A common mechanism of ATR activation by TOPBP1 and ETAA1

By

Vaughn Thada

Dissertation
Submitted to the Faculty of the
Graduate School of Vanderbilt University
in partial fulfillment of the requirements
for the degree of

DOCTOR OF PHILOSOPHY
In
Biochemistry
February 28, 2021
Nashville, Tennessee

Approved:
Walter Chazin, Ph.D.
David Cortez, Ph.D.
James Dewar, Ph.D.
Scott Hiebert, Ph.D.
William Tansey, Ph.D.

ACKNOWLEDGMENTS

Research for this dissertation was made possible with funding from the Vanderbilt environmental toxicology training program (5T32ES007028) and a Ruth L. Kirschstein NRSA pre-doctoral fellowship (1F31GM128334-01).

First and foremost, I would like to thank my advisor Dr. David Cortez for his mentorship during my Ph.D. studies. When I came to Vanderbilt, I did not know what I wanted to research specifically, but when I interacted with Dr. Cortez as a first-year student in FOCUS, I knew he was a very talented scientist. I joined Dr. Cortez's lab not only because I found his research interesting, but also because I knew he would challenge me and push me to become the best scientist I could be. Thank you, Dave, for all the outstanding mentoring and training.

I would also like to thank my committee members: Dr. Walter Chazin, Dr. James Dewar, Dr. Scott Hiebert, and Dr. William Tansey. The advice and suggestions you provided to me at committee meetings was much appreciated, and I am also thankful that as a group you helped me to identify my weaknesses and improve as a scientist during my graduate career. I would like to give a special thanks to Dr. Chazin for not only being my committee chair, but also for being the commissioner of 7:30 AM pickup basketball. Playing basketball on Tuesday and Friday mornings was my favorite non-science activity on campus, and I am thankful for all the people I met and relationships I developed because of this activity.

Finally, I would like to thank both past and present members of the Cortez lab. Another of the reasons that I joined Dr. Cortez's lab was because of the research atmosphere created by having so many outstanding scientists in the lab. I would especially like to thank former lab members Dr. Kareem Mohni, Dr. Jessica Luzwick, and Dr. Thomas Bass. Without your guidance

and mentorship, I would not have been as successful as I was. All three of you helped me immensely with technical and intellectual development. To the current members of the Cortez lab, Dr. Kavi Mehta, Dr. Sarah Wessel, Dr. Madison Adolph, Dr. Wenpeng Liu, Dr. Courtney Lovejoy, Dr. Matthew Cranford, Archana Krishnamoorthy, Taha Mohamed, Jorge Rua-Fernandez, Samika Joshi, and Runxiang Zhao, thank you for making this a great place to train. Thank you especially Kavi, Sarah, Madison, Courtney, and Archana for your technical and intellectual assistance. I wish all members of the Cortez lab the best of luck in the future.

TABLE OF CONTENTS

LIST OF TABLES

LIST OF FIGURES

LIST OF ABBREVIATIONS

53BP1	p53 binding protein 1
AAD	ATR activation domain
ATM	Ataxia telangiectasia mutated
ATR	ATM and Rad3 related
ATRi	ATR inhibitor
ATRIP	ATR interacting protein
BLM	Bloom syndrome protein
B-MYB	MYB proto-oncogene like 2
BRCA1	BRCA1 DNA repair associated
BRCA2	BRCA2 DNA repair associated
BRCT	BRCA1 C-terminus
CDC25	Cell division cycle 25
CDC45	Cell division cycle 45
CDK1	Cyclin dependent kinase 1
CENP-F	Centromere protein F
CHK1	Checkpoint kinase 1
CHK1i	CHK1 inhibitor
CHK2	Checkpoint kinase 2
CK2	Casein kinase 2
CMG	CDC45-MCM-GINS
CPT	Camptothecin

CtIP	CTBP-Interacting protein
Ddc1	DNA damage checkpoint 1
DDR	DNA damage response
DDX19	DEAD-box helicase 19
DMEM	Dulbecco's Modified Eagle Medium
Dna2	DNA synthesis defective 2
DNA-PK	DNA dependent protein kinase
DNA-PKcs	DNA-PK catalytic subunit
dNTPs	deoxyribonucleotide triphosphates
Dpb11	DNA replication regulator DPB11
DSB	Double strand break
dsDNA	Double-stranded DNA
EME1	Essential meiotic structure-specific endonuclease 1
ETAA1	ETAA1 activator of ATR kinase
EXO1	Exonuclease 1
EWS	Ewing sarcoma
F	Phenylalanine
FAM122A	PP2A A alpha (PPP2R1A) and B55A (PPP2R2A) interacting phosphatase regulator 1
FANCD2	Fanconi anemia complementation group D2
FANCM	Fanconi anemia complementation group M
FAT	Frap-ATM-TRRAP
FATC	FAT C-terminal

FKBP	FK-506 binding protein
FOXM1	Forkhead Box M1
FUS/TLS	Fused in sarcoma/translated in sarcoma
GFP	Green fluorescent protein
GST	Glutathione-S-transferase
HBSS	Hank's balanced salt solution
HEAT	Huntingtin, EF3A, ATM, TOR
HEK	Human Embryonic Kidney
H2A	Histone 2A
H2AX	Histone 2AX
HLTF	Helicase like transcription factor
HR	Homologous recombination
HU	Hydroxyurea
iPOND	isolation of proteins on nascent DNA
IR	Ionizing radiation
K	Lysine
LIG4	DNA ligase 4
MAD	Mec1 activation domain
MBP	Maltose binding protein
MCM	Minichromosome maintenance
MDC1	Mediator of DNA damage checkpoint 1
Mec1	Mitosis entry checkpoint 1
MLL	Mixed-lineage leukemia

MRI	Modulator of retrovirus infection
MRN	MRE11-RAD50-NBS1
mTOR	Mechanistic target of rapamycin kinase
MUS81	MUS81 structure-specific endonuclease subunit
NHEJ	Non-homologous end joining
PALB2	Partner and localizer of BRCA2
PARP1	Poly(ADP-ribose) polymerase 1
PAXX	PAXX non-homologous end-joining factor
PBS	Phosphate buffered saline
PD-1	Programmed cell death 1
PD-L1	CD274 molecule
PEI	Polyethylenimine
PI3K	Phosphoinositide 3-kinase
PIKK	Phosphoinositide 3-kinase related kinase
PLK1	Polo like kinase 1
POL α	DNA polymerase α
POL δ	DNA polymerase δ
POL ε	DNA polymerase ε
PP1	Protein phosphatase 1
PP2A	Protein phosphatase 2 phosphatase activator
PRD	PIKK regulatory domain
PTM	Post-translational modification
RFC	Replication factor C

RHINO	RAD9-RAD1-HUS1 interacting nuclear orphan
RIF1	Replication timing regulatory factor 1
RNF168	Ring finger protein 168
RNF8	Ring finger protein 8
RNR	Ribonucleotide reductase
ROS	Reactive oxygen species
RPA	Replication protein A
RRM2	Ribonucleoside-diphosphate reductase subunit M2
RSR	Replication stress response
RTEL1	Regulator of telomere elongation helicase 1
S	Serine
SAC	Spindle assembly checkpoint
SCE	Sister-chromatid exchange
seDSB	single-ended DSB
SLX1	Structure-specific endonuclease subunit SLX1
SLX4	Structure-specific endonuclease subunit SLX4
SSB	ssDNA-binding protein
ssDNA	Single-strand DNA
SMARCAL1	SWI/SNF, matrix associated, actin dependent regulator of chromatin A-like 1
SMC1	Structural maintenance of chromosomes 1
T	Threonine
TAF15	TATA box-binding protein-associated factor 68 KDa

TOPBP1	DNA topoisomerase II binding protein 1
TPR	Tetratricopeptide repeat
TRRAP	Transformation/transcription domain associated protein
UV	Ultraviolet
WEE1	WEE1 G2 checkpoint kinase
WRN	Werner syndrome ATP-dependent helicase
XLF	XRCC4-like factor
XRCC2	X-ray repair cross complementing protein 2
XRCC3	X-ray repair cross complementing protein 3
XRCC4	X-ray repair cross complementing protein 4
ZFP161	Zinc finger and BTB domain containing 14
ZRANB3	Zinc finger RANBP2-type containing 3

CHAPTER I

INTRODUCTION

The DNA damage response

Human cells must accurately replicate greater than 6 billion base pairs of DNA each time they divide. Human cells are also constantly exposed to exogenous agents, such as ultraviolet (UV) light, and endogenous agents, such as reactive oxygen species (ROS), that cause thousands of DNA lesions in each cell every day. Cells must carefully coordinate DNA replication and DNA repair to ensure that chromosomal aberrations are not passed from one generation to the next. An accumulation of such mutations can result in cell death or cause cancer. Coordination of DNA replication and DNA repair is controlled by a series of signaling pathways that are collectively known as the DNA damage response (DDR). The DDR regulates DNA replication and DNA repair, but it also coordinates these processes with the processes of cell cycle control, gene expression, senescence, and apoptosis (Ciccia and Elledge, 2010).

Initiation of DDR signaling pathways is primarily controlled by three proteins: ataxia telangiectasia mutated (ATM), ATM and Rad3 related (ATR), and DNA-dependent protein kinase (DNA-PK). ATM, ATR, and DNA-PK are large protein kinases that are activated in response to DNA damage. Activation of these kinases results in the phosphorylation of hundreds of additional proteins that function in the DDR. The importance of the DDR kinases to human health is underscored by the fact that mutations that disrupt their function cause severe physical and cognitive problems. Mutations in ATM cause ataxia-telangiectasia (A-T). Patients with A-T exhibit loss of cerebellar neuron function, which causes ataxia, and have abnormal blood vessel dilation (telangiectasia). Additionally, A-T patients are immunodeficient, profoundly sensitive to

ionizing radiation (IR), and have an increased cancer predisposition (Paull, 2015). Mutations in DNA-PK catalytic subunit (DNA-PKcs) cause severe combined immunodeficiency (SCID) as well as body dysmorphia, growth retardation, microcephaly, seizures, and impaired neurological function (Woodbine et al., 2013). Mutations that compromise ATR function cause Seckel syndrome, which is characterized by primordial dwarfism, microcephaly, craniofacial abnormalities, and mental retardation (O'Driscoll et al., 2003). Although mutations in all DDR kinases cause severe diseases, it is important to note that while complete loss of ATM and DNA-PKcs function is compatible with life, complete loss of ATR is not (Menolfi and Zha, 2020). Thus, ATR may be the most important of the three DDR kinases.

Below, I will discuss the specific functions of these kinases in the DDR. Their structures and mechanisms of regulation will also be examined. The work in this thesis describes how ATR activation is stimulated, so ATR will be the kinase most thoroughly discussed in the following sections. Finally, I will describe how our knowledge of the DDR is being used to improve cancer treatment, with a special focus on ATR.

DNA-PK and Non-homologous end joining

DNA double-strand breaks (DSBs) are the most deleterious DNA lesions that occur in cells. If unrepaired or repaired incorrectly, these lesions can result in cell death or chromosomal translocations, and possibly tumorigenesis. Cells have evolved two primary pathways to repair DSBs: non-homologous end joining (NHEJ) and homologous recombination (HR). NHEJ is the predominant DSB repair pathway and functions in all phases of the cell cycle. DSB repair by NHEJ occurs by direct ligation of the broken DNA ends and is generally considered to be error prone. Repair of DSBs by HR occurs in only S and G2 phase of the cell cycle and requires an

intact sister chromatid to serve as the repair template. As such, DSB repair by HR is error-free (Scully et al., 2019).

DNA-PK is required for DSB repair by NHEJ. Upon DSB formation, the KU70/80 complex binds the DNA ends and recruits the DNA-PKcs to form the DNA-PK holoenzyme, which is required for long range synaptic complex formation (Graham et al., 2016). Subsequently, additional proteins including XRCC4-LIG4 (Critchlow et al., 1997; Grawunder et al., 1997), XLF (Ahnesorg et al., 2006), PAXX, and MRI are recruited to DSBs (Fig 1.1). XRCC4-LIG4 and XLF are required for short range synaptic complex formation (Graham et al., 2016) and PAXX, through a direct interaction with KU, stabilizes the core NHEJ machinery to allow for efficient repair (Ochi et al., 2015). MRI also promotes retention of the core NHEJ proteins at DSBs via an interaction with KU and XLF (Hung et al., 2018). At a subset of DSBs, DNA-PKcs recruits and phosphorylates the end-processing enzyme Artemis (Fig 1.1). Phosphorylation by DNA-PK stimulates Artemis nuclease activity (Ma et al., 2002). DNA-PK also autophosphorylates at multiple sites, and these phosphorylation events are required for short-range synaptic complex formation (Graham et al., 2016; Jette and Lees-Miller, 2015). Current data suggests DNA-PKcs physically blocks DNA end-ligation and that autophosphorylation relieves this blockage (Jiang et al., 2015). DNA-PK phosphorylates several other NHEJ factors including XRCC4 (Critchlow et al., 1997); however, whether any of these phosphorylation events are required for NHEJ is unclear.

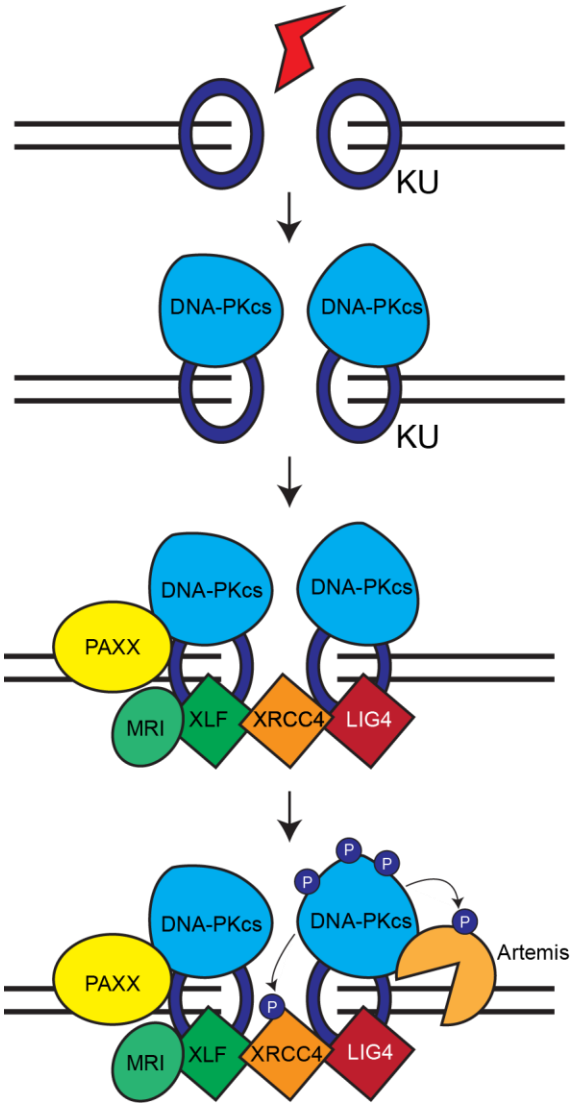

Figure 1.1 DNA-PK regulates NHEJ. NHEJ is the major form of DSB repair in human cells and occurs in all phases of the cell cycle. Upon DSB formation, the DNA ends are rapidly bound by the KU70/80 complex. KU recruits the DNA-PKcs to form the DNA-PK holoenzyme. Subsequently, additional factors XLF, MRI, XRCC4-LIG4, and PAXX are recruited to DSBs. Both MRI and PAXX, through an interaction with KU, stabilize the core NHEJ machinery, and XRCC4 stimulates LIG4 ligase activity to seal the break. At a subset of DSBs, DNA-PK recruits and phosphorylates the end-processing enzyme Artemis. Artemis function at DSBs with non-ligatable ends to ensure DSB ends are compatible prior to final ligation. DNA-PK phosphorylates several NHEJ proteins and also autophosphorylates. DNA-PK autophosphorylation is required for proper end-joining.

ATM and DNA DSB repair

Like DNA-PK, ATM primarily functions in response to DNA DSBs. However, ATM signaling is important for NHEJ and HR. ATM signaling also causes transcriptional changes and activates cell cycle checkpoints, and depending on the severity of the damage, can trigger senescence or apoptosis (Blackford and Jackson, 2017).

ATM activates a DNA damage signaling cascade at DSBs that recruits multiple downstream effectors needed for lesion repair. The MRE11-RAD50-NBS1 (MRN) complex is rapidly recruited to DSB sites where it then recruits and activates ATM (Falck et al., 2005; Lee and Paull, 2004, 2005) (Fig 1.2). Activated ATM phosphorylates the histone variant H2AX on S139, creating γH2AX (Scully and Xie, 2013). γH2AX recruits MDC1 (Stucki et al., 2005), another ATM substrate, and ATM-dependent phosphorylation stabilizes MDC1 at DSBs (Jungmichel et al., 2012; Liu et al., 2012) (Fig 1.2). MDC1 is simultaneously phosphorylated by CK2, and this phosphorylation promotes MDC1's interaction with MRN and increases MRN retention on chromatin (Melander et al., 2008; Spycher et al., 2008). This positive feedback loop increases ATM recruitment to DSBs, thereby amplifying ATM-dependent signaling.

MDC1 phosphorylation by ATM stabilizes MDC1 at DSBs, but it also generates a platform for the recruitment of additional DDR proteins. One such protein, the ubiquitin ligase RNF8, binds phosphorylated MDC1 (Huen et al., 2007; Kolas et al., 2007; Mailand et al., 2007). RNF8 ubiquitylates the linker histone H1, which results in the recruitment of another ubiquitin ligase, RNF168 (Thorslund et al., 2015) (Fig 1.2). RNF168 ubiquitylates K15 on H2A variants,

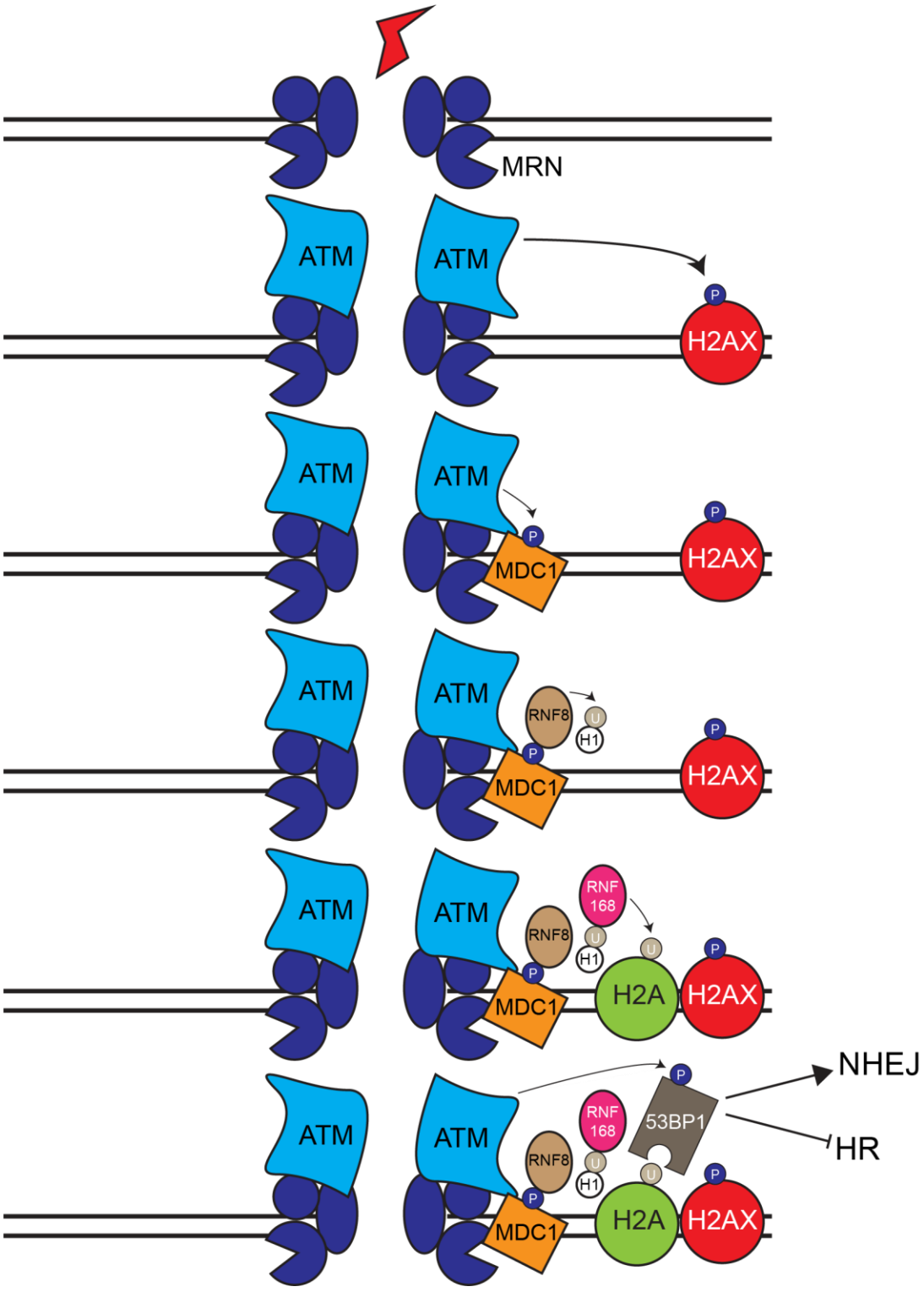
MRN
ATM
ATM
P
H2AX
ATM
ATM
P
MDC1
P
H2AX
ATM
ATM
RNF8
U
H1
P
MDC1
P
H2AX
ATM
ATM
RNF
168
RNF8
U
H1
P
MDC1
U
H2A
P
H2AX
ATM
ATM
P
RNF
168
53BP1
RNF8
U
H1
U
P
MDC1
H2A
H2AX
NHEJ
HR

Figure 1.2 ATM orchestrates DNA DSB repair. ATM is recruited to DSBs by the DSB sensor complex MRN, and MRN stimulates ATM kinase activity. At DSBs, ATM phosphorylates the histone variant H2AX to create γH2AX. γH2AX recruits MDC1, which interacts with MRN and promotes MRN retention at DSBs. ATM also phosphorylates MDC1, and phosphorylated MDC1 recruits the ubiquitin ligase RNF8. RNF8 ubiquitylates the linker histone H1, and ubiquitylated H1 is bound by another ubiquitin ligase, RNF168. RNF168 ubiquitylates K15 of H2A variants, and this facilitates recruitment of the adaptor protein 53BP1. ATM-dependent 53BP1 phosphorylation promotes DSB repair by NHEJ and suppress repair by HR.

and this ubiquitylation recruits the adaptor protein 53BP1 (Fradet-Turcotte et al., 2013). 53BP1 antagonizes DNA end-resection, the first step of HR, and thereby promotes DSB repair by NHEJ (Fig 1.2). In addition, 53BP1 is an ATM substrate and phosphorylated 53BP1 interacts with two additional proteins, PTIP and RIF1 (Munoz et al., 2007). Both the 53BP1-PTIP and 53BP1-RIF1 interactions are important for directing DSB repair to the NHEJ pathway (Blackford and Jackson, 2017). The 53BP1-RIF1 interaction may be especially important as this complex functions to recruit another multiprotein complex, Shieldin, that promotes DSB repair by NHEJ (Greenberg, 2018).

ATM signaling also promotes NHEJ through direct regulation of proteins that actively carry out NHEJ. ATM-dependent DNA-PK phosphorylation contributes to Artemis recruitment to DSBs (Jiang et al., 2015), and ATM-dependent Artemis phosphorylation is required for repair of a subset of DSBs by NHEJ (Riballo et al., 2004).

ATM phosphorylates numerous proteins in response to DNA damage, and although several of these proteins are important for DSB repair by NHEJ, ATM also phosphorylates proteins that are essential for DSB repair by HR. ATM phosphorylates all components of the MRN complex (Matsuoka et al., 2007), the DNA end-resection factor CtIP (Shibata et al., 2011; Wang et al., 2013), and BRCA1 (Cortez et al., 1999). ATM dependent CtIP phosphorylation promotes DNA end-resection (Fig 1.3), the first step in HR, and is also required for BLM and EXO1 recruitment to DSBs, two proteins that promote long-range resection (Wang et al., 2013). ATM-mediated DNA end-resection also facilitates ATR recruitment to DSBs, thereby promoting checkpoint activation (Adams et al., 2006; Cuadrado et al., 2006; Jazayeri et al., 2006; Myers and Cortez, 2006) (Fig 1.3). Importantly, ATM-dependent CtIP phosphorylation depends on

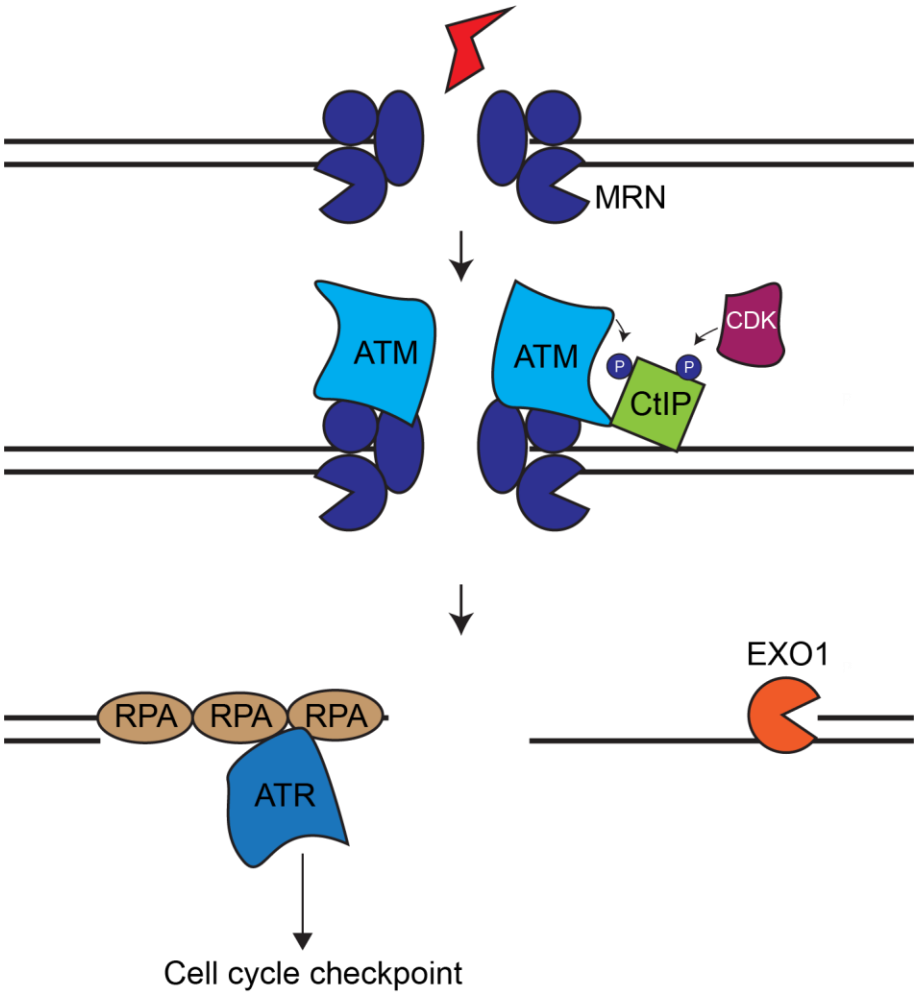

Figure 1.3 ATM regulates HR. ATM recruitment to DSBs by MRN promotes DSB repair by HR. ATM phosphorylates the essential resection factor CtIP, and together, MRN and CtIP perform short-range end-resection. Importantly, ATM-dependent CtIP phosphorylation is dependent on prior CtIP phosphorylation by CDK, thus ensuring ATM-dependent CtIP phosphorylation is restricted to S and G2 phase. Following short-range end-resection, long-range resection by EXO1 generates the 3' ended ssDNA needed for subsequent HR steps. ssDNA generated by DNA end-resection also recruits ATR to DSBs via the single-stranded DNA binding protein RPA. ATR signaling promotes DNA repair and activates cell cycle checkpoints.

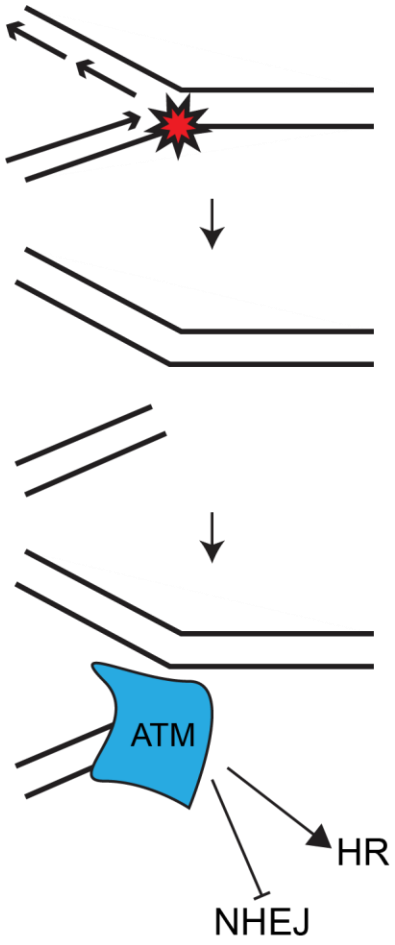

Figure 1.4 ATM promotes HR at collapsed replication forks. Replication forks that encounter DNA lesions such as single-strand breaks collapse and form single-ended DSBs (seDSBs). seDSBs are repaired exclusively by HR, and ATM activity at seDSBs promotes HR-mediated repair while suppressing NHEJ.

prior CtIP phosphorylation by CDK (Wang et al., 2013) (Fig 1.3). This regulatory mechanism ensures that ATM-dependent CtIP phosphorylation only occurs in S and G2 phase of the cell cycle, when a sister chromatid is available to serve as a repair template.

HR regulation by ATM is also critical at replication forks. Replication forks that encounter ssDNA breaks collapse and form single-end DSBs (seDSBs). ATM function at collapsed replication forks ensures these forks are repaired properly by HR, and not improperly by NHEJ, which would otherwise cause chromosomal aberrations that could lead to cell death or tumorigenesis (Fig 1.4). ATM-mediated DNA end-resection at seDSBs limits KU binding at these lesions and blocks XRCC4-LIG4 dependent end-joining (Balmus et al., 2019; Chanut et al., 2016).

ATM and cell cycle checkpoints

ATM coordinates DNA DSB break repair with cell cycle progression by activating cell cycle checkpoints in response to DNA damage. In G1 phase cells, DNA damage activates ATM and causes ATM-dependent p53 phosphorylation and stabilization (Fig 1.5). p53, often referred to as the "guardian of the genome," when stabilized, activates a transcriptional network that causes cellular senescence or apoptosis (Shiloh and Ziv, 2013). Through this mechanism, ATM signaling prevents cells with damaged DNA from beginning DNA replication.

ATM is also activated when cells undergoing DNA replication experience DNA damage. This intra-S phase checkpoint is initiated by ATM-dependent phosphorylation of CHK2. CHK2 subsequently phosphorylates CDC25A, a phosphatase that activates CDKs (Fig 1.5). CHK2-dependent CDC25A phosphorylation causes CDC25A degradation and thereby halts cell cycle

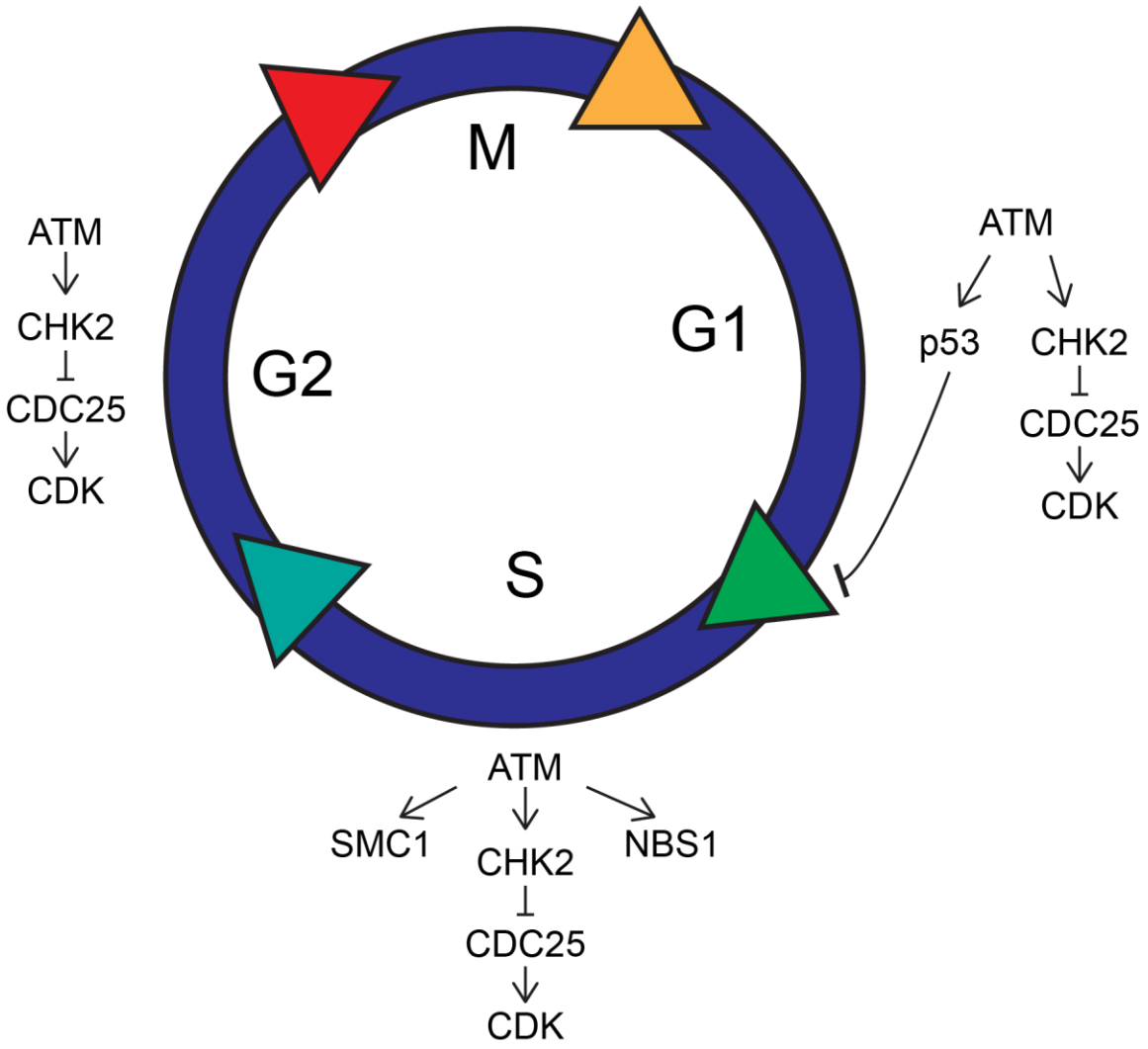

Figure 1.5 ATM activates cell cycle checkpoints. DNA damage activates ATM-dependent cell cycle checkpoints in G1, S, and G2 phase. In response to genotoxic stress, ATM phosphorylates its main downstream effector kinase CHK2. CHK2-dependent phosphorylation of the CDC25 phosphatases prevents CDC25 mediated activation of CDKs and slows cell cycle progression in G1, S, and G2 phase. Additionally, ATM-dependent p53 phosphorylation activates the G1/S checkpoint. p53 activates a transcriptional program that promotes cellular senescence or apoptosis, thereby preventing cells with damaged DNA from beginning DNA replication. During S-phase, ATM-dependent phosphorylation of SMC1 and NBS1 activates the intra-S phase checkpoint.

progression in S-phase (Falck et al., 2001), and in G1 and G2 phase (Lukas et al., 2004). ATM also phosphorylates SMC1 in response to DNA damage, which blocks radioresistant DNA synthesis (Yazdi et al., 2002), and NBS1, which is critical for activation of the intra-S phase checkpoint (Gatei et al., 2000; Lee et al., 2003; Lim et al., 2000; Zhao et al., 2000) (Fig 1.5).

ATR is the replication stress response kinase

ATR is activated by a greater variety of DNA lesions than DNA-PK and ATM. Lesions such as DNA inter-strand crosslinks (ICLs), UV light adducts, DSBs, and damaged replication forks all activate ATR, and the common structure that recruits ATR to these lesions is RPA-coated ssDNA (Cimprich and Cortez, 2008). ATR activation at both stalled and normal replication forks coordinates the processes of DNA replication, DNA repair, and cell cycle progression, and is essential for cellular proliferation. ATR regulates multiple cell cycle checkpoints including intra-S, S/G2, G2/M, and M phase checkpoints, controls origin firing, and stabilizes stressed replication forks (Saldivar et al., 2017).

ATR and cell cycle checkpoints

ATR exerts many of its effects, including the activation of cell cycle checkpoints, through its downstream effector kinase CHK1. In response to DNA damage, CHK1 is phosphorylated by ATR at residues S317 and S345 in a reaction that is mediated by the adaptor CLASPIN (Kumagai and Dunphy, 2000). Activated CHK1 phosphorylates numerous proteins including the CDC25 A/B/C phosphatases. CHK1-dependent CDC25A/B/C phosphorylation prevents CDK activation by these phosphatases and temporarily halts cell cycle progression. CDC25A phosphorylation results in its degradation (Mailand et al., 2000; Sorensen et al., 2003),

and CDC25C phosphorylation causes its localization to the cytoplasm via the 14-3-3 proteins (Peng et al., 1997; Sanchez et al., 1997).

During S-phase, CDK activity is required for origin firing. Specifically, CDK-dependent phosphorylation of TRESLIN is required for CDC45 loading at origins and helicase activation (Yekezare et al., 2013). As such, one way in which ATR activates the intra-S phase checkpoint is through decreased CDK activity, which causes a reduction in origin firing (Fig 1.6). ATR also blocks CDC45 loading at origins through other mechanisms. One such mechanism is CHK1-dependent phosphorylation of TRESLIN, which prevents CDC45 recruitment to chromatin (Guo et al., 2015), and another is ATR-dependent phosphorylation of MLL. MLL phosphorylation by ATR causes increased MLL retention on chromatin, and this antagonizes CDC45 loading at origins (Liu et al., 2010). Limiting origin firing ensures essential replication factors are not depleted, but it also prevents aberrant topological stress that would otherwise cause genome instability (Morafraile et al., 2019).

ATR also controls the S/G2 checkpoint. This checkpoint is regulated by ATR in the absence of any exogenous DNA damage and coordinates S-phase progression with a mitotic transcriptional program (Saldivar et al., 2018). During an unperturbed S-phase, basal levels of ATR activation signal through CHK1 and CDC25 to repress CDK1-dependent phosphorylation of B-MYB and FOXM1 (Fig 1.6). If ATR is inhibited during S-phase, aberrant B-MYB and FOXM1 phosphorylation results in premature expression of mitotic genes. The resulting discoordination between S-phase length and mitotic gene expression prevents complete DNA replication prior to mitotic entry and thus causes genomic instability (Saldivar et al., 2018). ATR-CHK1 repression of CDK1 activity in S-phase also blocks CDK1-dependent RIF1 phosphorylation, which restrains origin firing via stabilization of the RIF1-PP1 interaction

(Moiseeva et al., 2019) (Fig 1.6). In addition, ATR-CHK1-dependent suppression of another mitotic kinase, PLK1, coordinates DNA replication with mitotic onset (Lemmens et al., 2018). How ATR is activated to enforce cell cycle checkpoints in unstressed conditions is incompletely understood, but one mechanism involves inherent replication stress caused by low dNTP levels in early S-phase (Forey et al., 2020).

As with the intra-S and S/G2 checkpoints, ATR controls the G2/M checkpoint through phosphorylation of CHK1. In response to DNA damage in G2 or unresolved DNA damage from S-phase, ATR and CHK1 activation in G2 prevents CDC25-dependent activation of the CDK1/CYCLIN B complex, which is necessary for the transition from G2 phase to mitosis (Lukas et al., 2004). Although ATM-CHK2 signaling contributes to the G2/M checkpoint too (see above), ATR-CHK1 signaling is likely more important for this checkpoint (Lin and Dutta, 2007). Additionally, ATR-CHK1 signaling in G2 controls the G2/M checkpoint kinase WEE1. Upon DNA damage, CHK1 phosphorylates WEE1, which promotes WEE1 inhibitory phosphorylation of CDK1/CYCLIN B to delay mitotic entry (Lee et al., 2001; Oconnell et al., 1997) (Fig 1.6). CHK1 also regulates the G2/M checkpoint through phosphorylation of FAM122A. CHK1-dependent FAM122A phosphorylation activates PP2A, which results in PP2A dephosphorylation of WEE1 and subsequent WEE1 stabilization to activate checkpoint signaling (Li et al., 2020) (Fig 1.6).

ATR activation in mitosis is distinct from ATR activation in other cell cycle stages because it occurs independently of DNA damage and DNA replication. During mitosis, ATR is recruited to centromeres in an Aurora A kinase and CENP-F dependent manner and is activated

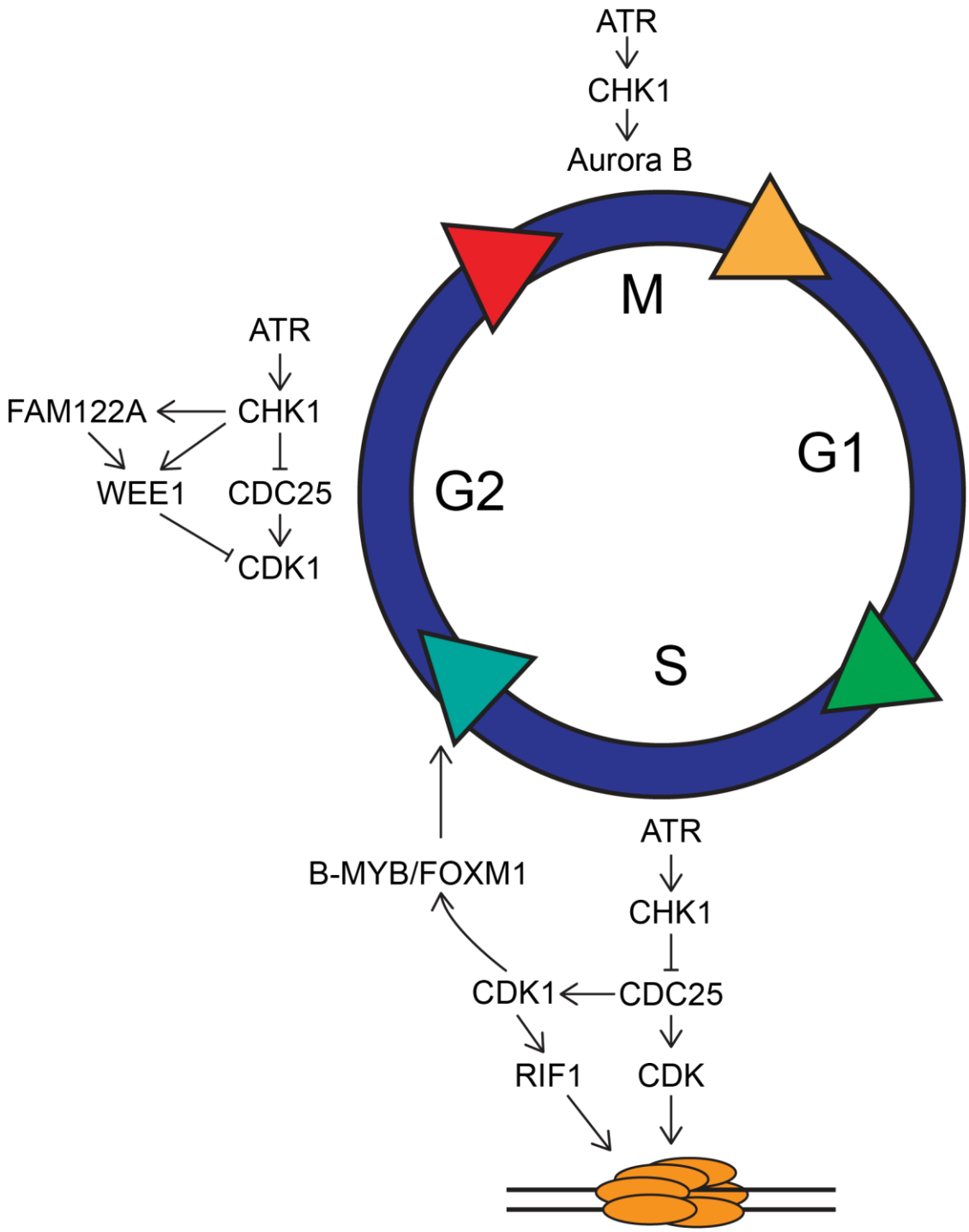

Figure 1.6 ATR activates cell cycle checkpoints. ATR-dependent cell cycle checkpoints occur in S, G2, and M phase. During S-phase, ATR-dependent CHK1 phosphorylation suppress CDC25-dependent CDK activation to slow cell cycle progression and restrain new origin firing. The ATR-CHK1 pathway also regulates the S/G2 checkpoint by ensuring CDK1-dependent B-

MYB and FOXM1 phosphorylation does not occur prematurely and activate a mitotic transcriptional network prior to S-phase completion. ATR-CHK1-dependent suppression of CDK1 activity also restrains origin firing through inhibition of RIF1. ATR-CHK1 signaling controls the G2/M checkpoint by inactivating the CDC25 phosphatases and through CHK1-dependent phosphorylation of WEE1 and FAM122A. Activated WEE1 phosphorylates CDK1/CYCLIN B, which delays progression from G2 to M phase. Mitotic ATR signaling activates Aurora B kinase to control the spindle assembly checkpoint (SAC) and ensure proper chromosome segregation.

upon binding to centromeric R-loops (Kabeche et al., 2018). ATR-CHK1 signaling at centromeres is required for efficient Aurora B kinase activation, which ensures maintenance of the spindle assembly checkpoint (SAC) and accurate chromosome segregation (Bass and Cortez, 2019; Kabeche et al., 2018; Zachos et al., 2007) (Fig 1.6).

ATR and replication fork stabilization

Replication forks frequently encounter obstacles that impede their progression such as transcription bubbles, DNA secondary structures, repetitive sequences, or DNA lesions induced by either endogenous or exogenous sources (Zeman and Cimprich, 2014). Stabilization of stalled replication forks such that they can resume DNA synthesis upon removal of the impeding lesion is a major function of ATR (Saldivar et al., 2017). Consistent with this idea, a recent study found that ATR is especially important for fork stabilization within, and the faithful replication of, structure-forming microsatellite sequences (Shastri et al., 2018).

Stalled replication forks that cannot resume DNA synthesis are said to have collapsed, and fork collapse is often accompanied by DSB formation. ATR activation at stalled replication forks is required for fork restart and to prevent DSB formation (Couch et al., 2013). Fork collapse that occurs when ATR is inhibited is not due to dissociation of replisome components (Dungrawala et al., 2015), but instead is likely due to inappropriate activity of fork remodeling enzymes and structure specific nucleases that can cleave stalled replication forks. Fork remodeling enzymes such as SMARCAL1, ZRANB3, and HLTF can remodel stalled replication forks to generate four-way junctions known as reversed forks (Cortez, 2019). Although fork reversal is likely a mechanism of DNA damage tolerance, aberrant fork reversal is detrimental and can lead to DSB formation (Neelsen and Lopes, 2015).

ATR likely regulates fork reversal in multiple ways, but one such way is through SMARCAL1 phosphorylation. ATR-dependent SMARCAL1 phosphorylation prevents excessive fork reversal and subsequent fork cleavage by SLX4-dependent nucleases (Couch et al., 2013) (Fig 1.7A). Additionally, ATR-dependent regulation of structure specific nucleases through down-regulation of CDK activity ensures reversed fork stability. In G2 phase and mitosis, elevated CDK activity stimulates SLX1-SLX4 and MUS81-EME1 resolution of Holliday junctions (Wyatt et al., 2013). While beneficial in G2 phase and mitosis for the separation of sister chromatids, aberrant nuclease activity in S-phase due to decreased ATR activity (and hence elevated CDK activity) could contribute to replication fork collapse (Fig 1.7A). Reversed forks are also stabilized by ATR-dependent XRCC2 phosphorylation, which prevents nascent strand degradation (NSD) (Saxena et al., 2019). Finally, ATR can inhibit NSD by promoting fork reversal-independent fork restart mechanisms. Indeed, in response to recurring cisplatin treatments, ATR-dependent PRIMPOL re-priming confers fork protection in BRCA1-deficient cells (Quinet et al., 2020) (Fig 1.7B).

ATR phosphorylates components of the replisome and many proteins that are recruited to stalled replication forks in addition to SMARCAL1. Although the significance of all these phosphorylation events is not known, ATR-mediated phosphorylation of replication stress response proteins likely contributes to fork stabilization and restart. One such example is ATR-dependent phosphorylation of the MCM complex (Cortez et al., 2004) (Fig 1.7B). Phosphorylated MCM recruits FANCD2 to replication forks, which in turn reduces fork speed and limits ssDNA generation (Lossaint et al., 2013). FANCD2, together with FANCM, also promotes fork traverse of ICLs upon ATR-dependent FANCM phosphorylation (Huang et al., 2019). ATR also phosphorylates the RECQ helicases BLM and WRN. ATR-dependent BLM

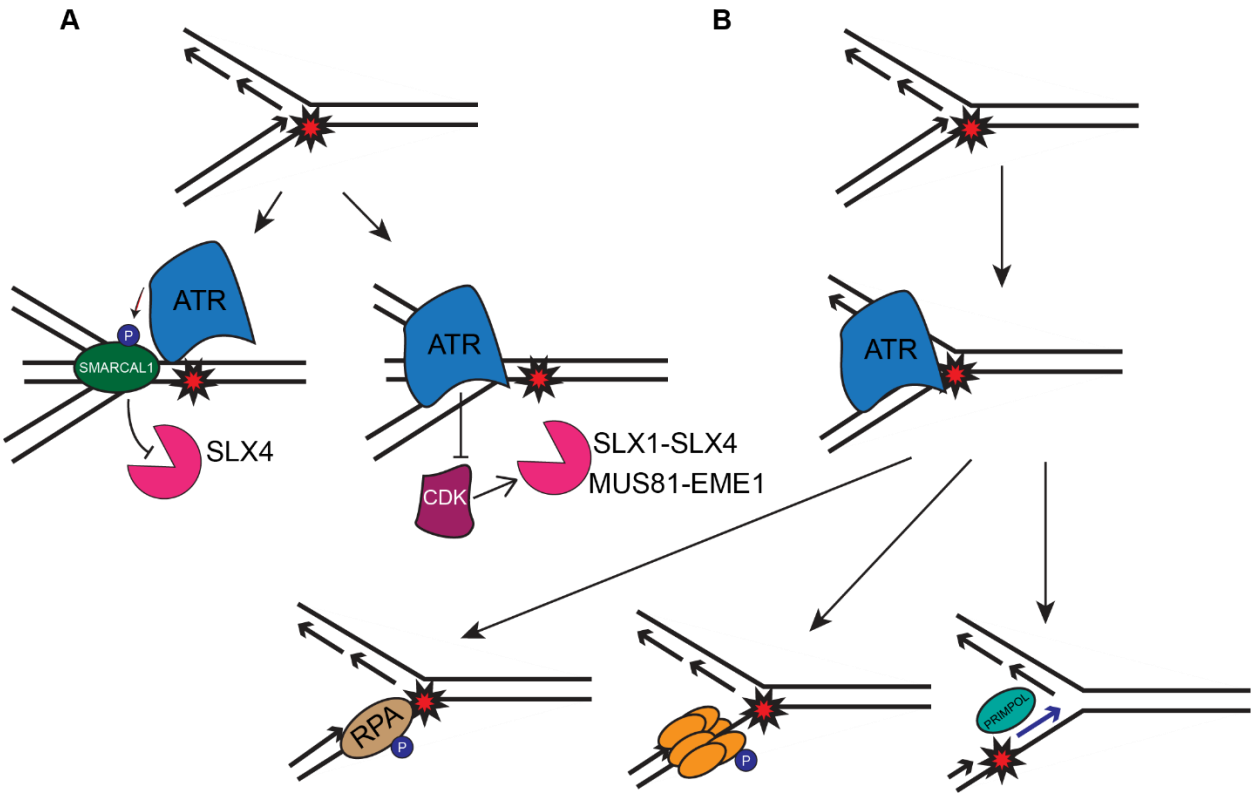

Figure 1.7 ATR stabilizes stressed replication forks. A) Replication stress promotes ATR-dependent SMARCAL1 phosphorylation, which restrains SMARCAL1-mediated fork reversal and prevents fork cleavage and DSB induction by SLX4-dependent nucleases. ATR-dependent CDK inactivation induced by fork stalling also ensures CDK-dependent activation of nucleases does not occur aberrantly/prematurely in S-phase and cause fork collapse. **B)** ATR phosphorylates numerous replisome and replication stress response proteins to stabilize stalled forks and promote fork restart. ATR-dependent RPA32 phosphorylation is required for fork stabilization, recruitment of additional DDR proteins to stalled forks, and fork restart. Likewise, ATR-dependent MCM phosphorylation promotes recruitment of other DDR proteins to damaged forks. Finally, ATR signaling at stalled forks upregulates PRIMPOL, which mediates fork restart.

phosphorylation is required for recovery from S-phase arrest due to replication fork stalling (Davies et al., 2004), and ATR-dependent WRN phosphorylation prevents replication fork collapse (Ammazzalorso et al., 2010).

Another important ATR substrate at stalled replication forks is RPA. ATR-dependent RPA32 phosphorylation is critical for stalled fork stabilization and recovery from replication stress (Murphy et al., 2014; Vassin et al., 2009) (Fig 1.7B). Additionally, ATR-dependent RPA32 phosphorylation promotes the recruitment of HR factors PALB2 and BRCA2 to damaged replication forks (Murphy et al., 2014), and ATR is required for PALB2 phosphorylation in response to replication stress (Ahlskog et al., 2016). Importantly, ATR-dependent PALB2 phosphorylation, in addition to ATR-dependent XRCC3 phosphorylation, is required for RAD51 recruitment to stalled replication forks (Ahlskog et al., 2016; Saxena et al., 2019). RAD51 is essential for HR, but it is also required for fork reversal and template switching (Saldivar et al., 2017). Finally, ATR promotes replication fork stabilization and repair by modulating nuclear F-actin polymerization (Lamm et al., 2020). Therefore, through phosphorylation of numerous replication stress response proteins, ATR stabilizes stalled replication forks and promotes fork restart likely by controlling multiple fork restart pathways.

ATR suppression of origin firing also contributes to replication fork stabilization in response to DNA damage. Although highly abundant, RPA pools become exhausted during conditions of replication stress when ATR is inhibited, causing widespread fork collapse (Toledo et al., 2013). RPA exhaustion caused by ATR inhibition may also contribute to exhaustion of HR factors needed for replication fork restart. Indeed, in response to ATR inhibition, aberrantly fired replication forks are bound by NHEJ factors instead of HR factors (Dungrawala et al., 2015).

Thus, ATR suppression of origin firing stabilizes stalled replication forks by preventing RPA exhaustion and by promoting HR-mediated fork restart.

Another important ATR regulated process that contributes to replication fork stabilization is maintaining an adequate level of deoxyribonucleotides (dNTPs). Ribonucleotide reductase (RNR) controls the rate limiting step of dNTP production, and RNR expression levels are controlled by ATR. ATR activity is required for expression of ribonucleoside-diphosphate reductase subunit M2 (RRM2) (a subunit of RNR) (Buisson et al., 2015), and in response to genotoxic stress, ATR-dependent downregulation of CDK activity increases RRM2 levels, thereby ensuring adequate dNTP levels are maintained (D'Angiolella et al., 2012). Interestingly, increasing Rrm2 levels in a mouse model of Seckel syndrome increases the size and lifespan of the mice (Lopez-Contreras et al., 2015), possibly indicating that regulation of dNTP levels is an important function of ATR during organismal development.

Structure of DDR PIKKs

The kinase domains of ATR, ATM, and DNA-PKcs exhibit structural similarity to the phospholipid kinase Phosphoinositide 3-kinase (PI3K) kinase domain and are so named PI3K-like kinases (PIKK). Other PIKKs include mammalian target of rapamycin (mTOR), which functions in cellular metabolism, SMG1, which functions in mRNA surveillance, and transformation/transcription domain-associated protein (TRRAP), which functions in chromatin remodeling (Imseng et al., 2018). All PIKKs share a similar domain architecture, with N-terminal α-solenoid Huntingtin, EF3A, ATM, TOR (HEAT) repeats followed by α-solenoid tetratricopeptide repeats (TPRs). The latter TPRs form a conserved structure known as the Frap, ATM, and TRRAP (FAT) domain, which is adjacent to the kinase domain. Following the kinase domain at the C-terminus are the PIKK regulatory domain (PRD) and FAT C-terminal (FATC)

motif. Together, the FAT, kinase, PRD, and FATC domains make up a single FATKIN unit (Imseng et al., 2018) (Fig 1.8A). Of all the PIKKs, the mTOR structure has been most extensively characterized, but in recent years, structural information about the DDR PIKKs have begun to emerge.

DNA-PKcs folds into three distinct structural units. The HEAT repeats form two of these units: the N-terminal unit and the circular cradle unit, and together these units form a ring shaped supersecondary structure (Sibanda et al., 2017). The third unit, the head, is composed of the bilobal kinase domain, FATC motif, and a poorly conserved fragment rapamycin binding (FRB) domain all surrounded by the FAT domain (Imseng et al., 2018) (Fig 1.8A and B). The DNA-PKcs head unit is similar in structure to the mTOR FATKIN unit. The DNA-PKcs is held in an inactive conformation by three α-hairpins that occupy the kinase active site. One of these α-hairpins originates from the Lst8 (a binding partner of mTOR)-binding element (LBE) and reaches into the active site. The other two α-hairpins are part of the PRD. One of the PRD α-hairpins blocks access to the PRD active site cleft, while the other binds the activation loop (Imseng et al., 2018). KU80 contacts DNA-PKcs at two sites in the circular cradle unit and initiates kinase activation through a long range allosteric mechanism (Sibanda et al., 2017), which may result in movement of the N-terminal HEAT repeat toward the FATKIN unit to create a wider active site cleft (Yin et al., 2017). This conformational change would also expose T3950 in the activation loop (Sibanda et al., 2017), a critical inhibitory autophosphorylation site that when phosphorylated decreases DNA-PK activity.

ATM is a dimer and adopts a butterfly-like architecture (Fig 1.8B). The HEAT repeats, which are important for protein-protein interactions, form a helical superstructure and are

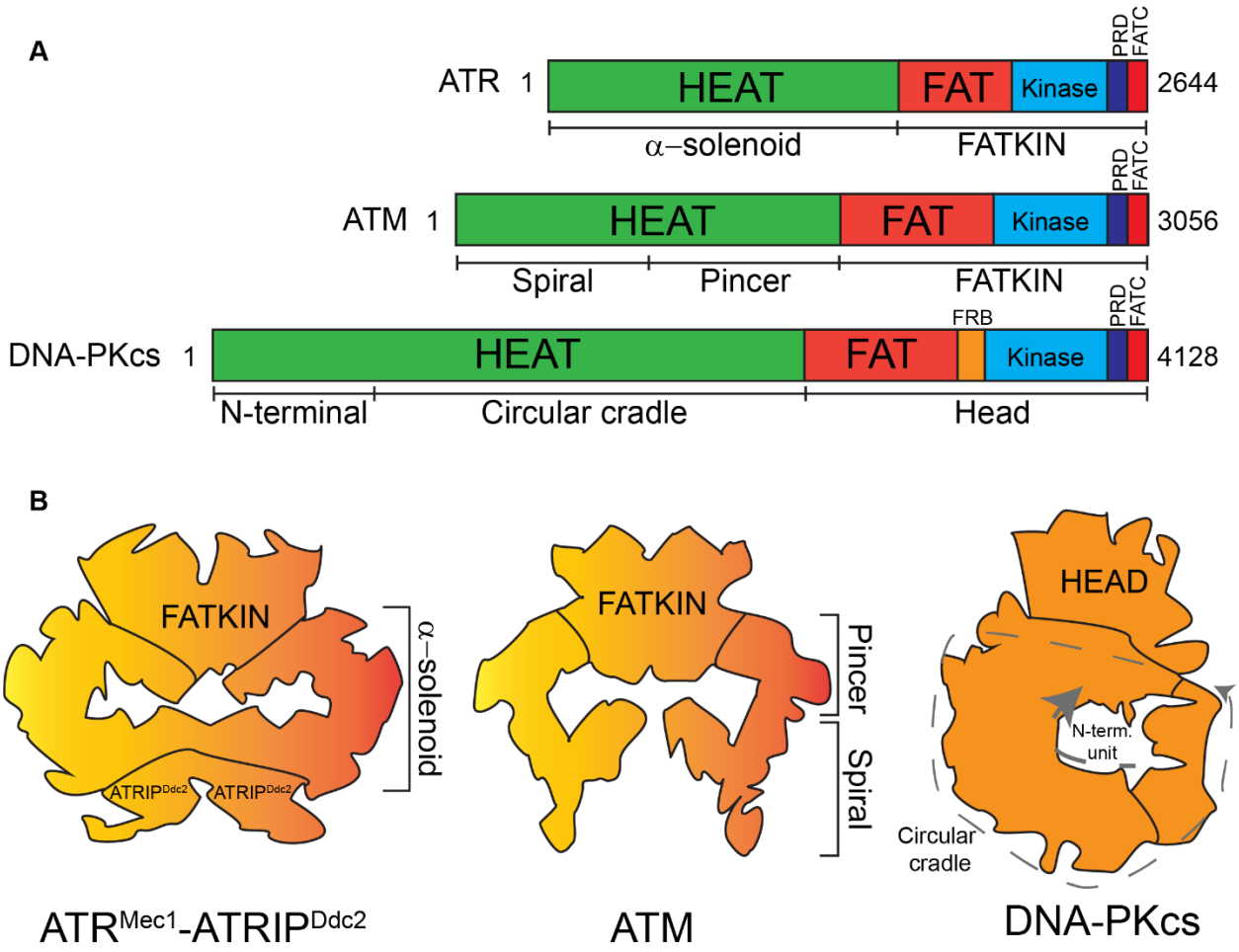

Figure 1.8 Structure of DDR PIKKs. A) Domain architecture of ATR, ATM, and DNA-PKcs. **B)** Three-dimensional structures of ATR^{Mec1}-$ATRIP^{Ddc2}$, ATM, and DNA-PKcs. The dimeric structures of ATR^{Mec1}-$ATRIP^{Ddc2}$ and ATM are represented by differential coloring (yellow and orange) of each protomer. The positions of the N-terminal unit and circular cradle regions in DNA-PKcs are denoted by the dashed arrows.

divided into the spiral and pincer regions (Wang et al., 2016) (Fig 1.8A and B). Unlike DNA-PKcs, ATM does not contain an FRB domain, but otherwise the ATM FATKIN unit generally aligns with the mTOR FATKIN unit (Imseng et al., 2018). ATM dimerization is mediated exclusively through the FATKIN unit with the main interface occurring at TPR domains 2 and 3 of the FAT domain (Baretic et al., 2017). Within the ATM FATKIN unit, the FATC, LBE equivalent region, activation loop, and PRD form a compact arrangement called the FLAP. The FLAP is pushed towards the kinase active site by the other protomer's FAT domain, thereby blocking substrate active site access and creating a closed conformation. Upon ATM activation, FATKIN dimeric interactions are reduced, and the FLAP repositions away from the active site to generate an open confirmation and presumably a more active kinase (Baretic et al., 2017).

Cryo-EM structures for both the ATR-ATRIP and Mec1-Ddc2 (ATR-ATRIP *S. cerevisiae* orthologs) complexes have been determined. Like ATM, the ATR^{Mec1}-$ATRIP^{Ddc2}$ complex forms a dimeric butterfly-like structure with two ATR^{Mec1} and two $ATRIP^{Ddc2}$ molecules in a single complex (Rao et al., 2018; Tannous et al., 2020; Wang et al., 2017) (Fig 1.8B). However, unlike ATM, which possesses only one dimer interface through the FATKIN unit, three dimer interfaces exist on the ATR^{Mec1}-$ATRIP^{Ddc2}$ complex. One of these dimer interfaces occurs through the FATKIN unit, another occurs through the PRD, and the third occurs through the $ATRIP^{Ddc2}$ coiled coil domain (Wang et al., 2017). Also, unlike ATM, the ATR^{Mec1} FATKIN unit possesses no inter-protomer inhibitory elements. The reported Mec1-Ddc2 structure is the closed, inactive form of the kinase where active site access and the activation loop are blocked by the PRD, FATC, and LBE (Wang et al., 2017). Binding of an ATR^{Mec1} activator (discussed below) to the PRD is hypothesized to relieve active site blockage through yet unknown conformational changes; however, the structure of a hyperactive Mec1

kinase with a mutation in the activation loop indicates Mec1 activation is achieved through PRD retraction from the activation loop concomitant with a reconfiguration of the FAT domain C-terminus and kinase domain N-lobe (Tannous et al., 2020).

Mechanisms of PIKK regulation

The similar structures of ATR, ATM, and DNA-PK imply that functional regulation of these kinases may also be similar, and indeed that is the case. Each DDR PIKK associates with a partner protein that localizes it to sites of DNA damage. ATR localizes to RPA-coated ssDNA through its interaction with ATRIP (Cortez et al., 2001; Zou and Elledge, 2003), ATM localizes to DSBs through its interaction with NBS1 (Falck et al., 2005), and DNA-PKcs localizes to DSBs through its interaction with KU80 (Gell and Jackson, 1999; Singleton et al., 1999) (Fig 1.9A). Additionally, ATRIP, NBS1, and KU80 all likely associate with their respective PIKKs in similar manners as all three proteins possess related C-terminal motifs required for PIKK binding (Falck et al., 2005).

Post-translational modifications (PTMs) of ATR, ATM, and DNA-PK also regulate their function. All three kinases autophosphorylate, with ATR and ATM each possessing one crucial site and DNA-PKcs possessing three (Fig 1.9B). DNA-PK undergoes autophosphorylation at S2056 and T2609 within the HEAT repeats and at T3950 in the kinase domain. Autophosphorylation at S2056 and T2609 promotes DNA-PK release from DSB sites to facilitate end-ligation (Jette and Lees-Miller, 2015), and autophosphorylation at T3950 inhibits DNA-PK activity (Sibanda et al., 2017). Additionally, because S2056 is near the KU binding site, autophosphorylation at this residue may alter the KU-DNA-PKcs interaction (Sibanda et al., 2017).

ATM autophosphorylates at S1981 within the FAT domain. Initial experiments in human cells indicated S1981 autophosphorylation was required for dissociation of inactive ATM dimers to active ATM monomers (or from closed to open ATM) and for full activation of ATM in response to DNA damage (Bakkenist and Kastan, 2003). However, mutation of the corresponding residue (S1987) in mice yields no observable deleterious phenotypes or defects in ATM activation (Daniel et al., 2008; Pellegrini et al., 2006). Furthermore, in a reconstituted *in vitro* system, the S1981A mutation does not reduce ATM activation (Lee and Paull, 2005).

Like ATM, ATR autophosphorylates at a residue within its FAT domain, T1989. Our lab demonstrated that T1989 phosphorylation occurs in response to DNA damage and is a marker of ATR activity, but that phosphorylation at this site is not required for recovery from replication stress and only causes a mild viability defect in cells (Nam et al., 2011). However, another study found that T1989 is essential for cellular viability and when mutated, causes a substantial reduction in checkpoint signaling. Furthermore, this same study found that T1989 phosphorylation is required for stable ATR-ATRIP association with the ATR activator DNA topoisomerase II binding protein 1 (TOPBP1) (Liu et al., 2011). Interestingly, the *S cerevisiae* ATR ortholog, Mec1, also undergoes autophosphorylation. However, this phosphorylation is distinct from ATR T1989 phosphorylation because Mec1 autophosphorylation at S1964 inhibits checkpoint signaling as opposed to stimulating it (Memisoglu et al., 2019). Thus, additional studies are needed to determine the functional relevance of both ATM and ATR autophosphorylation, and to more closely examine the similarities and differences between ATR T1989 and Mec1 S1964 autophosphorylation.

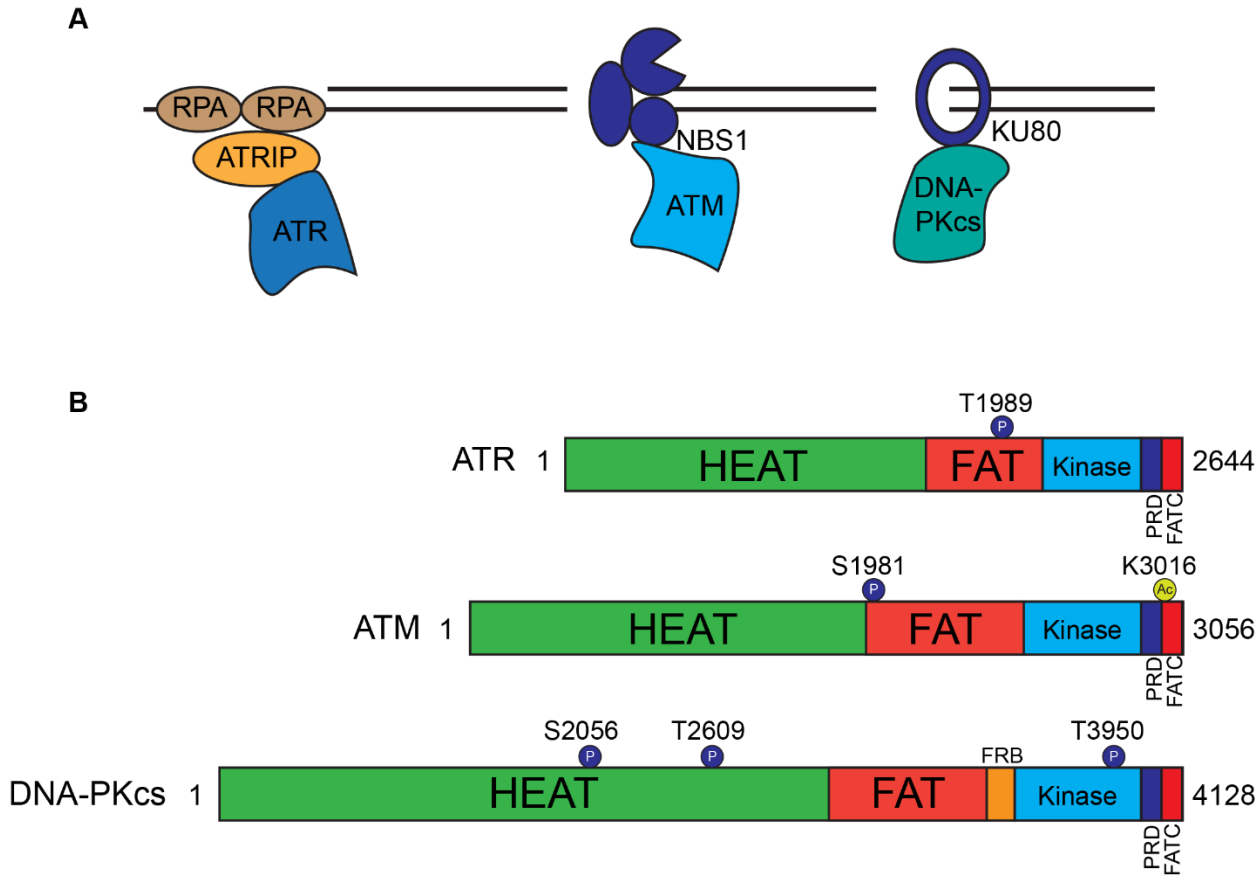

Figure 1.9 Mechanisms of DDR PIKK regulation. A) Each DDR PIKK is localized to DNA through an interaction with a partner protein. ATRIP localizes ATR to RPA-coated ssDNA, NBS1 recruits ATM to DSBs, and KU80 recruits DNA-PKcs to DSBs. **B)** The activities of all DDR PIKKs are regulated by post-translation modifications (PTMs). The locations of critical autophosphorylation sites are denoted on each kinase, and the location of a critical acetylation site on ATM is denoted.

Another PTM that regulates PIKK activation is acetylation. ATM is acetylated at K3016 in its FATC domain by Tip60 in response to genotoxic stress and this acetylation is required for damage-dependent ATM signaling (Sun et al., 2007) (Fig 1.9B). Tip60 loss also diminishes DNA-PK activation in response to DNA damage (Jiang et al., 2006), and mutation of possible acetylation sites in the DNA-PKcs FATC motif reduces DNA-PK signaling (Mordes et al., 2008a). The FATC motifs are highly conserved among ATR, ATM, and DNA-PKcs and remarkably, substitution of the ATM FATC motif with the ATR or DNA-PKcs FATC motif restores Tip60-dependent ATM acetylation and ATM activation in response to DNA damage (Jiang et al., 2006). To date, there is no evidence that the ATR FATC motif is acetylated, and although the ATR FATC motif can substitute for the ATM FATC motif, the reverse is not true (Mordes et al., 2008a). Thus, in addition to being regulated by PTMs, DDR PIKK FATC motifs likely have additional functions such as kinase domain stabilization.

ATR^{Mec1} regulation by ATR^{Mec1} activators

Each DDR PIKK requires an activator protein(s) to stimulate its kinase activity. KU stimulates DNA-PKcs activity and MRN stimulates ATM activity (Blackford and Jackson, 2017). In metazoan cells, there are at least two ATR activators, TOPBP1 and ETAA1 activator of ATR kinase (ETAA1), and in *S. cerevisiae*, there are at least three activators of Mec1: Dpb11, Ddc1, and Dna2 (Saldivar et al., 2017). Having multiple ATR^{Mec1} activators provides cells additional regulatory mechanisms to coordinate ATR^{Mec1} activation and signaling.

Mec1 coordinates DNA replication, DNA repair, and cell cycle progression by ensuring cells do not enter mitosis with damaged or incompletely replicated DNA. Like ATR, Mec1 is essential for cellular viability; however, Mec1 loss can be compensated for by deletion of the ribonucleotide reductase inhibitor Sml1 (Lanz et al., 2019). Mec1 is activated in response to

DNA damage in the G1, S, and G2 phases of the cell cycle, and signals through its downstream effector kinase Rad53 to slow cell cycle progression. Although Mec1-dependent Rad53 phosphorylation occurs in multiple cell cycle stages, this process is regulated differently in each stage. In response to genotoxic stress in G1, Mec1 activation is solely Ddc1 dependent (Kumar and Burgers, 2013; Navadgi-Patil and Burgers, 2009), but in G2, Mec1 activation of the G2/M checkpoint depends on both Ddc1 and Dpb11 (Navadgi-Patil and Burgers, 2009; Navadgi-Patil et al., 2011). During S-phase, Dpb11, Ddc1, and Dna2 all activate Mec1 to stimulate the checkpoint, and checkpoint signaling is only eliminated when all three activators are lost (Kumar and Burgers, 2013) (Fig 1.10). Dpb11 may be the most important S-phase specific Mec1 activator however, as overexpression of Dpb11, but not Ddc1, can rescue the hydroxyurea (HU) sensitivity of a Ddc2 mutant strain that does not support damage-dependent checkpoint signaling (Mordes et al., 2008b). Dpb11-dependent Mec1 activation is also CDK-dependent, and therefore only occurs in S and G2 phase (Pfander and Diffley, 2011).

Mec1 activation is regulated differently throughout the cell cycle in response to DNA damage, but Mec1 activation is also differentially regulated in S-phase between normal and stressed conditions. Large-scale phosphoproteomic experiments revealed that while most Mec1 phosphorylation events in response to DNA damage are also Rad53-dependent, during normal DNA replication, most Mec1 phosphorylation events are Rad53-independent. Furthermore, these experiments showed that Mec1 activation during unperturbed DNA replication is Dna2 and Ddc1 dependent and likely reflects Mec1 activation on the lagging strand at normal replication forks (de Oliveira et al., 2015) (Fig 1.10).

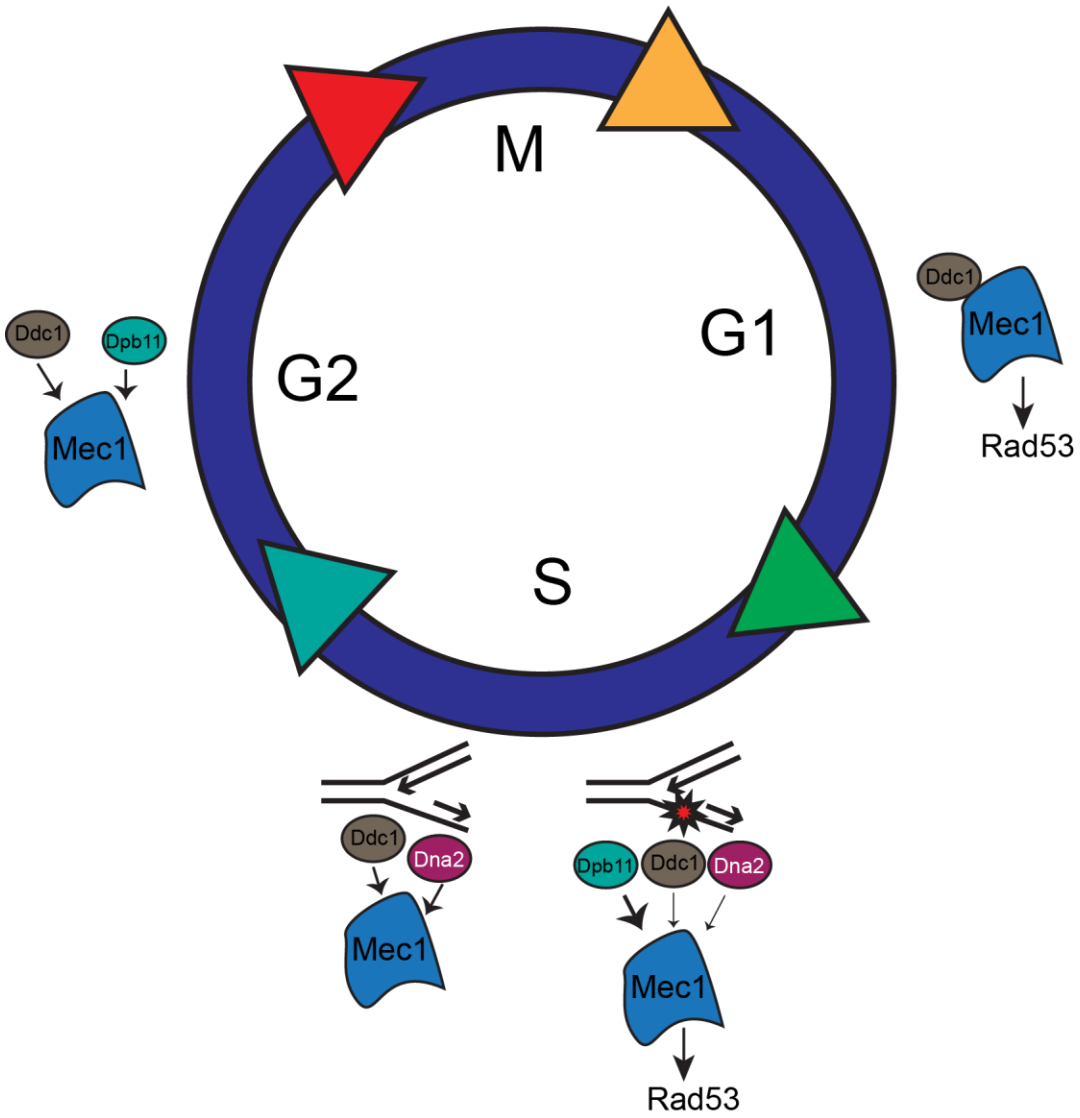

Figure 1.10 Cell cycle regulation of Mec1 activation. Mec1 activation is differentially regulated in G1, S, and G2 phase. Mec1 activation in G1 is solely Ddc1 dependent, and activation in G2 depends on both Ddc1 and Dpb11. During S-phase, Mec1 activation is regulated differently during normal replication than during replication stress. In unperturbed conditions, Mec1 activation is Ddc1 and Dna2 dependent and many Mec1-dependent phosphorylation events occur independently of Rad53. In response to replication stress, Mec1 activation is dependent on Dpb11, Ddc1, and Dna2, although Dpb11 is likely the primary activator, and most Mec1-dependent phosphorylation events are also Rad53-dependent.

Thus, normal versus stressed DNA replication regulates Mec1 activation and signaling differently.

ATR activation by TOPBP1 and ETAA1 is differentially regulated by cell cycle phase and by normal or stressed conditions. In response to exogenously induced replication stress, TOPBP1 is the predominant ATR activator (Bass and Cortez, 2019; Saldivar et al., 2018) (Fig 1.11). Quantitative phosphoproteomics revealed more DNA damage-dependent phosphorylation events are TOPBP1-dependent than ETAA1-dependent in response to replication stress (Bass and Cortez, 2019). Additionally, ATR-dependent γH2AX induction in response to replication stress is almost entirely TOPBP1-dependent (Saldivar et al., 2018). Replication stress-induced CHK1 phosphorylation is not ETAA1-dependent (Bass and Cortez, 2019; Bass et al., 2016; Haahr et al., 2016; Lee et al., 2016), and replication stress-induced MCM2 phosphorylation is TOPBP1-dependent and not affected by ETAA1 loss (Bass et al., 2016).

ETAA1 is the primary ATR activator during unperturbed DNA replication and regulates cell cycle transitions in the absence of exogenous stress (Fig 1.11). ATR-dependent γH2AX induction is ETAA1-dependent during normal DNA replication (Saldivar et al., 2018), and ETAA1-dependent ATR activation during unperturbed S phase is required for normal fork progression, suppression of origin firing (Haahr et al., 2016), and also suppresses the formation of mitotic chromosomal abnormalities (Achuthankutty et al., 2019). One study reported that ETAA1-dependent ATR activation is required for basal CHK1 activity and stability during S phase (Michelena et al., 2019), and while basal CHK1 activity may be ETAA1-dependent, no other groups have reported decreased CHK1 stability in the absence of ETAA1 (Bass et al., 2016; Haahr et al., 2016; Lee et al., 2016). The ATR-dependent mitotic checkpoint is also

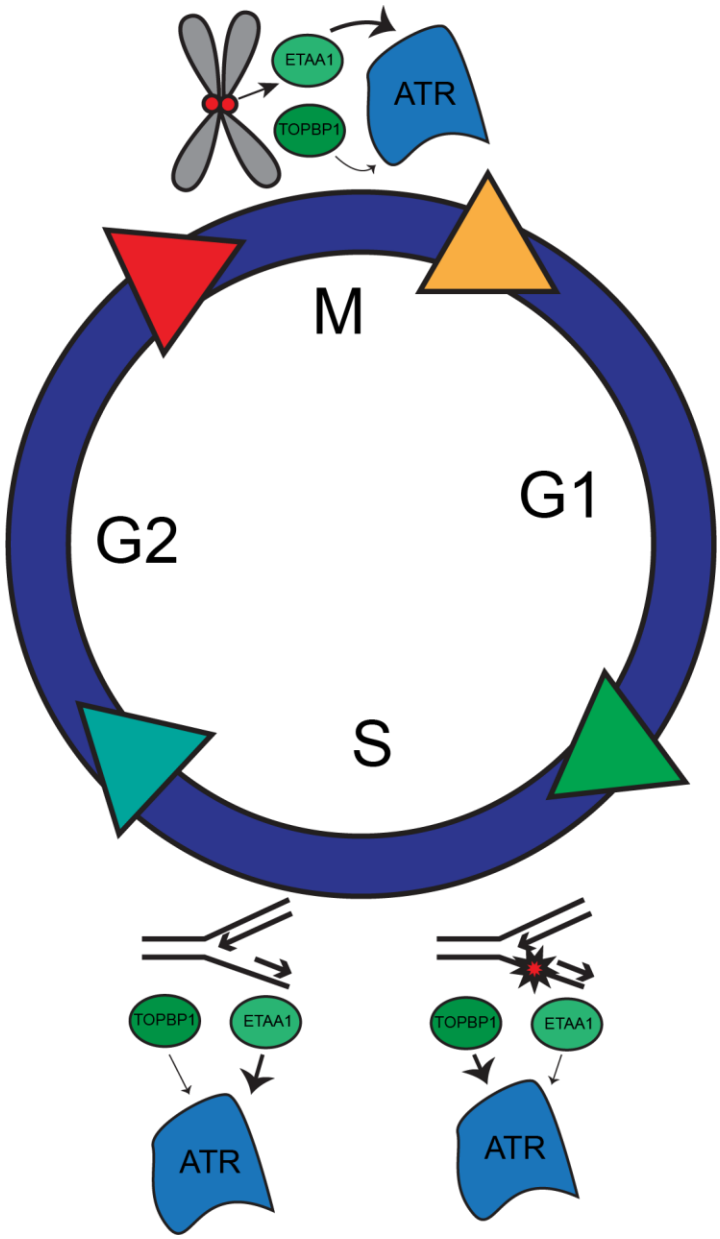

Figure 1.11 Cell cycle regulation of ATR activation. ATR activation is differentially regulated between normal DNA replication and conditions of replication stress. During normal replication, ATR activation is primarily ETAA1-dependent, but in response to replication stress, ATR activation is primarily TOPBP1-dependent. During mitosis, ATR-dependent Aurora B phosphorylation occurs in an ETAA1-dependent manner.

ETAA1-dependent. ETAA1 loss in mitosis impairs Aurora B phosphorylation, causes chromosomal alignment defects, and disrupts the SAC (Bass and Cortez, 2019).

Components required for ATR activation

ATR activation requires not just an ATR activating protein, but several other proteins that accumulate at sites of DNA replication stress. ATR is recruited to RPA-coated ssDNA through a direct interaction between ATRIP and RPA (Ball et al., 2007; Zou and Elledge, 2003), and the ATRIP-RPA interaction is mediated by ZFP161 (Kim et al., 2019). Simultaneously, the RAD17-replication factor C (RFC) 2-5 clamp loader loads the RAD9-RAD1-HUS1 (9-1-1) checkpoint clamp at 5' ssDNA-dsDNA junctions adjacent to RPA-coated ssDNA (Bermudez et al., 2003; Ellison and Stillman, 2003; Zou et al., 2003). TOPBP1 recruitment occurs via its interaction with the phosphorylated C-terminal tail of RAD9 (Delacroix et al., 2007; Rappas et al., 2011) and an interaction with the MRN complex (Duursma et al., 2013), which is also recruited to 5' ssDNA-dsDNA junctions. These interactions, in addition to an interaction with RAD9-RAD1-HUS1 interacting nuclear orphan (RHINO), are required for TOPBP1 to stimulate ATR kinase activity (Cotta-Ramusino et al., 2011) (Fig 1.12A).

5' ssDNA-dsDNA junctions are likely generated at stalled replication forks through multiple mechanisms. Replication fork stalling causes helicase-polymerase uncoupling which generates ssDNA ahead of the fork (Byun et al., 2005). While 5' ssDNA-dsDNA junctions are naturally formed on the lagging strand during DNA replication, upon fork stalling, continued primer synthesis ahead of the fork by DNA polymerase α (Pol α) can generate 5' junctions on the leading strand to recruit 9-1-1 and TOPBP1 (Fig 1.12B). Indeed, Pol α activity at stalled forks contributes to checkpoint activation (Byun et al., 2005; Van et al., 2010) and Pol α may also be important for 9-1-1 loading (Yan and Michael, 2009). Fork reversal could also generate 5'

ssDNA-dsDNA junctions at stalled forks. If the nascent leading strand is longer than the nascent lagging strand, fork reversal would generate the appropriate structure to support TOPBP1-dependent ATR activation. If the nascent lagging strand is longer, 5'-3' resection by nucleases would be required to generate the appropriate structure (Saldivar et al., 2017) (Fig 1.12C). Consistent with this model, a previous study found that depletion of DNA2, which mediates 5'-3' resection, disrupts ATR signaling (Thangavel et al., 2015).

In contrast to TOPBP1, ETAA1 is recruited to replication forks through a direct interaction with RPA (Bass et al., 2016; Haahr et al., 2016; Lee et al., 2016) (Fig 1.12A). The ETAA1-RPA interaction promotes ETAA1-dependent ATR activation two ways. First, it co-localizes ETAA1 with ATR-ATRIP, and second, the ETAA1-RPA interaction stimulates ATR activation (Lyu et al., 2019).

5' ssDNA-dsDNA junctions are the canonical ATR activating structure, but in recent years, R-loops have emerged as another prominent ATR activating structure (Crossley et al., 2019). R-loops are formed when newly transcribed RNA hybridizes with complementary DNA to generate an RNA-DNA hybrid and a displaced strand of ssDNA (Fig 1.12D). In mitosis, R-loop formation at centromeres recruits and activates ATR to regulate chromosome segregation (Kabeche et al., 2018). During S-phase, R-loops formed in response to exogenous replication stress activate ATR (Hamperl et al., 2017; Matos et al., 2020). In addition, mutations in splicing factors that cause increased R-loops also activate ATR (Chen et al., 2018). ATR signaling in response to R-loop formation promotes R-loop resolution likely via multiple mechanisms, but one such mechanism includes regulation of DDX19. ATR-dependent DDX19 nuclear translocation mediates DDX19-dependent R-loop unwinding, which relieves replication-

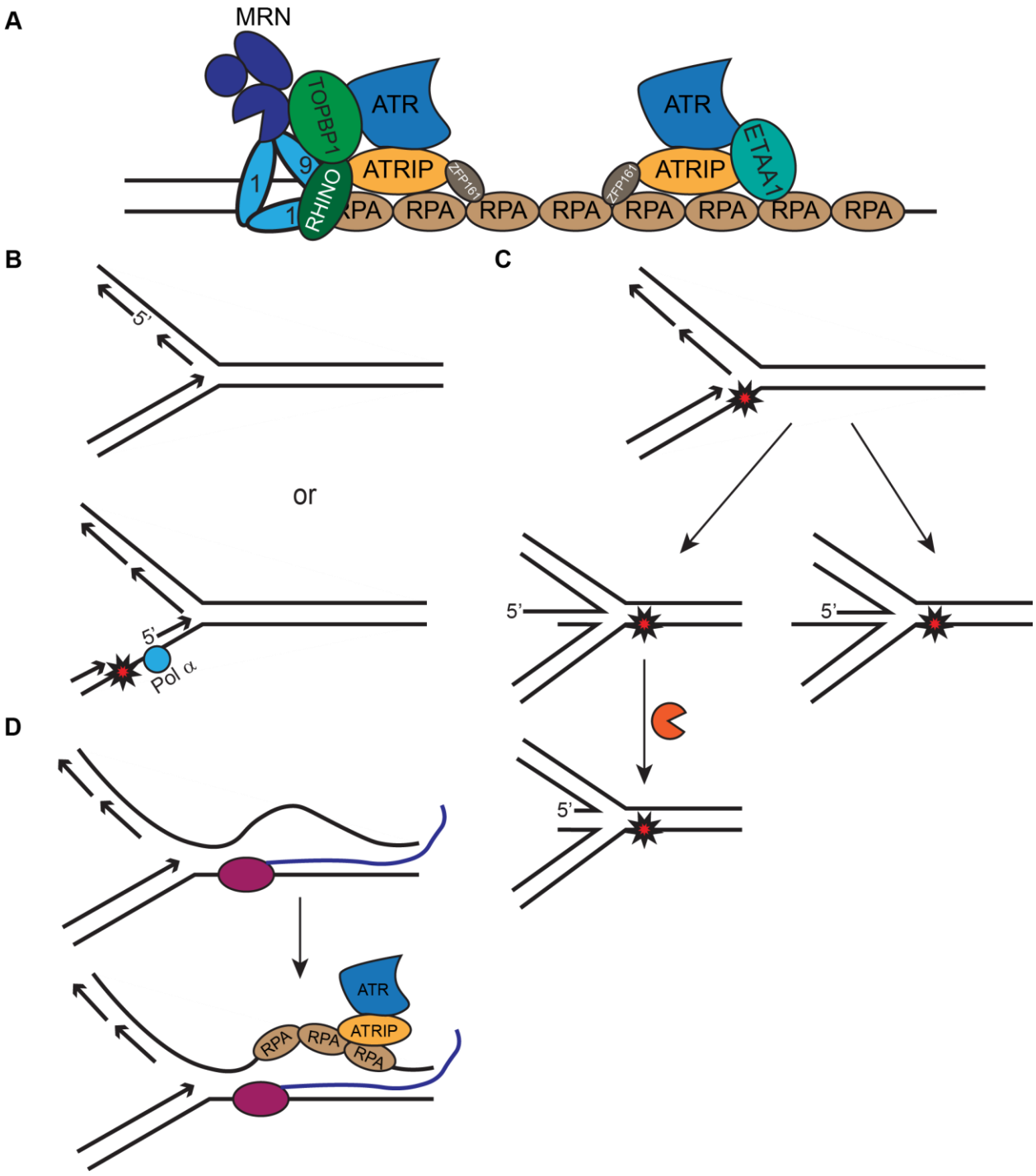

Figure 1.12 Components of ATR signaling pathway. A) Different proteins are required for TOPBP1-dependent ATR activation than for ETAA1-dependent ATR activation. TOPBP1-dependent activation occurs at 5' ssDNA-dsDNA junctions. ATR-ATRIP binds to RPA-coated ssDNA and simultaneously, the 9-1-1 complex is loaded at the 5' ssDNA-dsDNA junction by the RAD17-RFC2-5 clamp loader. The ATRIP-RPA interaction is mediated by ZFP161. TOPBP1 recruitment occurs by TOPBP1 binding to the phosphorylated C-terminal tail of RAD9 and

through an interaction with MRN. The interactions of TOPBP1 with RAD9, MRN, and RHINO are all required for TOPBP1 to activate ATR. In contrast, ETAA1 is recruited to RPA-coated ssDNA through a direct interaction with RPA. **B-C)** 5' ssDNA-dsDNA junctions can be generated at replication forks in multiple ways. **B)** 5' junctions normally form on the lagging strand during unperturbed replication. In response to replication stress, a 5' junction can be generated on the leading strand by Pol α-dependent repriming ahead of the stalled fork. **C)** Fork reversal is a common mechanism of fork stabilization. Upon fork reversal, if the nascent leading strand is longer than the nascent lagging strand, an appropriate 5' junction is generated. If the opposite occurs, 5'-3' resection of the lagging strand would generate the necessary 5' junction. **D)** Conflicts between replication and transcription machineries can generate R-loops, a structure formed when nascent RNA (colored blue) hybridizes to the template DNA causing displacement of the non-template DNA strand. ssDNA generated by R-loops is bound by RPA, which recruits ATR-ATRIP.

transcription conflicts (Hodroj et al., 2017). Data from recent genetic screens also indicates R-loop resolution may be a critical function of ATR signaling. Indeed, loss of RNASEH2, which resolves R-loops, confers ATR inhibitor (ATRi) hypersensitivity in multiple cell types (Hustedt et al., 2019; Wang et al., 2019).

Mechanism of ATR^{Mec1} activation

The Mec1 activators activate Mec1 in different cell cycle stages, but the mechanism by which they activate Mec1 appears to be the same. Each of the Mec1 activators contains an experimentally defined Mec1 activation domain (MAD) that is predicted to be intrinsically disordered (Wanrooij et al., 2016). Furthermore, each MAD contains two essential aromatic amino acids that are required for Mec1 activation *in vitro* and in cells (Kumar and Burgers, 2013; Navadgi-Patil and Burgers, 2009; Navadgi-Patil et al., 2011; Wanrooij et al., 2016) (Fig 1.13A). The MADs are predicted to bind and activate Mec1 via a two-step process where initial Mec1 binding is mediated by the two aromatic residues and then subsequent binding by adjacent residues stimulates full Mec1 activation (Wanrooij et al., 2016) (Fig 1.13B).

Prior to the work described in this thesis, less was known about the TOPBP1 and ETAA1 ATR activation domains (AADs), and the mechanism by which they activate ATR. Each activator contains an experimentally defined AAD (Fig 1.13A), but no structural information about the AADs is available. The AADs share no primary sequence similarity except for residues that immediately flank a conserved tryptophan in both domains. Mutation of this tryptophan in TOPBP1 and ETAA1 abrogates their interaction with ATR and impairs ATR activation *in vitro* and in cells (Bass et al., 2016; Haahr et al., 2016; Kumagai et al., 2006; Lee et al., 2016). Chapter III describes new discoveries made about the TOPBP1 and ETAA1 AADs and further

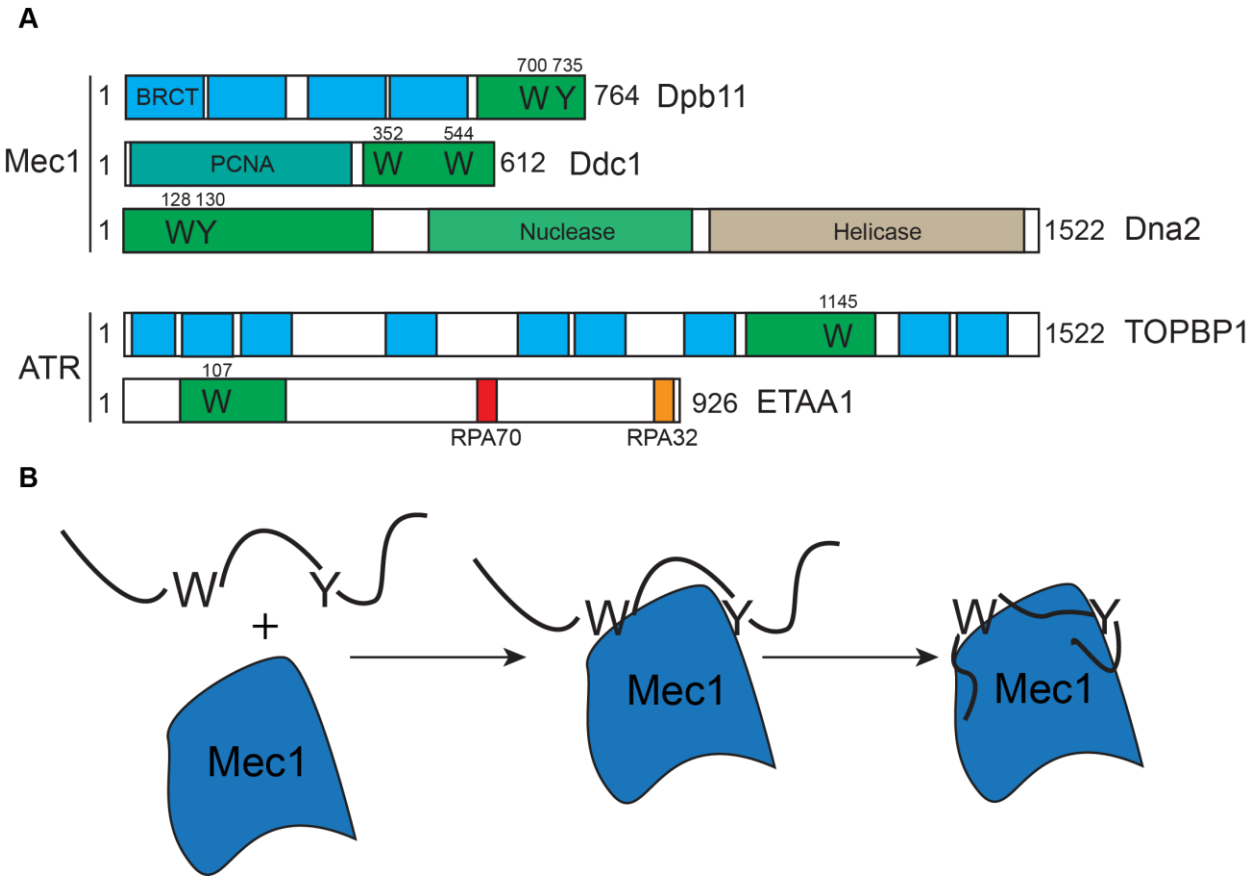

Figure 1.13 Mechanism of ATR^{Mec1} activation. A) Domain architecture of the Mec1 and ATR activators. The MADs and AADs are colored green and the location of the critical aromatic residues in each is denoted. The BRCT domains in Dpb11 and TOPBP1 are colored cyan. **B)** Proposed two-step activation mechanism of Mec1 by the MADs. Initial binding is mediated by the two critical aromatic residues, followed by binding of adjacent residues to stimulate full kinase activation.

delineates the mechanism by which they activate ATR. Specifically, the data in this chapter shows that both AADs contain predicted coiled-coil motifs that are required for ATR binding and activation. Chapter IV also examines the mechanism by which the AADs activate ATR, and describes how AAD dimerization is required for efficient ATR activation. In addition, Chapter IV also documents that ETAA1 forms oligomeric complexes in cells and that forced dimerization of an ETAA1 oligomerization-defective mutant restores ATR activation in ETAA1-deficient cells. Together, the results of Chapters III and IV are consistent with the hypothesis that TOPBP1 and ETAA1 activate ATR via the same biochemical mechanism.

Chapter V examines whether leading and lagging strand synthesis is coupled during DNA replication. The results indicate that when lagging strand synthesis is inhibited, leading strand replication continues, albeit at a reduced rate. Uncoupling of leading and lagging strand synthesis activates ATR to prevent replication fork collapse, but it does not induce robust replication checkpoint signaling. Thus, Chapter V more specifically defines the determinants of ATR-checkpoint signaling at stalled replication forks.

The DDR and cancer

One of the hallmarks of cancer is genome instability (Hanahan and Weinberg, 2011). Genomic instability in cancer cells often increases replication stress, and as such, causes an increased dependence on ATR signaling for survival. Both ATR inhibitors (ATRi) and CHK inhibitors (CHK1i) have been developed and their efficacy is currently being assessed in preclinical and clinical studies (Qiu et al., 2018), both as single agents and in combination with more traditional genotoxic chemotherapies (Forment and O'Connor, 2018). ATR and CHK1 inhibition may be a particularly effective strategy for treating cancer cells with non-functional p53. TP53 (gene encoding p53) is the most commonly mutated gene in cancer, and cells lacking

p53 have a defective G1/S checkpoint, and thus, are more dependent on the ATR controlled intra-S and G2/M checkpoints for survival. Indeed, ATR inhibition in a p53 deficient chronic lymphocytic leukemia (CLL) cell line causes increased cell death due to mitotic catastrophe, and in a p53 deficient xenograft model, ATR inhibition reduces tumor load (Kwok et al., 2016). ATM deficient tumors also have a defective G1/S checkpoint, and similar to p53 deficient tumors, exhibit increased sensitivity to ATR inhibitors in *in vitro* and in vivo models (Kwok et al., 2015; Menezes et al., 2015; Min et al., 2017; Perkhofer et al., 2017; Schmitt et al., 2017).

Overexpression of certain oncogenes can also cause increased reliance on ATR for cancer cell survival. MYC and CYCLIN E overexpression cause increased replication stress due to de-regulation of origin firing and aberrant conflicts between the replication and transcriptional machinery (Macheret and Halazonetis, 2015). Not surprisingly, cells overexpressing CYCLIN E are hypersensitive to ATR inhibition (Luis et al., 2011), and CHK1 inhibition has proved efficacious in killing MYC overexpressing cells *in vitro* and in vivo (Ferrao et al., 2012; Matilde et al., 2011; Sen et al., 2017).

More recently, combining DNA damaging chemotherapy with immunotherapy has emerged as a promising therapeutic strategy for treating cancer (Brown et al., 2018). Cancer cells with DNA repair defects generally have a high mutational burden, which renders them more susceptible to immune checkpoint inhibitors (Berti et al., 2020). Consistent with this notion, a combinatorial platinum chemotherapy and anti-PD-1 treatment regimen increases survival in patients with non-small-cell lung cancer (Gandhi et al., 2018). Furthermore, irradiation combined with ATR inhibition enhances innate immune signaling via disruption of cell cycle checkpoints to promote increased anti-tumor immune responses (Chen et al., 2020). ATR signaling also upregulates PD-L1 expression (Sato et al., 2017); therefore, ATR inhibition may increase

antitumor immunity in two ways: first by causing increased inflammatory signaling through abrogation of cell cycle checkpoints and second, by increasing proliferation and activation of effector T cells through reduced PD-L1 expression. Together, these mechanisms are likely to promote enhanced immune cell infiltration in tumors.

Continued research on mechanisms of ATR activation and signaling should contribute to increased efficacy of ATR inhibitors in the cancer clinic. Although several synthetic lethal interactions with ATR have been established, a more comprehensive understanding of TOPBP1- and ETAA1-dependent ATR signaling and mechanisms of TOPBP1- and ETAA1-dependent ATR activation will prove useful in determining which patients should be treated with ATR inhibitors. Developing ATR inhibitors that specifically inhibit TOPBP1- or ETAA1-dependent signaling may also be a way to more specifically inhibit ATR in certain genetic contexts.

CHAPTER II

MATERIALS AND METHODS

Table 2.1 Antibodies. Information about antibodies used for immunoblotting (IB) and immunofluorescence (IF).

Antibody	Dilution	Species	Company	Catalog number	Location	Molecular weight (KDa)	Use
ATR (N-19)	1:1000	Goat	Santa Cruz	SC-1887	Box 1 A3	301	IB
ATRIP-N	1:1000	Rabbit	Cortez		Box 2 A2	85	IB
BrdU	1:150	Rat	Abcam	6326			IF
CHK1	1:1000	Mouse	Santa Cruz	SC-8408	Box 3 D3	55	IB
CHK1 pS317	1:1000	Rabbit	Cell Signaling	2344	Box 4 A1	55	IB
CHK1 pS345	1:1000	Rabbit	Cell Signaling	2348	Box 9 C8	55	IB
ETAA1	1:1000	Rabbit	Cortez (Covance)		Box 10 D9	103	IB
Anti-Flag	1:1000	Rabbit	Sigma	F7425	Box 9 E8		IB
Flag M2	IB: 1:1000 IF: 1:200	Mouse	Sigma	F3165			IB IF
GST	1:20,000	Goat	Amersham	27457701	Box 1 I2	27	IB
HA	1:2000	Rat	Roche	11867423001			IB
HA.11	1:1000	Mouse	Biolegend	901501	Box 10 G5		IB
γH2AX	1:200	Rabbit	Cell Signaling	2577	Box 4 F4	14	IF
MCM2 pS108	1:1000	Rabbit	Cortez	92232311	Box 1 H6	102	IF
RAD9	1:2000	Rabbit	Bethyl	A300-890A	Box 6 G2	42	IB
RPA32	1:1000	Mouse	Abcam	2175	Box 1 B9	32	IB
RPA70	1:200	Rabbit	Cell Signaling	2267	Box 4 G5	70	IF
RPA 32 pS4/S8	1:1000	Rabbit	Bethyl	A300-245A	Box 6 A4	32	IB
RPA32 pS33	1:1000	Rabbit	Bethyl	A300-246A	Box 10 E9	32	IB
TOPBP1	1:1000	Rabbit	Bethyl	A300-111A	Box 3 E3	170	IB

Table 2.2 Cell lines. Cell line growth mediums and transfection reagents

Cell line	Growth media	Plasmid transfection	siRNA transfection
HCT116	McCoy's + 7.5% FBS	PEI	
HEK293T	DMEM + 7.5% FBS	PEI	
HeLa	DMEM + 7.5% FBS	PEI	RNAi max
RPE-hTERT	DMEM F12 + 7.5% FBS		
U2OS	DMEM + 7.5% FBS	PEI	RNAi max

Bioinformatic analysis

ETAA1 and TOPBP1 predicted disorder was determined using IUPred2A (Meszaros et al., 2018) and coiled coil predictions were determined using Paircoil2 (McDonnell et al., 2006). ETAA1 and TOPBP1 predicted coiled coil sequence alignments were assembled using ClustalOmega.

GST protein purification

GST-tagged AADs were purified from ArcticExpress *Escherichia coli* (Agilent Technologies). Bacteria were resuspended in NET Buffer (25 mM Tris pH 8, 50 mM NaCl, 0.1 mM EDTA, 5% glycerol, 1 mM DTT, 5 µg/mL aprotinin, 5 µg/mL leupeptin) and sonicated three times (Setting 4, Duty cycle 90, 20 seconds) with one minute of cooling between each sonication. Triton X-100 was then added to a final concentration of 1%, and lysates were incubated on ice for 30 minutes. After centrifugation at 5,000 x g for 10 minutes, cleared lysates were incubated with glutathione sepharose beads (GE Healthcare) for 2.5 hours at 4°C. Beads were then washed three times with NET Buffer + 1% Triton X-100. Bound proteins were eluted using elution buffer (75 mM Tris pH 8, 15 mM glutathione, 5 µg/mL leupeptin). For AADs used in gel-filtration chromatography experiments and kinase assays without a GST tag, GST was

removed by incubating beads with cleavage buffer (50 mM Tris pH 7, 150 mM NaCl, 1 mM EDTA, 1 mM DTT) containing Prescission Protease (GE Healthcare) overnight at 4°C. Purified proteins were dialyzed (20 mM HEPES-KOH pH 7.5, 50 mM NaCl, 1 mM DTT) twice, once for 2 hours, and then again overnight.

His protein purification

His-MBP-AADs and His-FKBP F36V-AADs were purified from ArcticExpress *Escherichia coli*. Bacteria were resuspended in native purification buffer (50 mM NaH_2PO_4, 500 mM NaCl, 10 mM imidazole, 5 μg/mL aprotinin, 5 μg/mL leupeptin, 4 mm DTT) containing lysozyme and incubated on ice for 30 minutes. Cells were sonicated six times (Setting 4, Duty cycle 90, 10 seconds) with ten seconds of cooling between each sonication, and lysates were cleared by centrifugation at 3,000 x g for 15 minutes. Cleared lysates were incubated with Ni-NTA agarose beads (Invitrogen) for 3 hours at 4°C. Beads were washed four times with native wash buffer (50 mM NaH_2PO_4, 500 mM NaCl, 20 mM imidazole, 5 μg/mL aprotinin, 5 μg/mL leupeptin, 4 mm DTT). Bound proteins were eluted by incubation with native elution buffer (50 mM NaH_2PO_4, 500 mM NaCl, 250 mM imidazole, 5 μg/mL aprotinin, 5 μg/mL leupeptin, 4 mm DTT), and dialyzed (20 mM HEPES-KOH pH 7.5, 50 mM NaCl, 1 mM DTT) for 2 hours, and then again overnight at 4°C.

Nuclear Extract Preparation

HEK293T cells were resuspended in a volume of hypotonic buffer (10 mM HEPES pH 7.9, 1.5 mM MgCl2, 10 mM KCl, 0.5 mM DTT) five times the packed cell volume and then centrifuged at 2,553 x g for 5 minutes at 4°C. Cells were resuspended in hypotonic buffer three times the packed cell volume and incubated on ice for 10 minutes. Cells were transferred to a

glass Dounce homogenizer and homogenized with 10 slow strokes using a B type pestle. Cells were then transferred to microcentrifuge tubes and centrifuged at 3,300 x g for 15 minutes at 4°C. After removal of supernatant, cells were resuspended in a volume of low-salt buffer (20 mM HEPES pH 7.9, 1.5 mM MgCl2, 20 mM KCl, 25% glycerol, 0.5 mM DTT) equal to 1/3 the packed nuclear volume. High-salt buffer (20 mM HEPES pH 7.9, 1.5 mM MgCl2, 1.2 M KCl, 25% glycerol, 0.5 mM DTT) equal to 1/3 the packed nuclear volume was then added dropwise to tubes. Resuspended nuclei were incubated at 4°C for 30 minutes on a moving rotator, then centrifuged at 21,130 x g for 30 minutes at 4°C. Supernatant (nuclear extract) was transferred to 3,500 molecular weight cutoff dialysis tubing and dialyzed (20 mM HEPES pH 7.9, 100 mM KCl, 20% glycerol, 0.5 mM DTT) for 1 hour at 4°C, and then centrifuged at 21,130 x g for 20 minutes at 4°C to obtain the final nuclear extract (supernatant).

For kinase and binding assays, nuclear extracts were prepared differently. HEK293T cells (from two, 15 cm plates) were resuspended in 1 mL of hypotonic buffer (20 mM HEPES pH 7.9, 1.5 mM MgCl2, 10 mM KCl, 0.5 mM DTT) and then centrifuged at 2,500 x g for 3 minutes at 4°C. Cells were resuspended in 400 µl of hypotonic buffer and incubated on ice for 10 minutes. Cells were transferred to Dounce homogenizer and homogenized with 15 slow strokes using a B type pestle. Cells were transferred to microcentrifuge tubes and centrifuged at 3,300 x g for 6 minutes at 4°C. Supernatant was discarded and 250 µl of high-salt buffer (20 mM HEPES pH 7.9, 25% glycerol, 1.5 mM MgCl2, 350 mM NaCl, 0.5 mM DTT, 1 mM NaF, 1 mM sodium orthovanadate, 10 mM β-glycerol phosphate, 5 µg/mL aprotinin, 5 µg/mL leupeptin) was added to nuclei slowly with periodic mixing. Resuspended nuclei were then incubated on a moving rotator for 30 minutes at 4°C and centrifuged at 21,130 x g for 10 minutes at 4°C. 200 µl of no-salt buffer (20 mM HEPES pH 7.9, 20% glycerol, 0.1% Tween 20) was added to supernatant

prior to another 5-minute centrifugation at 21,130 x g for 5 minutes at 4°C. Remaining supernatant (nuclear extract) was collected and used for HA immunoprecipitation.

Whole cell lysis and immunoblotting

Harvested cells were resuspended in NP-40 lysis buffer (50 mM Tris pH 7.5, 150 mM NaCl, 10% glycerol, 0.5% NP-40, 5 μg/mL aprotinin, 5μg/mL leupeptin, 1 mM sodium orthovanadate, 10 mM β-glyercol phosphate, 1 mM NaF, 1 mM DTT, 1 mM $MgCl_2$, 1 μL/mL Pierce Universal nuclease for cell lysis) and incubated on ice for 30 minutes. Cells were centrifuged at 21,130 x g for 30 minutes at 4°C. The supernatant (whole cell lysate) was retained, while the pellet was discarded. Appropriate volumes of 2x or 6x SDS sample buffer were added to lysates before incubation at 95°C for 3-5 minutes. Equal amounts of lysates were separated by SDS-PAGE and proteins were detected by immunoblotting. In some experiments, 0.5% NP-40 was substituted with 0.75% CHAPS.

Kinase assays

Flag-ATR – HA-ATRIP complexes were purified from HEK293T cell nuclear extracts using monoclonal anti-HA agarose beads (Sigma-Aldrich). Beads were washed three times with TGN buffer (50 mM Tris pH 7.5, 150 mM NaCl, 10% glycerol, 1% Tween20, 0.5 mM DTT, 1 mM NaF, 1 mM sodium orthovanadate, 10 mM β-glycerol phosphate, 5 μg/mL aprotinin, 5 μg/mL leupeptin). Beads were then washed once in TGN buffer containing 500 mM LiCl and twice with kinase buffer (10 mM HEPES-KOH pH 7.5, 50 mM NaCl, 10 mM $MgCl_2$, 10 mM $MnCl_2$, 1 mM DTT, 50 mM β-glycerol phosphate). Kinase reactions containing purified ATR-ATRIP, substrate (GST-MCM2 79-138 or MCM2 79-138), [γ-^{32}P]ATP, and GST, GST-AADs, MBP-AADs, untagged AADs, or FKBP F36V-AADs were incubated for 20 minutes at 30°C and

stopped upon addition of 2X SDS sample buffer. Reaction products were separated by SDS-PAGE and detected by coomassie staining or immunoblotting. Substrate phosphorylation was detected and quantified by phosphoimaging. In experiments performed with FKBP F36V-AADs, the FKBP F36V-AADs were incubated with DMSO or 5 μM AP20187 for 1 hour at room temperature prior to beginning kinase reactions. Kinase reactions also contained either DMSO or 5 μM AP20187.

Gel-filtration chromatography

Proteins were loaded onto a Superdex^{TM} 200 Increase 10/300 GL column (GE Healthcare) previously equilibrated with buffer (20 mM HEPES-KOH pH 7.5, 50 mM NaCl, 10 mM DTT) and eluted at 0.25 mL min^{-1}. 0.25 mL fractions were collected and equal volumes of fractions corresponding to peaks were separated by SDS-PAGE and visualized by coomassie staining. Purified FKBP F36V-AADs were incubated with DMSO or 5 μM AP20187 for 1 hour at room temperature prior to loading onto column.

Co-immunoprecipitation from nuclear extracts

Equal amounts of HEK293T cell nuclear extracts expressing GFP-Flag or GFP-Flag AADs were incubated with EZview^{TM} Red Anti-Flag M2 affinity gel (Sigma-Aldrich) for 1-2 hours at 4°C. Beads were washed three times with dialysis buffer (20 mM HEPES-KOH pH 7.9, 100 mM KCl, 20% glycerol, 0.5 mM DTT) and once with flag elution buffer (10 mM HEPES-KOH pH 7.9, 300 mM KCl, 1.5 mM $MgCl_2$, 0.05% NP-40, 0.5 mM DTT). Bound proteins were eluted with flag elution buffer containing 0.3 mg/mL 3X FLAG peptide (Sigma-Aldrich), separated by SDS-PAGE, and detected by immunoblotting.

Co-immunoprecipitation from whole cell lysates

HEK293T cells were lysed in NP-40 lysis buffer (50 mM Tris pH 7.5, 150 mM NaCl, 10% glycerol, 0.5% NP-40, 5μg/mL aprotinin, 5 μg/mL leupeptin, 1 mM sodium orthovanadate, 10 mM β-glycerol phosphate, 1 mM NaF, 1 mM DTT) for 30 minutes on ice and cleared by centrifugation (21,130 x g, 30 minutes, 4°C). Supernatants were incubated with EZ View^{TM} Red Anti-Flag M2 affinity gel or monoclonal anti-HA agarose beads for 1-2 hours at 4°C. Beads were then washed three times with NP-40 lysis buffer and once with Flag elution buffer (10 mM HEPES-KOH pH 7.9, 300 mM KCl, 1.5 mM $MgCl_2$, 0.05% NP-40, 0.5 mM DTT). Proteins bound to EZ View^{TM} Red Anti-Flag affinity gel were eluted with Flag elution buffer containing 0.3 mg/mL 3x Flag peptide. Immunoprecipitated proteins were separated by SDS-PAGE and detected by immunoblotting. In some experiments, 0.5% NP-40 was substituted with 0.75% CHAPS. For experiments assessing inducible dimerization, cells were incubated with 100 nM AP20187 for 1 hour prior to harvesting, and lysis and elution buffers contained 4 μM AP20187.

Binding assays

GST-tagged proteins were purified as described above. After washes with NET Buffer + 1% Triton X-100, glutathione beads were incubated with equal amounts of HEK293T cell nuclear extracts (prepared as described above for kinase assays) expressing Flag-ATR – HA-ATRIP overnight at 4°C. Beads were washed three times with low-salt buffer (20 mM HEPES-KOH pH 7.9, 150 mM NaCl, 20% glycerol, 0.05% Tween20, 0.5 mM DTT). Bound proteins were eluted (75 mM Tris pH 8, 15 mM glutathione, 5 μg/mL leupeptin), separated by SDS-PAGE, and detected by coomassie staining or immunoblotting.

Immunofluorescence

U2OS or HeLa cells grown on glass coverslips were washed once with PBS, and then fixed in 3% paraformaldehyde/2% sucrose in PBS for 10 minutes at room temperature. Cells were washed three times with PBS, and then permeabilized with 0.5% Triton X-100 in PBS for 5 minutes at room temperature. Cells were then washed four times with PBS prior to blocking with 5% BSA in PBS for at least 15 minutes at room temperature. Cells were washed once with PBS and incubated with primary antibodies diluted in 1% BSA in PBS for 1 hour at room temperature. Cells were washed three times with PBS and incubated with secondary Alexa fluor antibodies diluted in 1% BSA in PBS for at least 20 minutes at room temperature in the dark. Finally, cells were washed three times with PBS and coverslips were mounted on slides with Prolong Gold antifade reagent containing DAPI. Images were obtained using a Nikon microscope and Flag, γH2AX, MCM2 pS108, and BrdU nuclear intensities were quantitated using Elements software.

Micronuclei assays

Cells were untreated or treated with 100 nM AP20187 for 24 hours. Cells were washed once with PBS and fixed with 3% paraformaldehyde/2% sucrose in PBS for 10 minutes at room temperature. Cells were washed three times with PBS, permeabilized with 0.5% Triton X-100 in PBS for 5 minutes at room temperature, washed four times with PBS, and stained with DAPI. Cells were imaged using a Nikon microscope and micronuclei were quantitated manually. All samples were blinded to the experimenter.

Clonogenic survival assays

U2OS, U2OS ΔETAA1, and U2OS ΔETAA1 cells complemented with FKBP F36V-mini-ETAA1 were plated, left untreated, treated with 1 mM HU +/- 100 nM AP20187, or treated with 5 nM CPT +/- 100 nM AP20187 for 24 hours. Following drug removal, cells were allowed to grow for 10 days before staining with methylene blue solution (48 % methanol, 2% methylene blue, 50% water). The number of colonies on each plate was quantitated manually and for each condition, percent viability was normalized to viability of the corresponding untreated control.

Lentivirus production

Day 1: Plate 4.5 x 10^6 HEK293T cells in 10 cm dishes

Day2: Transfect cells with 3 μg psPAX2, 1 μg pMD2.G, and 4 μg of pVT174, pVT179, or pVT185

Day 3: Aspirate media from plates, wash with PBS, and add 7 mL of media

Day 4: Remove media from plates and store at 4°C. Add another 7 mL of media

Day 5: Remove media from plates and combine with media from Day 4. Make 1 mL aliquots and store virus-containing media at -80°C

Lentiviral Infection

Day 1: Plate 2 x 10^5 U2OS ΔETAA1 #17 cells in 60 mm dishes

Day 2: Infect plates with 1 mL of virus-containing media. Leave one plate uninfected

Day 3: Expand cells from 60 mm dishes to 10 cm dishes with media containing 2 μg/mL puromycin

Day 5: Expand surviving cells into multiple 10 cm dishes without puromycin to harvest for immunoblotting, to freeze, and to continue passaging

Neutral comet assays

Neutral Comet assays were performed following the manufacturer's protocol (Trevigen). HeLa cells were synchronized overnight with 2 mM thymidine. Cells were washed once with PBS, incubated with fresh media for 1 hour, and then incubated with media containing no drugs, CD437, ATRi, or CD437+ATRi for 0.5 – 3 hours. Cells were harvested and resuspended in PBS. Cells in PBS were then combined with molten LMAgarose at a ratio of 1:10 and spread onto CometSlides. Slides were incubated at 4°C for 30 minutes in the dark, and then immersed in lysis solution overnight at 4°C in the dark. Slides were immersed in neutral electrophoresis buffer (100 mM Tris, 300 mM sodium acetate, pH 9) for 30 minutes at 4°C in the dark prior to electrophoresis (21 volts for 45 minutes). Slides were immersed in DNA precipitation solution (1 M NH_4AC in 95% ethanol) for 30 minutes at room temperature in the dark and then immersed in 70% ethanol for 30 minutes at room temperature in the dark. Slides were dried at 37°C in the dark before a 30-minute incubation with diluted SYBR Gold. Slides were rinsed with water and allowed to dry overnight at room temperature in the dark. Slides were imaged using a Nikon microscope and tail moments were quantitated using OpenComet software.

DNA Combing

HeLa cells were pulsed with 20 μM CldU, washed twice with HBSS, pulsed with 100 μM IdU, and washed twice with HBSS. Pulse times and absence or presence of drugs is indicated in individual experiments. Cells were harvested and resuspended in ice cold PBS. Cells were centrifuged at 150 x g for 5 minutes at 4°C. Cells were then resuspended in 45 μl of PBS, warmed to 50°C, and resuspended again by addition of 45 μl of buffer 2. Resuspended cells were transferred to plug molds and incubated at 4°C for at least 30 minutes. Solidified plugs were transferred to buffer 3 and incubated at 50°C overnight. Plugs were washed three times with 15

mL of buffer 4 (1x TE Buffer), transferred to 2 mL collection tubes containing 1 mL of buffer 7, and incubated at 68°C for 20 minutes. Collection tubes were then incubated at 42°C for 10 minutes prior to addition of 1.5 µl of β-agarase. Tubes were incubated at 42°C overnight. DNA solutions from collection tubes were gently poured into combing reservoirs containing 1.2 mL of buffer 7 and DNA was combed onto silanized coverslips using the FiberComb molecular combing system (Genomic Vision). Coverslips were incubated at 65°C for 2 hours, and then incubated at -20°C overnight. Coverslips were warmed to room temperature prior to incubation with 1 M NaCl + 0.5 M NaOH for 8 minutes. Coverslips were washed three times with PBS, incubated with 70% ethanol for 5 minutes, with 90% ethanol for 5 minutes, and with 100% ethanol for 5 minutes. Coverslips dried at room temperature and then were washed once with PBS. Coverslips were blocked with 10% goat serum + 0.1% Triton X-100 in PBS for 1 hour and washed once with PBS. Coverslips were incubated with primary antibodies diluted in 10% goat serum + 0.1% Triton X-100 in PBS for 1 hour, washed three times with PBS, incubated with Alexa fluor secondary antibodies diluted in 10% goat serum + 0.1% Triton X-100 for 30 minutes, washed three times with PBS, and then mounted on slides with Prolong Gold antifade reagent without DAPI. Images were obtained using a Nikon microscope and analyses were performed manually.

CHAPTER III

COMMON MOTIFS IN ETAA1 AND TOPBP1 REQUIRED FOR ATR KINASE ACTIVATION

This chapter is adapted from [Common motifs in ETAA1 and TOPBP1 required for ATR kinase activation] published in [Journal of Biological Chemistry 294(21): 8395-8402] and has been reproduced with the permission of the publisher and my co-author [David Cortez]

Introduction

Cells are constantly exposed to exogenous and endogenous sources of DNA damage that cause thousands of DNA lesions in each cell every day (Ciccia and Elledge, 2010). These lesions can interfere with processes such as DNA replication and transcription, and must be accurately repaired to preserve genome stability (Zeman and Cimprich, 2014). The recognition and repair of DNA lesions is coordinated by a series of signaling pathways collectively known as the DNA damage response (DDR). The DDR also regulates cell cycle progression, cellular senescence, and apoptosis (Ciccia and Elledge, 2010). The phosphatidylinositol 3-kinase related protein kinases (PIKKs) ATM, ATR, and DNA-PK, activate the DDR (Blackford and Jackson, 2017; Ciccia and Elledge, 2010). ATM and DNA-PK signaling is initiated primarily in response to DNA double-strand breaks (DSBs), while ATR is activated at lesions containing replication protein A (RPA)-coated ssDNA (Blackford and Jackson, 2017; Saldivar et al., 2017).

ATR is recruited to sites of RPA-coated ssDNA through its obligate binding partner ATRIP, which directly binds RPA (Cortez et al., 2001; Zou and Elledge, 2003). However, recruitment to RPA-coated ssDNA alone is not sufficient to trigger ATR activation. Several other proteins, including at least one ATR activating protein, must also be recruited to trigger

maximal ATR signaling. One ATR activating protein is TOPBP1 (Kumagai et al., 2006). TOPBP1 is recruited to DNA lesions that possess a ssDNA-dsDNA 5' junction through its interaction with the MRE11/RAD50/NBS1 (MRN) complex and the phosphorylated C-terminal tail of RAD9, a component of the RAD9-RAD1-HUS1 (9-1-1) checkpoint clamp (Delacroix et al., 2007; Duursma et al., 2013; Rappas et al., 2011). TOPBP1 also interacts with RHINO at DNA damage sites (Cotta-Ramusino et al., 2011; Lindsey-Boltz et al., 2015). All these interactions are required for TOPBP1 to fully stimulate ATR kinase activity, which is specifically mediated by the TOPBP1 ATR activation domain (AAD) (Kumagai et al., 2006).

The other known ATR activator is ETAA1. Unlike TOPBP1, ETAA1 is recruited to RPA-coated ssDNA through a direct interaction with RPA, where it then activates ATR through its AAD (Bass et al., 2016; Haahr et al., 2016; Lee et al., 2016). ETAA1 is especially important to activate ATR to regulate cell cycle transitions even in the absence of DNA damage or replication stress (Bass and Cortez, 2019; Saldivar et al., 2018).

The ATR and ATRIP orthologues in *Saccharomyces cerevisiae* are Mec1 and Ddc2 respectively. Like ATR-ATRIP, Mec1-Ddc2 localizes to DNA lesions containing RPA-coated ssDNA via a direct interaction between RPA and Ddc2 (Ball et al., 2007). Mec1 kinase activity can then be stimulated by Dpb11 (TOPBP1 orthologue), Ddc1 (human RAD9 orthologue), or the multifunctional nuclease/helicase Dna2 (Kumar and Burgers, 2013; Mordes et al., 2008b; Navadgi-Patil and Burgers, 2008, 2009). The biochemical mechanism by which these proteins activate Mec1 appears to be the same. Each Mec1 activation domain (MAD) is predicted to be intrinsically disordered and contains two essential aromatic amino acids that when mutated, abrogate Mec1 activation both *in vitro* and *in vivo* (Kumar and Burgers, 2013; Navadgi-Patil and Burgers, 2009; Navadgi-Patil et al., 2011). Additionally, it has been proposed that the Mec1

activators bind Mec1 via a two-step binding mechanism whereby the two aromatic residues bind first followed by binding of the surrounding residues to stimulate full kinase activation (Wanrooij et al., 2016).

In contrast to the Mec1 activators, how TOPBP1 and ETAA1 activate ATR is less well understood. The AAD structures have not been solved, and the AAD primary sequences contain no similarities except for a few amino acids that flank a conserved tryptophan (Bass et al., 2016). Mutation of this tryptophan, in both TOPBP1 and ETAA1, prevents ATR activation (Bass et al., 2016; Haahr et al., 2016; Kumagai et al., 2006; Lee et al., 2016). However, whether a second critical aromatic residue or any other motifs in these domains are required for ATR activation is unknown. To better determine how ETAA1 and TOPBP1 activate ATR, we more specifically defined the ETAA1 and TOPBP1 AADs. We found that each of the AADs contains a predicted coiled coil motif that is required for ATR activation *in vitro* and in cells. Our data indicates that the predicted coiled coils are required for ATR activation because these motifs bind the ATR-ATRIP complex.

Results

Identification of the ETAA1 ATR activation domain

ETAA1 is a 926 amino acid protein that contains two RPA interaction motifs and an AAD (Bass et al., 2016; Haahr et al., 2016; Lee et al., 2016). However, it contains no other defined domains and several regions within the protein are predicted to be unstructured (Fig 3.1A). To better understand how ETAA1 activates ATR, we sought to more specifically define the AAD. We previously identified the ETAA1 AAD to be residues 75-250, as this fragment stimulates robust ATR kinase activity *in vitro* (Bass et al., 2016). Like the yeast MADs, the

ETAA1 AAD is predicted to be intrinsically disordered without clear secondary structure except for a predicted coiled coil motif spanning residues 183-215 (p score = 0.01) (Fig 3.1A and B). To determine if this predicted coiled coil is important for ATR activation, we incubated purified ATR-ATRIP with recombinant GST-ETAA1 AADs containing or lacking the predicted coiled coil, an ATR substrate (an MCM2 fragment containing S108 (Cortez et al., 2004)), and ATP [γ-^{32}P], and measured substrate phosphorylation. ETAA1 75-250 and 75-215, which contain the predicted coiled coil, stimulate ATR kinase activity, while ETAA1 75-182, which lacks the predicted coiled coil, does not (Fig 3.1C). ETAA1 75-204 has partial activity, but removal of six more residues eliminates virtually all activation (Fig 3.1D and G). We also tested ETAA1 AADs that had amino acids deleted from the N-terminus. Compared to ETAA1 75-215, ETAA1 85-215 activates ATR less efficiently, ETAA1 95-215 activates ATR very little, and ETAA1 100-215 does not activate ATR at all (Fig 3.1E). A direct comparison between ETAA1 75-250, 75-215, 75-204, and 85-215 revealed that 75-250 and 75-215 activate ATR to a similar extent and more robustly than 75-204 and 85-215 (Fig 3.1F and G). Therefore, we conclude that in addition to the critical tryptophan (W107), ETAA1 contains a predicted coiled coil motif that is required for stimulation of maximal ATR kinase activity and the minimal AAD that retains complete activity contains residues 75-215.

Identification of the TOPBP1 ATR activation domain

TOPBP1 is a multiple BRCT-domain containing protein with an AAD located between BRCT domains 6 and 7 composed of residues 978-1192 (Kumagai et al., 2006). Like the ETAA1 AAD and yeast MADs, the TOPBP1 AAD is predicted to be mostly unstructured (Fig 3.2A). Since the ETAA1 AAD contains a predicted coiled coil that is required for ATR activation, we hypothesized that the TOPBP1 AAD may contain a similar motif. Indeed, a secondary structure

prediction algorithm identified a possible coiled coil in the TOPBP1 AAD from residues 1054-1083 albeit with a more modest p-score of 0.074 (Fig 3.2B). Therefore, we assessed whether this motif was required for TOPBP1-dependent ATR activation. GST-TOPBP1 fragments containing the predicted coiled coil as small as amino acids 1057-1173 stimulate ATR kinase activity (Fig 3.2C and D). However, TOPBP1 1083-1173, which lacks the predicted coiled coil, does not activate ATR (Fig 3.2D). Thus, like ETAA1, TOPPB1 contains a critical tryptophan (W1145) and a predicted coiled coil within an otherwise disordered domain that is required for full stimulation of ATR kinase activity.

A single point mutation in the predicted coiled coils disrupts ATR activation

A sequence alignment of the ETAA1 and TOPBP1 predicted coiled coil motifs reveals some sequence similarity (Fig 3.3A). Both contain a conserved phenylalanine (F198 in ETAA1 and F1071 in TOPBP1), which we hypothesized could be a second critical aromatic residue in each AAD required for ATR activation similar to the requirement in the Mec1 activators. Mutation of ETAA1 F198 to alanine completely abolishes ATR activation (Fig 3.3B). Mutation of TOPBP1 F1071 to alanine also reduces ATR activation, although not to the extent observed for ETAA1 (Fig 3.3C).

Over-expression of either the TOPBP1 or ETAA1 AAD in cells results in ATR activation that can be assessed by measuring histone variant H2AX phosphorylation at serine-139 (γH2AX) (Ball et al., 2007; Bass et al., 2016; Haahr et al., 2016). We expressed the full length AADs, AADs lacking the predicted coiled coils, or AADs with the phenylalanine mutations in U2OS cells and measured γH2AX induction by immunofluorescence. Expression of ETAA1 75-215 induces a large increase in γH2AX, while ETAA1 75-182 and ETAA1 75-215 F198A expression

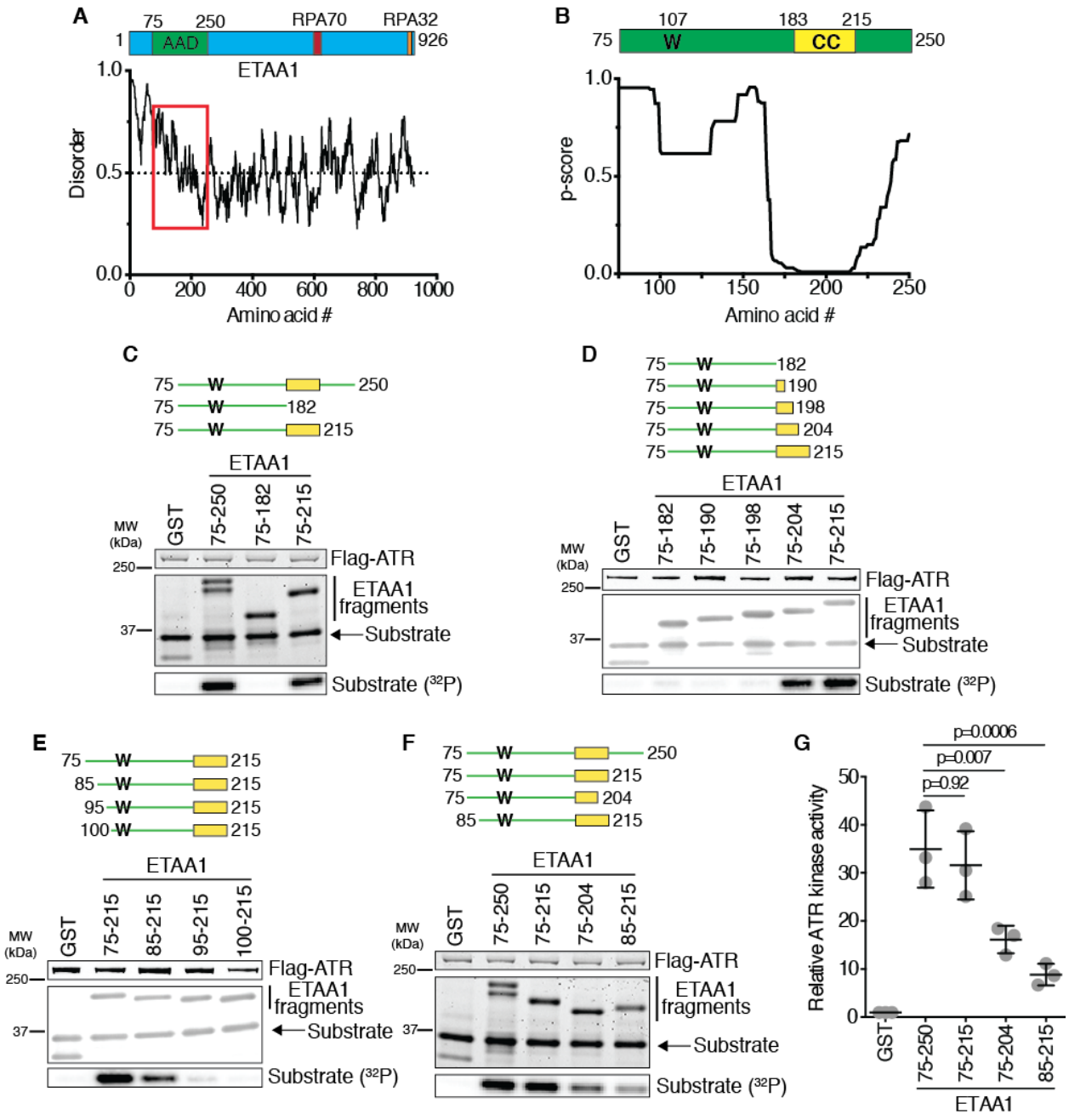

Figure 3.1 Identification of the ETAA1 ATR activation domain. A) Schematic of ETAA1 with the AAD and RPA interaction motifs indicated. ETAA1 predicted disorder was calculated using IUPred2A (Meszaros et al., 2018). AAD region is indicated by red box. **B)** Schematic of the ETAA1 AAD, with the critical tryptophan and predicted coiled coil (CC) indicated. Predicted coiled coil per residue scores were calculated using Paircoil2 (McDonnell et al., 2006). **C-F)** Purified ATR-ATRIP complexes were incubated with GST or the indicated GST-ETAA1 AADs, an ATR substrate, and ATP γ-^{32}P. Reaction products were separated by SDS-PAGE and detected by coomassie staining and immunoblotting. Substrate phosphorylation was detected by autoradiography. **G)** Quantification of three experiments as shown in **F**. Statistical significance

was calculated using a one-way ANOVA and Tukey's multiple comparisons test. Black bars are mean +/- SD.

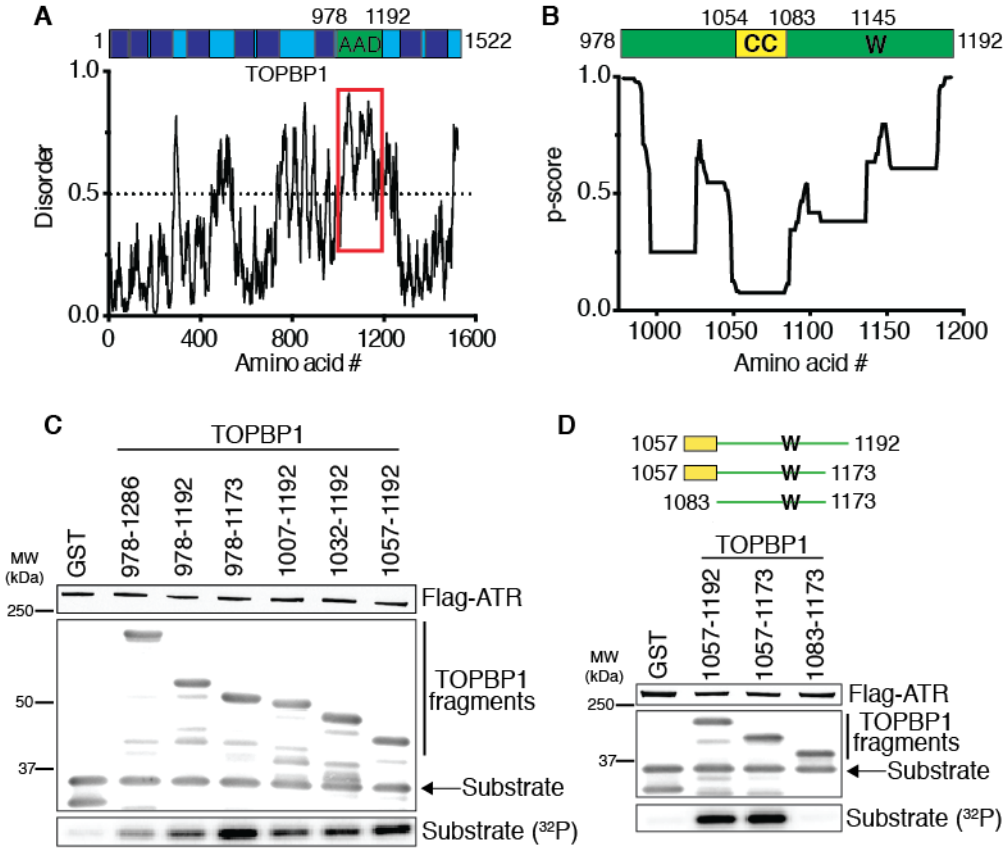

Figure 3.2 Identification of the TOPBP1 ATR activation domain. A) Schematic of TOPBP1 with the AAD indicated. BRCT domains are indicated as dark blue boxes. TOPBP1 predicted disorder was calculated using IUPred2A (Meszaros et al., 2018). AAD region is indicated by red box. **B)** Schematic of the TOPBP1 AAD, with the critical tryptophan and predicted coiled coil (CC) indicated. Predicted coiled coil per residue scores were calculated using Paircoil2 (McDonnell et al., 2006). **C-D)** Purified ATR-ATRIP complexes were incubated with GST or the indicated GST-TOPBP1 AADs, an ATR substrate, and ATP γ-^{32}P. Reaction products were separated by SDS-PAGE and detected by coomassie staining and immunoblotting. Substrate phosphorylation was detected by autoradiography.

do not (Fig 3.3D and E). We also assessed MCM2 S108 phosphorylation as a second measure of ATR activation and observed that expression of ETAA1 75-215, but not ETAA1 75-182 or ETAA1 75-215 F198A, causes a modest increase in MCM2 S108 phosphorylation (Fig 3.3F).

Next, we measured γH2AX induction and MCM2 S108 phosphorylation in cells expressing our newly defined TOPBP1 AADs. Expression of TOPBP1 1057-1173 causes a large increase in γH2AX, while expression of TOPBP1 1083-1173, which lacks the predicted coiled coil, results in no increase in γH2AX (Fig 3.3G and H). Expression of TOPBP1 1057-1173 F1071A causes moderate γH2AX induction, (Fig 3.3G and H) consistent with the result of the *in vitro* kinase assay where the F1071A mutation reduces, but does not abolish, ATR activation by TOPBP1 (Fig 3.3C). Expression of TOPBP1 1057-1173 also causes a modest increase in MCM2 S108 phosphorylation, while expression of TOPBP1 1083-1173 does not. Expression of TOPBP1 1057-1173 F1071A, as for γH2AX, causes an intermediate level of MCM2 S108 phosphorylation (Fig 3.3I). Taken together, these results indicate that the ETAA1 and TOPBP1 predicted coiled coils are required for efficient ATR activation in cells.

The coiled coil point mutations do not alter AAD oligomerization

Coiled coils often function as oligomerization domains (Burkhard et al., 2001). To determine if mutation of the predicted coiled coils altered AAD oligomerization, we compared the elution profiles of ETAA1 75-215 and ETAA1 75-215 F198A on a size exclusion column. Both ETAA1 75-215 and ETAA1 75-215 F198A elute at a retention volume of 15.2 mL, indicating that the F198A mutation does not disrupt function by preventing homo-oligomerization (Fig 3.4A). Both the wild-type and mutant proteins elute at a position that does not match their predicted molecular weight (approximately 38.6 kDa compared to the predicted

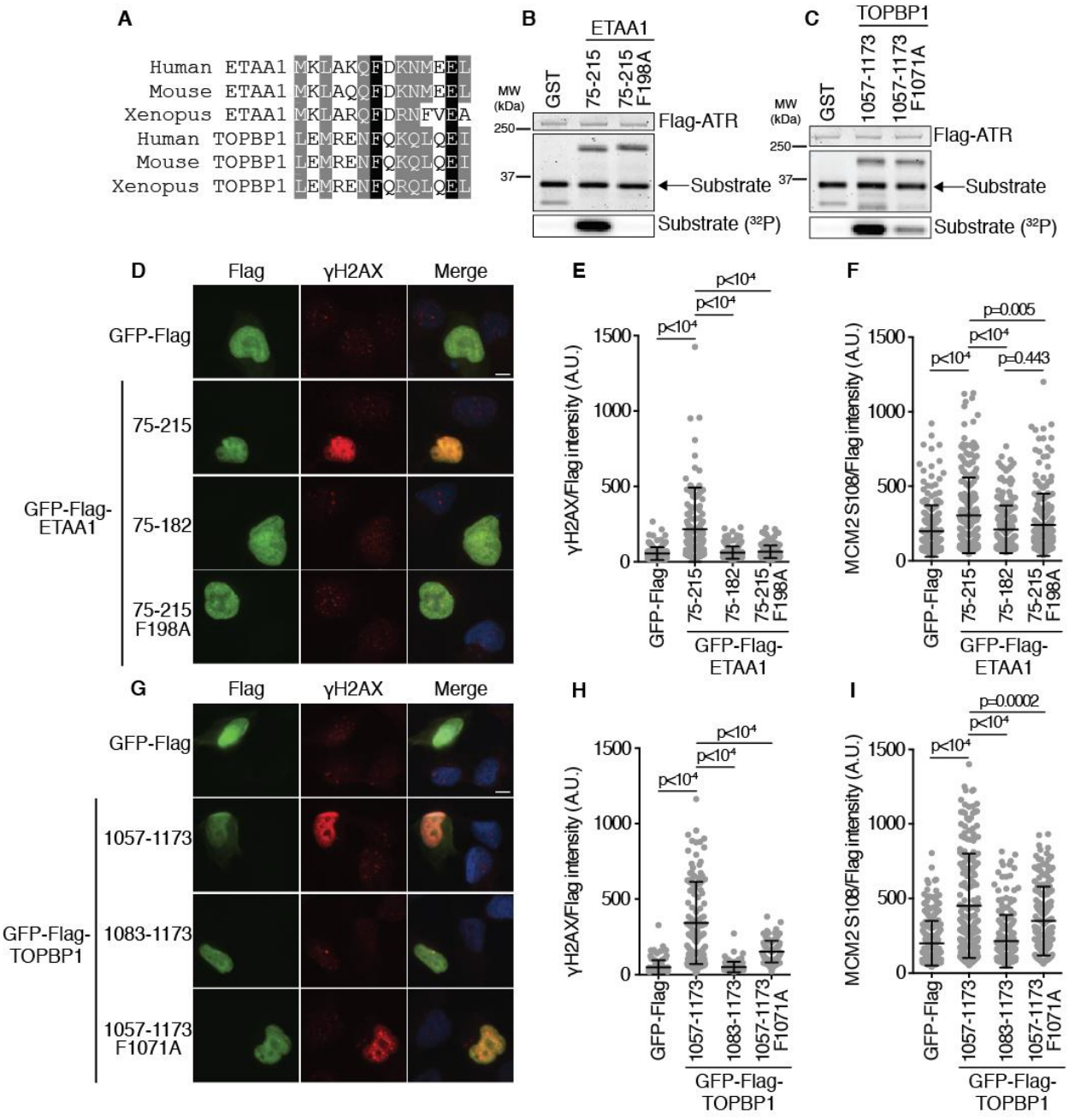

Figure 3.3 Mutation of a conserved phenylalanine disrupts ETAA1 and TOPBP1-dependent ATR activation. A) Sequence alignment of ETAA1 and TOPBP1 predicted coiled coil residues flanking ETAA1 F198 and TOPBP1 F1071. **B-C)** Purified ATR-ATRIP complexes were incubated with GST or the indicated GST-ETAA1 or GST-TOPBP1 AADs, an ATR substrate, and ATP γ-^{32}P. Reaction products were separated by SDS-PAGE and detected by Coomassie staining. Substrate phosphorylation was detected by autoradiography. **D-I)** Empty vector or the indicated ETAA1 or TOPBP1 AAD proteins were expressed in U2OS cells. γH2AX (**D-E** and **G-H**) or MCM pS108 (**F** and **I**) was visualized in Flag positive nuclei. Scale bar is 10 μm. γH2AX and MCM2 pS108 intensity is normalized to Flag expression level.

Statistical significance was calculated using a one-way ANOVA and Tukey's multiple comparisons test. Black bars are mean +/- SD.

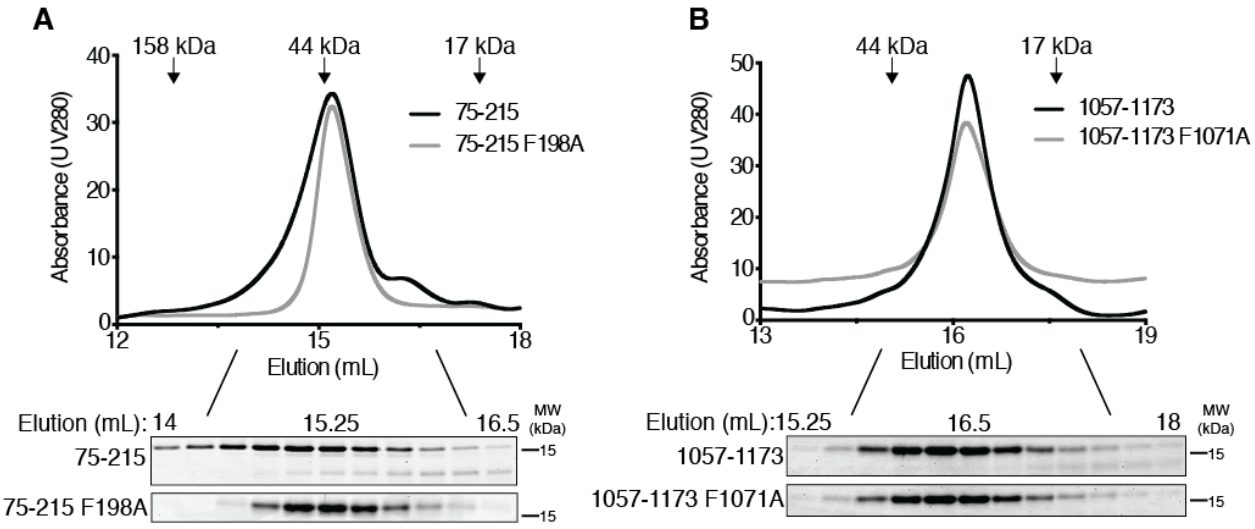

Figure 3.4 Mutation of the AADs does not alter AAD oligomerization. A-B) The indicated ETAA1 (**A**) or TOPBP1 (**B**) AADs were eluted from a Superdex^{TM} 200 Increase 10/300 GL column while measuring UV absorbance at 280 nm. Equal amounts of fractions corresponding to peaks were separated by SDS-PAGE and visualized by coomassie staining. Elution volume of molecular weight standards is indicated.

16.3 kDa). However, since the ETAA1 AAD is predicted to be intrinsically disordered (Fig 3.1A), it is unlikely to be globular likely explaining this difference.

We also assessed TOPBP1 AAD oligomerization using gel-filtration chromatography. TOPBP1 1057-1173 elutes at a retention volume of 16.23 mL, while TOPBP1 1057-1173 F1071A elutes at a retention volume of 16.2 mL (Fig 3.4B). These retention volumes correspond to molecular weights of 21.8 kDa and 22.2 kDa respectively compared to the predicted molecular weights of 13.4 kDa and 13.3 kDa. These results indicate that the F1071A mutation does not alter TOPBP1 AAD oligomerization, despite impairing ATR activation.

The predicted coiled coils promote the AAD-ATR interaction

Since mutation of the predicted coiled coils had no apparent effect on AAD oligomerization, we next tested how these mutations affected the AAD-ATR interactions. The F198A mutation almost completely abolishes the ETAA1 AAD-ATR interaction as measured by co-immunoprecipitation (Fig 3.5A). Similarly, the F1071A mutation diminishes the TOPBP1 AAD-ATR interaction (Fig 3.5B).

Given that mutation of the predicted coiled coils disrupts the ETAA1 and TOPBP1 AAD-ATR interactions, we considered the possibility that the predicted coiled coils might directly contact ATR and/or ATRIP. To test this hypothesis, we purified the full length ETAA1 AAD, the ETAA1 predicted coiled coil, and the ETAA1 predicted coiled coil containing the F198A mutation all as recombinant GST-fusion proteins, bound the proteins to glutathione beads, and incubated the beads with nuclear extracts expressing Flag-ATR and HA-ATRIP. As expected, the full length ETAA1 AAD binds the ATR-ATRIP complex. The ETAA1 predicted coiled coil also binds a small amount of ATR-ATRIP, whereas no appreciable binding above background is

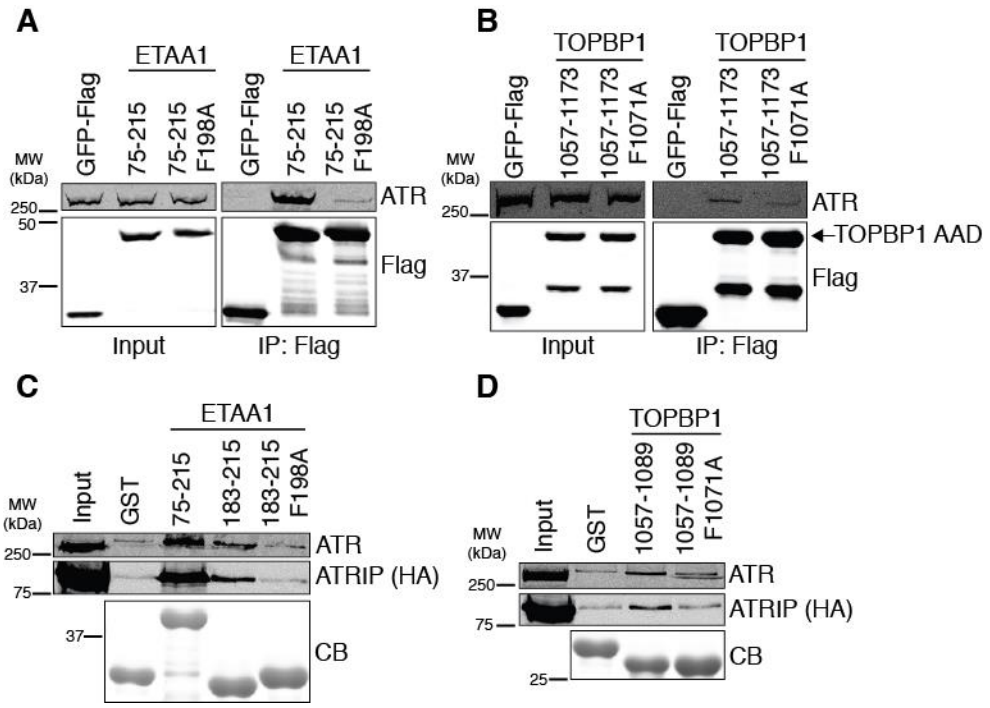

Figure 3.5 The predicted coiled coils promote the ETAA1 and TOPBP1 AAD-ATR interaction. A-B) Empty vector or the indicated ETAA1 (**A**) or TOPBP1 (**B**) AADs were immunoprecipitated from HEK293T cell nuclear extracts. Immunoprecipitated proteins were separated by SDS-PAGE and detected by immunoblotting. **C-D)** Purified GST or recombinant GST-ETAA1 (**C**) or GST-TOPBP1 (**D**) proteins bound to glutathione beads were incubated with HEK293T cell nuclear extracts expressing Flag-ATR and HA-ATRIP. Bound proteins were eluted, separated by SDS-PAGE, and detected by coomassie staining (CB) or immunoblotting.

observed with the F198A mutant (Fig 3.5C). We performed the same experiment with the TOPBP1 predicted coiled coil, and similarly, observed that this protein binds a small amount of ATR-ATRIP. In contrast, the TOPBP1 predicted coiled coil with the F1071A mutation exhibits no ATR-ATRIP binding above background (Fig 3.5D). Taken together, these results suggest that the ETAA1 and TOPBP1 predicted coiled coils are important for ATR activation because these motifs contribute to the AAD interaction with ATR-ATRIP.

Discussion

Combined with previously published data, our results suggest that the defining features of an ATR activation domain include: 1) the presence of an evolutionary conserved tryptophan within a region predicted to be mostly disordered, and 2) a predicted coiled coil motif that mediates binding to ATR-ATRIP. Both ATR and ATRIP are thought to contain AAD interaction surfaces needed for ATR activation (Mordes et al., 2008a), perhaps explaining the requirement of more than one ATR-ATRIP binding motif in the AADs. With this more specific definition of an AAD, it may be possible to combine phenotypic data, secondary structure predictions, and primary sequence alignments to identify or evaluate additional AADs.

NBS1 was previously proposed to be a direct ATR activator (Kobayashi et al., 2013). The ATR interaction domain on NBS1 was mapped to BRCT domain 2, which does not have any similarity to the ETAA1 or TOPBP1 AAD motifs. The authors concluded that NBS1 activates ATR differently than TOPBP1. Therefore, we cannot rule out the possibility that additional ATR activators, such as NBS1, may activate ATR using mechanisms other than through AADs.

Like the MADs, which contain two aromatic residues required for Mec1 activation (Kumar and Burgers, 2013; Navadgi-Patil and Burgers, 2009; Navadgi-Patil et al., 2011), we identified a second critical aromatic residue, a phenylalanine, in the ETAA1 and TOPBP1 AADs within the predicted coiled coils. The critical aromatic residues in the Mec1 activators are always either tryptophan or tyrosine, and interestingly, although one of the critical aromatics in Dna2, Trp-128, can be substituted with Tyr, mutation of this residue to Phe causes a defect in Mec1 activation (Wanrooij et al., 2016). The MADs also contain no obvious predicted coiled coils (McDonnell et al., 2006). Thus, there may be some differences between the yeast MAD and vertebrate AAD domains. Atomic resolution structural information will be required to fully determine how the MADs and AADs actually bind to and activate Mec1 and ATR respectively.

ATR inhibitors are currently being tested as single agents and in conjunction with genotoxic chemotherapies to treat various malignancies (Forment and O'Connor, 2018). Identification of ATR activating proteins and the mechanism by which they activate ATR should reveal more detailed information about how, when, and where ATR is activated and about downstream activator-specific signaling cascades. This information, in turn, may be useful in identifying which patients would most benefit from ATR inhibitor treatment regimens and contribute to improved efficacy of these drugs.

Conclusions

Budding yeast contain at least three Mec1 activating proteins, and these proteins are predicted to stimulate Mec1 kinase activity by a common mechanism. Each Mec1 activator possesses two aromatic amino acids that are essential for Mec1 activation because these residues directly bind Mec1 to stimulate kinase activity. Metazoans contain at least two ATR activating proteins, TOPBP1 and ETAA1, and although each of these proteins contain an essential

tryptophan that is required for ATR binding and activation, less is known about the mechanism by which these proteins activate ATR. We identified a common motif in the ETAA1 and TOPBP1 AADs, a predicted coiled coil, that is essential for ATR binding and activation. Furthermore, we found that the predicted coiled coils exhibit primary sequence similarity and contain an essential phenylalanine that is required for ATR binding and activation. Our data indicates that the predicted coiled coils directly contact the ATR-ATRIP complex.

CHAPTER IV

REGULATION OF ATR ACTIVATION BY DIMERIZATION OF ATR ACTIVATING DOMAINS

This chapter is adapted from [Regulation of ATR activation by dimerization of ATR activating domains] currently in revision at [Journal of Biological Chemistry] and is expected to be accepted for publication in February 2021

Introduction

Replication forks frequently encounter obstacles such as DNA damage and transcriptional machinery that impede their progression (Cortez, 2019). Stalled replication forks must be stabilized to avoid collapse into double-strand breaks and to facilitate resumption of DNA synthesis. Upon fork stalling, the phosphoinositide-3 kinase related kinase ataxia telangiectasia and Rad3 related (ATR) activates the replication stress response, which slows cell cycle progression, suppresses new origin firing, and stabilizes stalled replication forks (Saldivar et al., 2017).

ATR activation occurs not only in response to replication stress, but also during normal DNA replication and in mitosis (Bass and Cortez, 2019; Buisson et al., 2015; Kabeche et al., 2018; Saldivar et al., 2018). ATR signaling in S-phase suppresses CDK1-dependent activation of a mitotic transcriptional network to enforce an S/G2 checkpoint (Saldivar et al., 2018). In mitosis, ATR signaling ensures proper chromosome alignment and segregation, and regulates the spindle assembly checkpoint (Bass and Cortez, 2019; Kabeche et al., 2018).

ATR is recruited to replication forks through its obligate binding partner ATR interacting protein (ATRIP) via a direct interaction between ATRIP and replication protein A (RPA) (Cortez

et al., 2001; Zou and Elledge, 2003). In mitosis, RPA recruits ATR to centromeric R-loops (Kabeche et al., 2018). However, ATR localization to RPA-coated ssDNA is not sufficient for ATR activation. Several additional proteins, including an ATR activating protein, must also be recruited and assembled with ATR (Saldivar et al., 2017). In metazoan cells, there are at least two ATR activating proteins, TOPBP1 and ETAA1 (Bass et al., 2016; Haahr et al., 2016; Kumagai et al., 2006; Lee et al., 2016), whereas *S. cerevisiae* contains at least three activators (Kumar and Burgers, 2013; Mordes et al., 2008b; Navadgi-Patil and Burgers, 2008, 2009). Whether ATR activation occurs via TOPBP1 or ETAA1 is dependent on cell cycle phase and the presence of exogenous DNA damage. In response to replication stress caused by replication inhibitors or DNA damaging agents, ATR signaling is predominantly TOPBP1-dependent, whereas ETAA1 is the primary ATR activator during normal DNA replication and in mitosis (Bass and Cortez, 2019; Saldivar et al., 2018).

TOPBP1 and ETAA1 can activate different ATR signaling pathways in cells, but the mechanism by which these proteins stimulate ATR activity appears to be the same. Both TOPBP1 and ETAA1 possess experimentally defined ATR activation domains (AADs) that are required to bind and activate ATR-ATRIP complexes (Bass et al., 2016; Haahr et al., 2016; Kumagai et al., 2006; Lee et al., 2016). Although the AADs do not exhibit significant primary sequence similarity, both are predicted to be intrinsically disordered, and both possess a critical tryptophan and predicted coiled coil motif that are essential for ATR binding and activation (Thada and Cortez, 2019). Additionally, a mutation in ATR that reduces TOPBP1-dependent activation also reduces activation by ETAA1 (Bass et al., 2016; Mordes et al., 2008a).

Human and yeast ATR-ATRIP complexes form a dimeric butterfly-like structure similar to ataxia telangiectasia mutated (ATM) with two ATR molecules and two ATRIP molecules in a

single complex (Rao et al., 2018; Sawicka et al., 2016; Tannous et al., 2021; Wang et al., 2016; Wang et al., 2017), and dimerization of the complex is required for function (Ball and Cortez, 2005). ATM is activated by the MRE11-RAD50-NBS1 (MRN) complex (Lee and Paull, 2004, 2005), and like ATM, MRN is a dimer with two MRE11, RAD50, and NBS1 molecules in a single complex (Syed and Tainer, 2018). In addition, RAD50 dimerization is required for ATM activation (Lee et al., 2013). Thus, activation of ATM may require dimerization of the ATM activation protein.

TOPBP1 forms oligomeric complexes in cells (Liu et al., 2006), but how TOPBP1 oligomerization affects ATR activation is not clear. While one study concluded that TOPBP1 dimerization augments ATR signaling (Zhou et al., 2013), another concluded that TOPBP1 oligomerization mediated by AKT-phosphorylation reduces ATR signaling (Liu et al., 2013). In our studies, we observe increased ATR activation when the AADs are fused to a dimeric GST tag but not a monomeric maltose binding protein (MBP) tag. We assessed how AAD dimerization affects ATR activation, and found that dimerization of both the TOPBP1 and ETAA1 AADs enhances ATR activation. Additionally, ETAA1 forms oligomeric complexes in cells. Expression of a dimeric, but not monomeric, mini-ETAA1 protein complements the hydroxyurea (HU) and camptothecin (CPT) hypersensitivity of ETAA1-deficient cells, and restores genome stability. Our results indicate that ETAA1 and TOPBP1 dimerization are likely important for optimal ATR checkpoint signaling.

Results

GST tag enhances ATR activation by AADs

We previously identified the minimal TOPBP1 and ETAA1 AADs by determining which TOPBP1 and ETAA1 fragments were capable of activating ATR in an *in vitro* kinase assay (Thada and Cortez, 2019). All AADs used in that study had a GST tag. Interestingly, we found that cleavage and removal of the GST tag reduces the ability of the AADs to activate ATR. Even at a three-fold higher concentration, ATR activation by untagged TOPBP1 or ETAA1 AADs is still less than activation by the corresponding GST-AADs (compare lanes 2 and 5 and 6 and 9) (Fig 4.1A). The substrate used in this experiment (GST-MCM2 79-138) possesses a GST tag that may form a dimer (McTigue et al., 1995); therefore, we assessed whether increased ATR activation by GST-AADs was due to a GST-mediated interaction between substrate and AAD. To do this, we performed kinase assays with the same substrate lacking the GST tag. Again, compared to GST alone, GST-TOPBP1 AAD strongly stimulates ATR kinase activity towards the untagged substrate, while the untagged TOPBP1 AAD does not (Fig 4.1B). We also determined how another tag that does not dimerize, MBP, affects ATR activation by the AADs. In contrast to the GST-TOPBP1 AAD, the MBP-TOPBP1 AAD induces minimal if any ATR activation towards the untagged substrate (Fig 4.1B). We observed the same result with GST-tagged, MBP-tagged, and untagged ETAA1 AADs (Fig 4.1C). Together, these results indicate that a GST tag fused to the TOPBP1 and ETAA1 AADs enhances ATR activation without facilitating an interaction with the kinase substrate.

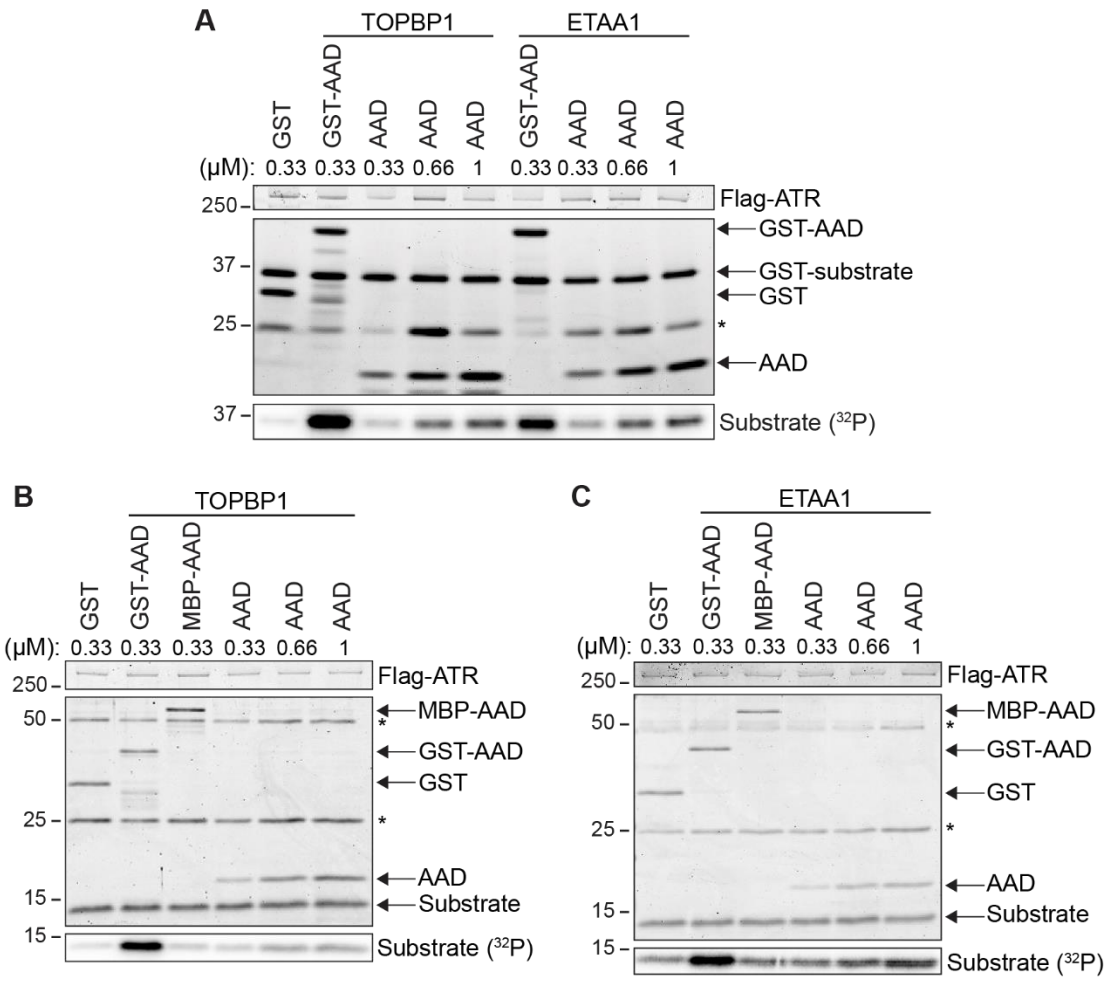

Figure 4.1 Fusion of GST to AADs enhances their ability to activate ATR. A) The kinase activity of ATR-ATRIP towards a GST-MCM2 substrate was measured in the presence of purified GST, AAD, or GST-AAD proteins. Reaction products were separated by SDS-PAGE and detected by coomassie blue staining. Substrate phosphorylation was detected by phosphoimaging. **B-C)** Kinase activity of ATR-ATRIP towards an untagged MCM2 substrate was measured in the presence of GST-, MBP-, or untagged AADs. Asterisks (*) denote antibody heavy and light chains.

AAD dimerization enhances ATR activation

Because GST can form a dimer (McTigue et al., 1995), we hypothesized that GST-mediated AAD dimerization might be the cause of the increased ATR activation. To test this hypothesis directly, we generated AADs with a FKBP F36V tag. Dimerization of proteins fused to FKBP F36V (hereafter referred to as FK) occurs upon incubation with the rapamycin analog AP20187 (Fig 4.2A) (Clackson et al., 1998). We first determined whether AP20187 induces dimerization of FK-TOPBP1 AAD and/or FK-ETAA1 AAD. In the absence of AP20187, purified FK-TOPBP1 AAD elutes from a size exclusion column at a retention volume of 15.7mL, which corresponds to a molecular weight of 29 KDa (Fig 4.2B). FK-TOPBP1 AAD has a predicted molecular weight of 28.5 KDa, suggesting that in the absence of AP20187, FK-TOPBP1 AAD is a monomer. Upon preincubation with AP20187, a second FK-TOPBP1 AAD elution peak is observed at a retention volume of 14.6 mL (Fig 4.2B). This elution volume corresponds to a molecular weight of 54 KDa, approximately twice the predicted molecular weight of FK-TOPBP1 AAD. Thus, as expected, AP20187 induces FK-TOPBP1 AAD dimerization.

FK-ETAA1 AAD has a predicted molecular weight of 31.5 KDa, but in the absence of AP20187 elutes from a size exclusion column at a retention volume (14.6 mL) corresponding to a molecular weight of 54 KDa (Fig 4.2C). The ETAA1 AAD is predicted to be intrinsically disordered and unlikely to form a globular fold (Thada and Cortez, 2019), which may explain this result. Upon preincubation with AP20187, FK-ETAA1 AAD elutes at a second peak of 12.6 mL, which corresponds to a predicted molecular weight of 163 KDa (Fig 4.2C). This result is consistent with AP20187 inducing FK-ETAA1 AAD dimerization or oligomerization. Like the FK-ETAA1 AAD, we previously found that the untagged ETAA1 and TOPBP1 AADs elute

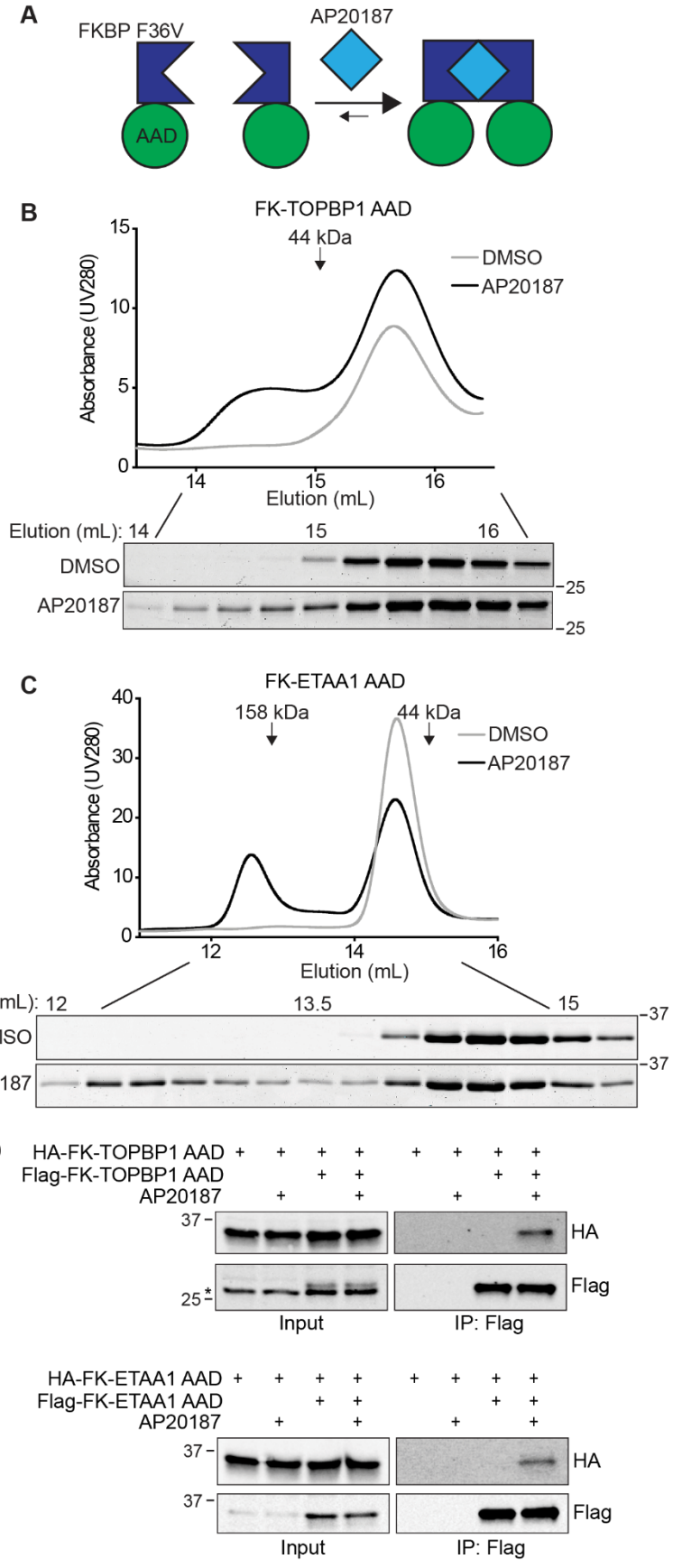
A
FKBP F36V
AP20187
AAD
B
FK-TOPBP1 AAD
44 kDa
DMSO
AP20187
Absorbance (UV280)
Elution (mL)
Elution (mL): 14
15
16
DMSO
AP20187
25
25
C
FK-ETAA1 AAD
158 kDa
44 kDa
DMSO
AP20187
Absorbance (UV280)
Elution (mL)
Elution (mL): 12
13.5
15
DMSO
AP20187
37
37
D
HA-FK-TOPBP1 AAD
Flag-FK-TOPBP1 AAD
AP20187
37
25
HA
Flag
Input
IP: Flag
E
HA-FK-ETAA1 AAD
Flag-FK-ETAA1 AAD
AP20187
37
37
HA
Flag
Input
IP: Flag

Figure 4.2 FKBP F36V (FK)-AADs dimerize when incubated with AP20187. A) Schematic depicting the FK inducible dimerization system. **B-C)** Purified FK-TOPBP1 AAD (**B**) or FK-ETAA1 AAD (**C**) were pre-incubated with either DMSO or 5μM AP20187 for 1 hour prior to application to a Superdex^{TM} 200 Increase 10/300 GL column. Samples from the indicated fractions were analyzed by SDS-PAGE and coomassie blue staining. **D-E)** The indicated HA- or Flag-tagged proteins were expressed in HEK293T cells. Cells were incubated with DMSO or 100 nM AP20187 for 1 hour prior to lysis with buffer containing DMSO or 4 μM AP20187. Immunoprecipitated proteins were separated by SDS-PAGE and detected by immunoblotting. Asterisk denotes non-specific band at similar MW as Flag-FK-TOPBP1 AAD (**D**).

from a size exclusion column at larger than predicted molecular weights (Thada and Cortez, 2019). These results could be due to the predicted intrinsic disorder of the AADs, or to AAD dimerization. To assess whether the TOPBP1 and/or ETAA1 AADs dimerize, we performed co-immunoprecipitation experiments. Immunoprecipitation of Flag-FK-TOPBP1 AAD co-precipitates HA-FK-TOPBP1 AAD in the presence, but not the absence of AP20187 (Fig 4.2D). The same result is observed when Flag- and HA-FK-ETAA1 AAD are co-expressed in cells (Fig 4.2E). These results suggest the AADs alone are not capable of dimerizing, and that their elution profiles in size-exclusion chromatography is likely because they do not fold into a globular structure as is predicted from their high degree of disorder in prediction algorithms.

Next, we determined how AAD dimerization affects ATR activation by performing kinase assays with the FK-AADs in the absence or presence of AP20187. FK-TOPBP1 AAD activates ATR more efficiently in the presence of AP20187, and this result is observed regardless of AAD concentration (Fig 4.3A and B). AP20187 also increases ATR activation by the FK-ETAA1 AAD (Fig 4.3C and D). These results are not due to AP20187 off-target effects since basal ATR activation levels and ATR activation by GST-AADs are not changed in the presence of AP20187 (Fig 4.3E). Thus, AAD dimerization enhances ATR activation *in vitro*.

ETAA1 forms oligomeric complexes in cells

Based on our biochemical data, we wondered whether dimerization (or oligomerization) of ATR activating proteins in cells is important for ATR signaling. TOPBP1 oligomerization has been reported to enhance or attenuate ATR signaling (Liu et al., 2013; Zhou et al., 2013), but whether ETAA1 oligomerization affects ATR signaling is not known. To determine if ETAA1 forms oligomeric complexes, we expressed Flag-ETAA1 and HA-ETAA1 in cells either alone or in combination and examined potential oligomerization by co-immunoprecipitation.

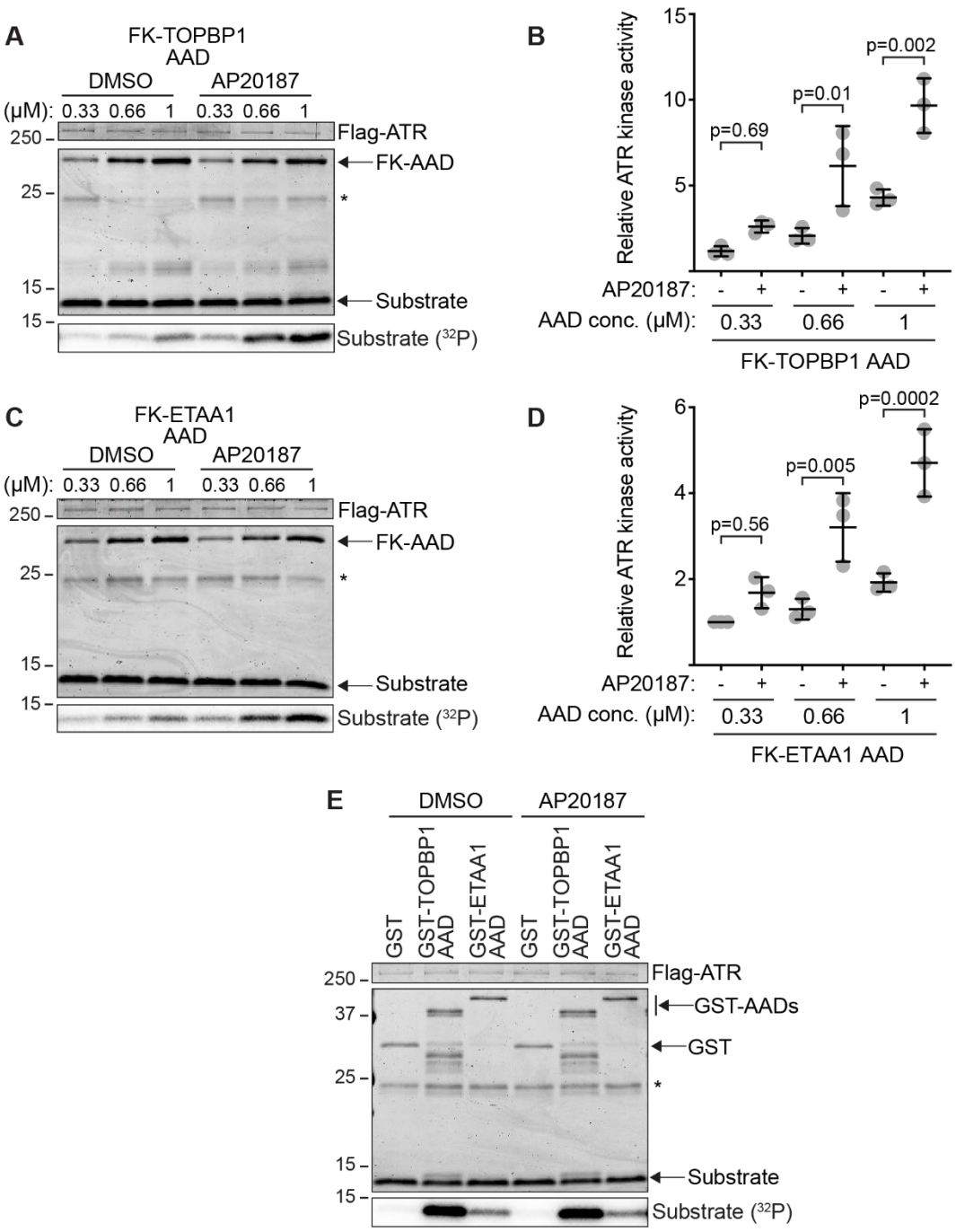

Figure 4.3 AAD dimerization enhances ATR activation. A-D) Kinase activity of ATR-ATRIP towards untagged MCM2 substrate in the presence of FK-TOPBP1 AAD (**A**) or FK-ETAA1 AAD (**C**) was measured in the presence of DMSO or 5 μM AP20187. Reaction products were separated by SDS-PAGE and detected by coomassie staining. Quantification of substrate phosphorylation in three independent experiments (**B** and **D**) was measured using a phosphoimager. Statistical significance was calculated using a one-way ANOVA and Tukey's multiple comparisons test (Mean +/- SD). **E)** Kinase activity of ATR-ATRIP towards untagged

MCM2 substrate in the presence of GST or the indicated GST-AADs in the presence of DMSO or 5 μM AP20187. Asterisks (*) denote antibody light chain.

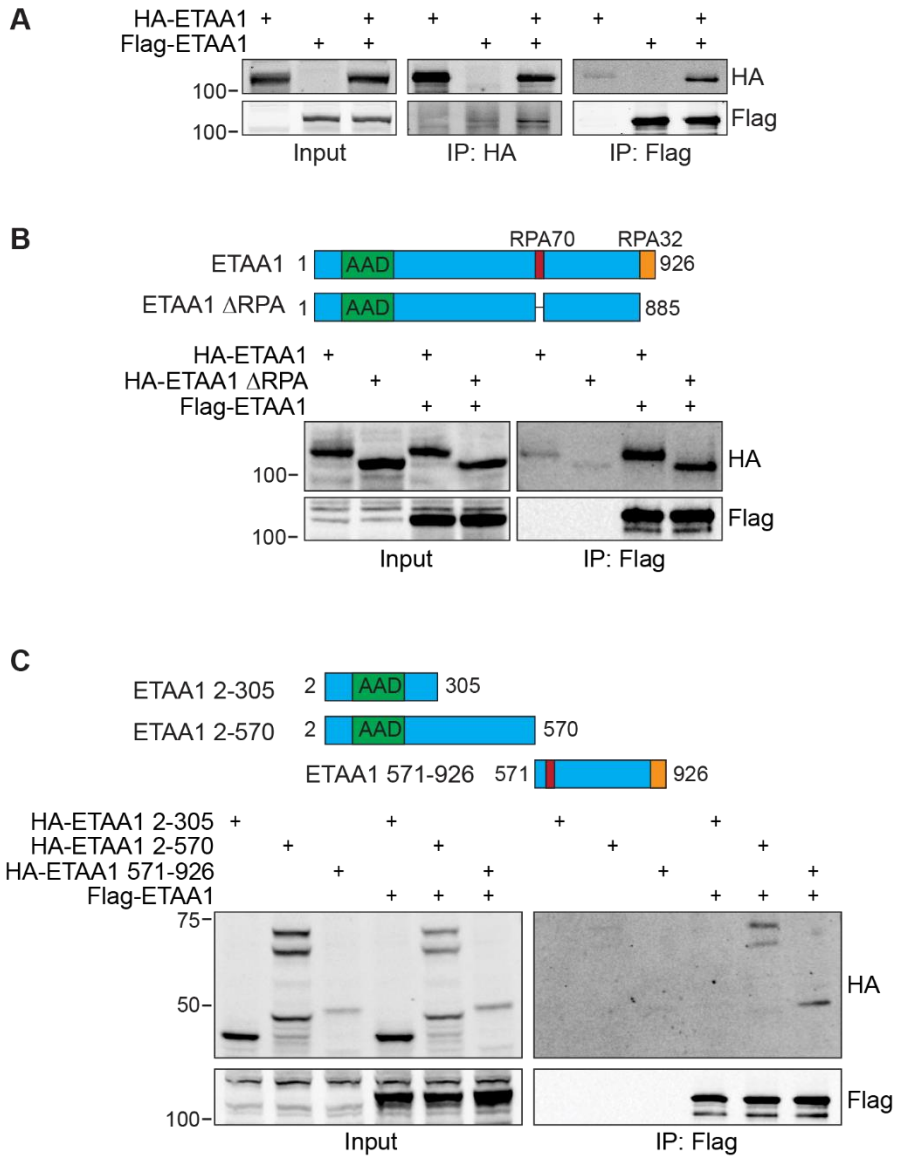

Figure 4.4 ETAA1 forms oligomeric complexes in cells. A) Flag-ETAA1 and HA-ETAA1 were expressed either alone or in combination in HEK293T cells prior to lysis, immunoprecipitation, and immunoblotting. **B)** HA-ETAA1 or HA-ETAA1 ΔRPA were expressed either alone or in combination with Flag-ETAA1 in HEK293T cells prior to lysis, immunoprecipitation, and immunoblotting. **C)** HA-ETAA1 2-305, 2-570, or 571-926 were expressed either alone or in combination with Flag-ETAA1 in HEK293T cells prior to lysis, immunoprecipitation, and immunoblotting.

Immunoprecipitation of HA-ETAA1 co-precipitates Flag-ETAA1, and immunoprecipitation of Flag-ETAA1 co-precipitates HA-ETAA1 (Fig 4.4A). ETAA1 localizes to ssDNA through a direct interaction with RPA (Bass et al., 2016; Haahr et al., 2016; Lee et al., 2016). Because ETAA1 contains two RPA interaction motifs that interact with two different RPA subunits, we tested whether ETAA1 oligomerization was dependent on the ETAA1-RPA interaction. Immunoprecipitation of Flag-ETAA1 results in similar co-precipitation of HA-ETAA1 and HA-ETAA1 ΔRPA (a mutant lacking both RPA interaction motifs), indicating that ETAA1 oligomerization occurs independently of RPA binding (Fig 4.4B).

Next, we attempted to identify a discreet oligomerization domain within ETAA1. We expressed HA-ETAA1 fragments 2-305, 2-570, and 571-926 in cells either alone or in combination with Flag-ETAA1. Immunoprecipitation of Flag-ETAA1 co-precipitates both HA-ETAA1 2-570 and 571-926, but not 2-305 (Fig 4.4C). This data suggests ETAA1 oligomerization may occur through multiple interaction surfaces.

Dimeric mini-ETAA1 restores function in ETAA1-deficient cells

We have been unsuccessful in further narrowing the oligomerization surfaces in part because of the instability of ETAA1 fragments and lack of predicted folded domains. Nonetheless, we were interested in determining if ETAA1 oligomerization affects ATR signaling in cells, so investigated whether we could prevent oligomerization by removing most of the ETAA1 regions predicted to be disordered while retaining known functional motifs. To do this, we created a protein we have termed mini-ETAA1, in which we fused ETAA1 amino acids 2-305 to the RPA70 (residues 600-622) and RPA32 (residues 885-926) interaction motifs (Fig 4.5A). In addition to the AAD and RPA interaction motifs, mini-ETAA1 also retains CDK-

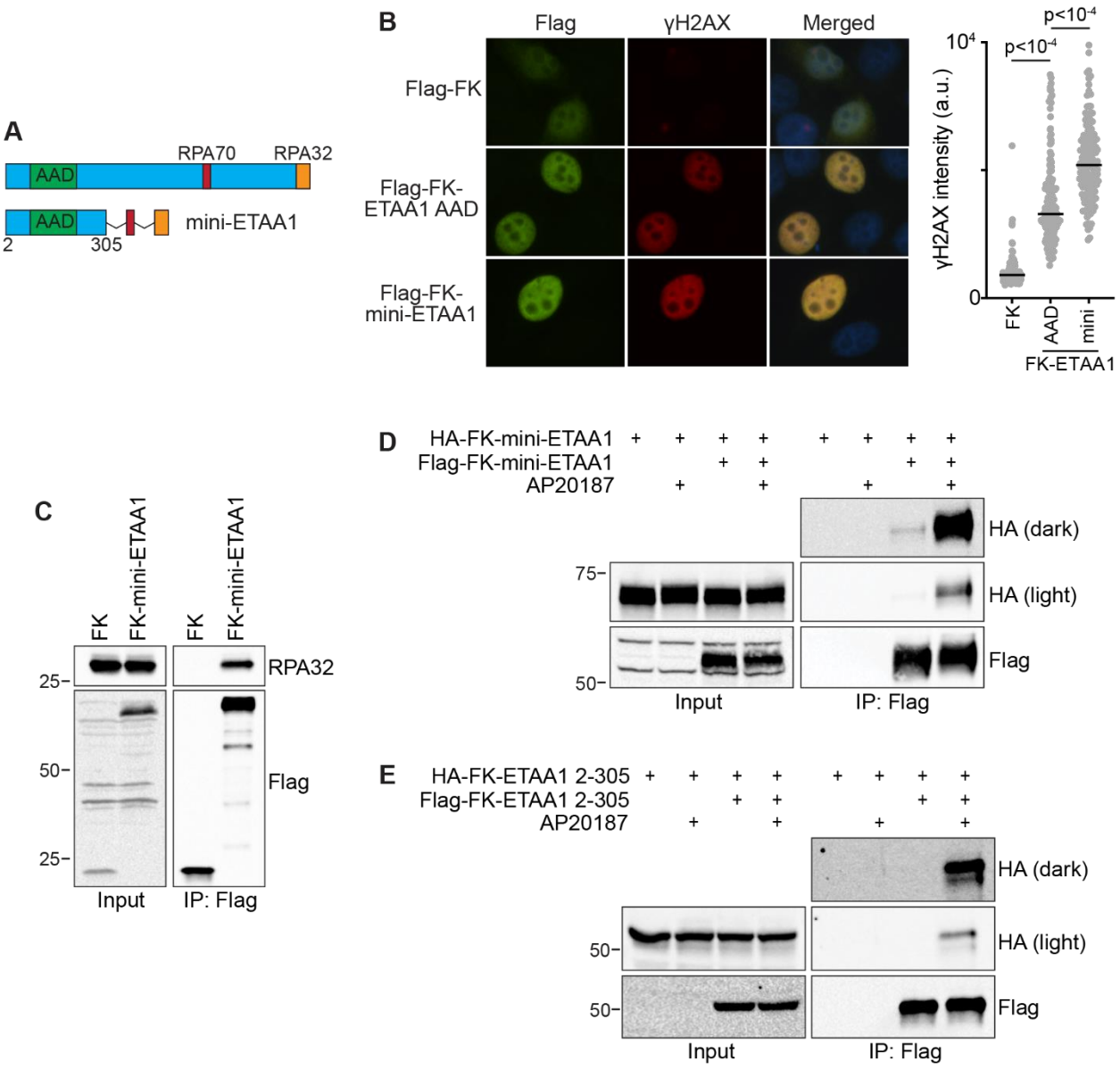

Figure 4.5 Creation and characterization of a mini-ETAA1 protein. A) Schematic comparing ETAA1 to mini-ETAA1. Domains of mini-ETAA1 are separated by a flexible linker $(GGGGS)_3$. **B)** HeLa cells expressing either Flag-FK, Flag-FK-ETAA1 AAD, or Flag-FK-mini-ETAA1 in the absence of AP20187 were fixed and stained for Flag and γH2AX. Representative images and γH2AX quantification of at least 100 Flag positive cells per condition are shown. Statistical significance was calculated with a Kruskal-Wallis test and Dunn's multiple comparisons test. Black bars indicate median. **C)** FK or FK-mini-ETAA1 were expressed in HEK293T cells. Cell were lysed, and immunoprecipitated proteins were detected by immunoblotting. **D)** HA-FK-mini-ETAA1 was expressed either alone or in combination with Flag-FK-mini-ETAA1 in HEK293T cells. Cells were preincubated with DMSO or 100 nM AP20187 for 1 hour prior to lysis in buffer containing DMSO or 4μM AP20187. Immunoprecipitated proteins were detected by immunoblotting. **E)** HA-FK-ETAA1 2-305 was expressed either alone or in combination with

Flag-FK-ETAA1 2-305 in HEK293T cells. Cells were preincubated with DMSO or 100 nM AP20187 for 1 hour prior to lysis in buffer containing DMSO or 4μM AP20187. Immunoprecipitated proteins were detected by immunoblotting.

dependent phosphorylation sites that are required for ETAA1-dependent suppression of chromosomal instability (Achuthankutty et al., 2019).

We assessed the functionality of mini-ETAA1 by measuring ATR activation and RPA binding. Overexpression of both full-length ETAA1 and the ETAA1 AAD results in ectopic ATR activation that can be measured by γH2AX induction (Achuthankutty et al., 2019; Bass et al., 2016; Thada and Cortez, 2019). FK-mini-ETAA1 overexpression causes a large increase in γH2AX induction, and an even greater increase in γH2AX than is caused by FK-ETAA1 AAD overexpression (Fig 4.5B). In addition, immunoprecipitation of FK-mini-ETAA1 co-precipitates RPA32 (Fig 4.5C). These results indicate FK-mini-ETAA1 is capable of activating ATR and binding RPA.

Next, we examined mini-ETAA1 oligomerization. As expected, immunoprecipitation of Flag-FK-mini-ETAA1 results in co-precipitation of HA-FK-mini-ETAA1 in the presence of AP20187. We also detect a substantially attenuated interaction between Flag- and HA-FK-mini-ETAA1 in the absence of AP20187 (Fig 4.5D). The small residual interaction is mediated by RPA since immunoprecipitation of Flag-FK-ETAA1 2-305 (which lacks the RPA interaction motifs) only co-precipitates HA-FK-ETAA1 2-305 in the presence, but not absence, of AP20187 (Fig 4.5E).

We next tested whether monomeric and/or dimeric mini-ETAA1 is sufficient to restore function to ETAA1-deficient cells. First, we assessed ATR-dependent RPA32 phosphorylation in response to CPT, which is reduced in ETAA1-deficient cells (Bass et al., 2016; Haahr et al., 2016; Lee et al., 2016). As previously reported, ΔETAA1 cells generated by CRISPR-Cas9 gene editing have reduced RPA32 S33 phosphorylation upon CPT treatment compared to wild-type controls or ΔETAA1 cells complemented with FK-full-length ETAA1 (Fig 4.6A). Expression of

the FK tag by itself does not complement the defect whether or not the dimerization ligand AP20187 is added to the culture media (Fig 4.6A). In contrast, ΔETAA1 cells expressing FK-mini-ETAA1 in the absence of AP20187 exhibit partial restoration of RPA32 phosphorylation upon CPT treatment. Importantly, phosphorylation is further increased in these cells in the presence of AP20187 (Fig 4.6A and B). This result is likely due to more potent ATR activation by dimeric FK-mini-ETAA1, but also due to increased recruitment of dimeric FK-mini-ETAA1 to damaged replication forks. Indeed, FK-mini-ETAA1 co-localization with RPA in response to CPT is increased upon addition of AP20187 (Fig 4.6C).

ETAA1-deficient cells also exhibit increased genome instability, including a greater number of cells with micronuclei due to defective ATR signaling (Bass et al., 2016). To examine micronuclei formation, we first generated U2OS ΔETAA1 stable cell lines expressing either FK, FK-ETAA1, or FK-mini-ETAA1 (Fig 4.6D). Although we have been unable to detect expression of FK-ETAA1 by immunoblot in these cells, our phenotypic data indicates it is expressed since it complements ETAA1-deficient phenotypes (Fig 4.6D and E). As expected, ΔETAA1 cells, or ΔETAA1 cells expressing only the FK protein exhibit increased micronuclei formation irrespective of whether AP20187 is present (Fig 4.6E). In contrast, ΔETAA1 cells expressing FK-full length ETAA1 have reduced micronuclei formation (Fig 4.6E). ΔETAA1 cells expressing FK-mini-ETAA1 in the absence of AP20187 have micronuclei levels similar to ΔETAA1 and ΔETAA1+FK cells. However, incubation of ΔETAA1+FK-mini-ETAA1 cells with AP20187 reduces the percentage of cells with micronuclei to the same level as ΔETAA1 cells expressing FK-full length ETAA1 (Fig 4.6E).

Finally, we examined whether FK-mini-ETAA1 dimerization complements the HU and CPT sensitivity of ΔETAA1 cells. As shown previously, ETAA1 loss decreases viability in a

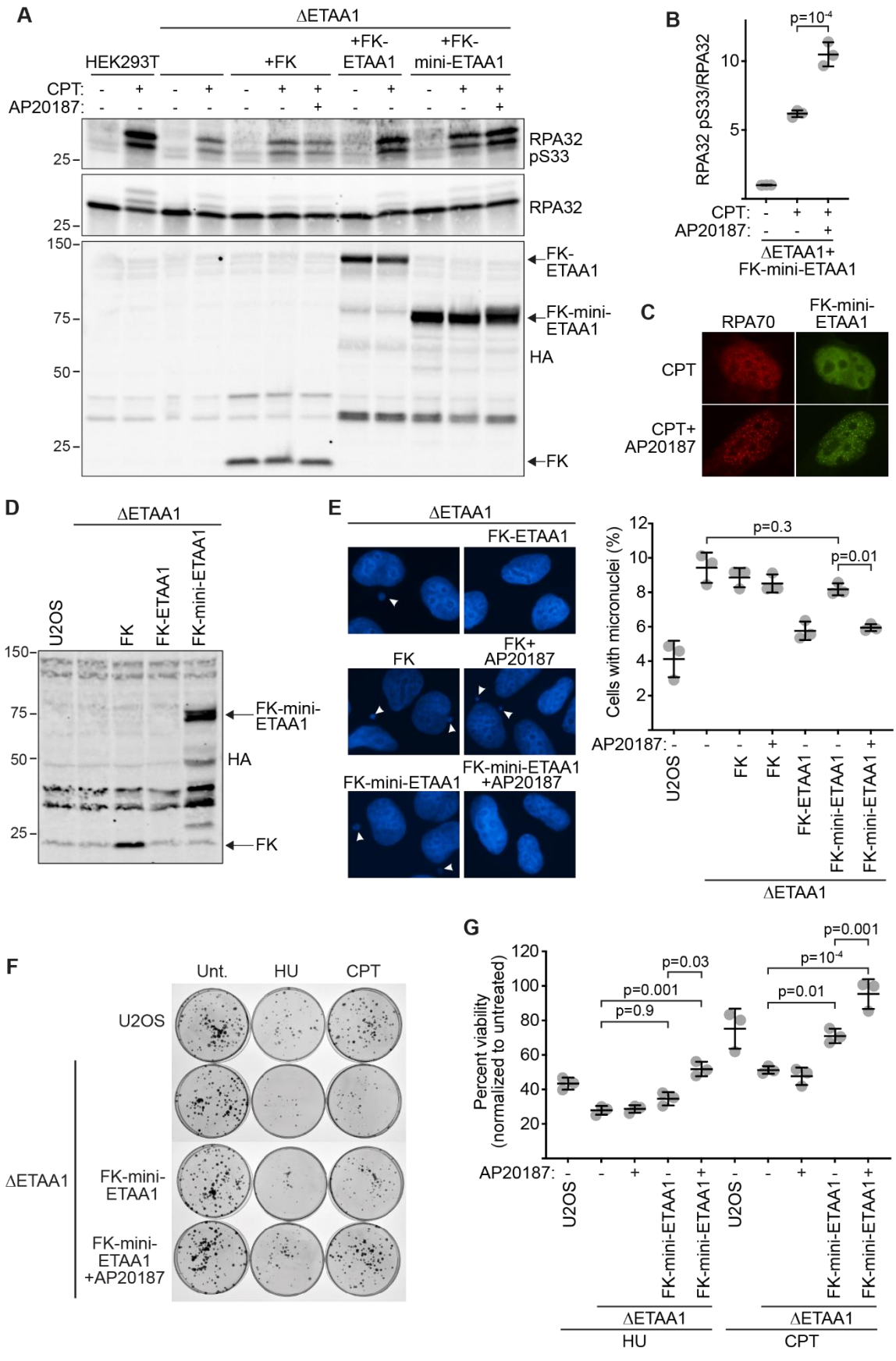
A
ΔETAA1
HEK293T
+FK
+FK-ETAA1
+FK-mini-ETAA1
CPT:
AP20187:
RPA32 pS33
RPA32
FK-ETAA1
FK-mini-ETAA1
HA
FK
B
p=10-4
RPA32 pS33/RPA32
ΔETAA1+ FK-mini-ETAA1
C
RPA70
FK-mini-ETAA1
CPT
CPT+ AP20187
D
ΔETAA1
U2OS
FK
FK-ETAA1
FK-mini-ETAA1
E
ΔETAA1
FK-ETAA1
FK
FK+ AP20187
FK-mini-ETAA1
FK-mini-ETAA1 +AP20187
Cells with micronuclei (%)
p=0.3
p=0.01
F
Unt.
HU
CPT
U2OS
ΔETAA1
FK-mini-ETAA1
FK-mini-ETAA1 +AP20187
G
Percent viability (normalized to untreated)
p=0.9
p=0.001
p=0.03
p=0.01
p=10-4
p=0.001
HU
CPT

Figure 4.6 Induced dimerization of mini-ETAA1 restores function in ETAA1-deficient cells. A) HEK293T, HEK293T ΔETAA1, or HEK293T ΔETAA1 cells complemented with the indicated cDNAs were preincubated with 100 nM AP20187 for 2 hours before incubation with 300 nM CPT +/- 100 nM AP20187 for 6 hours as indicated. Cells were lysed and proteins were separated by SDS-PAGE and immunoblotted with the indicated antibodies. **B)** Quantification of RPA32 S33 phosphorylation in HEK293T ΔETAA1 cells expressing FK-mini-ETAA1 treated with 300 nM CPT and/or 100 nM AP20187 as indicated. Statistical significance was calculated with a one-way ANOVA and Tukey's multiple comparisons test (Mean +/- SD, n=3). **C)** U2OS cells expressing HA-FK-mini-ETAA1 were treated with 300 nM CPT for 3 hours or pre-treated with 100 nM AP20187 for 1 hour before treatment with 300 nM CPT and 100 nM AP20187 for 3 hours. Cells were fixed and stained for RPA70 and HA-FK-mini-ETAA1. Representatives images for each condition are shown. **D)** U2OS ΔETAA1 cells expressing HA-FK, HA-FK-ETAA1, or HA-FK-mini-ETAA1 were generated by lentiviral infection. HA-FK-ETAA1 expression is below limit of detection. **E)** Micronuclei quantification and representative images in the indicated cell types incubated in the absence or presence of 100 nM AP20187 for 24 hours. Statistical significance was calculated with a one-way ANOVA and Tukey's multiple comparisons test (Mean +/- SD, n=3). **F)** Representative images of a clonogenic survival assay of the indicated cell types treated with 1 mM HU +/- 100 nM AP20187 or 5 nM CPT +/- 100 nM AP20187 for 24 hours. **G)** Quantification of survival assay shown in (**F***).* Percent viability for each condition is normalized to the corresponding untreated control. Statistical significance was calculated with a one-way ANOVA and Tukey's multiple comparisons test (Mean +/- SD, n=3 technical triplicate).

clonogenic survival assay upon HU and CPT treatment (Fig 4.6F and G). In the absence of AP20187, expression of FK-mini-ETAA1 has minimal impact on HU sensitivity although it does reduce hypersensitivity to CPT. Induction of mini-ETAA1 dimerization by AP20187 further reduces sensitivity to both HU and CPT (Fig 4.6F and G). These results are not due to other effects of AP20187 as AP20187 does not alter the HU and CPT sensitivity of ΔETAA1 cells (Fig 4.6G). Altogether, these results indicate dimerization of mini-ETAA1 restores functionality and largely rescues the genome instability and HU and CPT sensitivities caused by defective ATR signaling in ETAA1-deficient cells.

Discussion

ATR-ATRIP is a dimer of dimers with two ATR and two ATRIP molecules in a single complex, and this dimerization is required for signaling and checkpoint activity (Ball and Cortez, 2005; Rao et al., 2018; Wang et al., 2017). We now find that dimerization of the TOPBP1 and ETAA1 AADs is also important for ATR activation and function. Like TOPBP1, ETAA1 forms oligomeric complexes in cells. An ETAA1 protein that cannot dimerize (mini-ETAA1) is unable to restore function in ETAA1-deficient cells until it is induced to dimerize with a heterologous dimerization domain. These results are consistent with the hypothesis that TOPBP1 and ETAA1 activate ATR as dimers via the same biochemical mechanism.

Consistent with this conclusion, ATR activation in *Xenopus* egg extracts was previously shown to be strongly stimulated by a GST-TOPBP1 AAD recombinant protein, but only weakly stimulated by an MBP-TOPBP1 AAD (Kim et al., 2020). Addition of an FK tag to MBP-TOPBP1 AAD causes increased ATR activation in the presence, but not absence, of AP20187. The TOPBP1 AAD elutes from a size-exclusion column at a larger than predicted molecular weight (Thada and Cortez, 2019). This difference has been suggested to be because the TOPBP1

AAD itself is a dimer (Kim et al., 2020). However, our data indicate that the TOPBP1 and ETAA1 AADs only form dimers when fused to heterologous dimerization domains or are embedded within the full-length proteins. Therefore, the aberrant elution profiles of these proteins from size-exclusion columns is likely because they are intrinsically disordered and do not form globular domains.

Previous studies examining how TOPBP1 oligomerization affects ATR activation reported conflicting results. Our findings are consistent with those of Zhou et al., (Zhou et al., 2013) who reported that forced TOPBP1 dimerization enhances ATR signaling. In contrast, Liu et al., (Liu et al., 2013) reported that TOPBP1 oligomerization mediated by AKT phosphorylation reduces ATR signaling. These differences could be attributable to differences in the specific oligomeric structures formed in these circumstances. Consistent with our conclusions, a study published during revisions of this manuscript found that TOPBP1 oligomerization occurs via liquid-liquid phase separation and that micron-sized TOPBP1 condensates promote ATR activation (Frattini et al., 2021).

Our domain mapping studies of ETAA1 suggests it contains at least two separable regions that mediate oligomerization. Similar findings have been reported for TOPBP1 oligomerization. One study found that AKT-dependent AAD phosphorylation mediates TOPBP1 oligomerization via the BRCA1 C-terminus 7/8 (BRCT7/8) domains (Liu et al., 2013), while another study reported that the BRCT1/2 and BRCT4/5 domains mediate TOPBP1 oligomerization (Kim et al., 2020). Unlike TOPBP1, ETAA1 is mostly devoid of predicted folded domains and several regions within ETAA1 are predicted to be intrinsically disordered (Thada and Cortez, 2019). Although disordered regions in other proteins often promote phase separation due to self-assembly (Banani et al., 2017), a previous report found no evidence of

ETAA1 biomolecular condensate formation (Frattini et al., 2021). Thus, elucidating specially how ETAA1 oligomerization occurs will require additional studies.

FK-mini-ETAA1, when expressed in ΔETAA1 cells, increases RPA32 phosphorylation in response to CPT treatment, reduces micronuclei formation to the level observed in ΔETAA1 cells expressing full-length ETAA1, and restores the HU and CPT sensitivities of ΔETAA1 cells to wild-type levels only upon mini-ETAA1 induced dimerization. Thus, in addition to ATR-ATRIP and RPA binding, ETAA1 dimerization is needed for its function in the DNA damage response. This result also suggests that these ETAA1 biochemical activities may be sufficient to mediate at least some functions of ETAA1. However, the FK-mini-ETAA1 protein is expressed at higher levels than the full-length protein, which could obscure the need for additional domains or motifs in ETAA1. ETAA1 forms complexes with several other DNA damage response proteins (Bass et al., 2016). Thus, further studies will be needed to determine if there are additional functional motifs within the disordered regions of ETAA1. Nonetheless, the mini-ETAA1 protein may be useful in future structural studies aimed at visualizing the activated form of ATR since the mini-ETAA1 lacks most of the disordered regions and is sufficient induce an active ATR conformation.

In conclusion, dimerization of the ATR activators ETAA1 and TOPBP1 is important for their function in ATR activation. Regulation of TOPBP1 and ETAA1 oligomerization, possibly mediated by post-translation modifications and/or phase separation, may facilitate precise spatiotemporal control of ATR signaling.

Conclusions

The ATR^{Mec1}-ATRIP^{Ddc2} complex is a dimer of dimers that forms a butterfly like structure, and complex dimerization is required for function. We now show that TOPBP1 and ETAA1 AAD dimerization is required for ATR activation. ETAA1 forms oligomeric complexes in cells, and oligomerization is mediated by at least two distinct regions of the protein. Fusion of ETAA1 amino acids 2-305 to the RPA70 and RPA32 interaction motifs creates a mini-ETAA1 protein that retains all known function motifs, but unlike full-length ETAA1, mini-ETAA1 does not form oligomeric complexes. Mini-ETAA1 expression fully rescues defective ATR signaling and genomic instability in ETAA1-deficient cells only upon mini-ETAA1 induced dimerization. These results support a model whereby TOPBP1 and ETAA1 activate ATR as dimers via the same biochemical mechanism.

CHAPTER V

ATR PREVENTS FORK COLLAPSE IN RESPONSE TO LAGGING STRAND REPLICATION STRESS

Introduction

Each time a cell divides, it must accurately duplicate its genome to ensure each daughter cell receives the correct amount of genetic material. This process, called DNA replication, requires a plethora of proteins that function in a spatiotemporally regulated manner (Burgers and Kunkel, 2017). DNA replication begins at origins of replication and involves DNA unwinding by helicases and synthesis of nascent DNA by polymerases. In eukaryotes, the CMG helicase unwinds DNA while polymerases α, δ, and ε (Pol α, δ, and ε) synthesize DNA (Burgers and Kunkel, 2017). Based on the polarity of DNA and because DNA polymerases synthesize DNA in the 5'-3' direction, DNA replication occurs differently on the leading and lagging strands. On the leading strand after priming and initial synthesis by Pol α-Primase, nascent DNA is synthesized continuously by Pol ε (Pursell et al., 2007). On the lagging strand, DNA synthesis occurs discontinuously via the generation of Okazaki fragments (Okazaki et al., 1968). Following initial priming and DNA synthesis by Pol α-Primase, Okazaki fragment synthesis is completed by Pol δ (McElhinny et al., 2008). Thus, while leading strand synthesis only requires Pol α-Primase for initiation, lagging strand synthesis requires Pol α-Primase for the synthesis of every Okazaki fragment.

DNA lesions, repetitive sequences, and collisions with transcriptional machinery can interfere with DNA replication (Cortez, 2019). Obstacles that stop or slow DNA replication forks activate the replication stress response (RSR). The RSR coordinates DNA replication with DNA

repair to ensure replication accuracy is maintained, and coordinates DNA replication with cell cycle progression to ensure cells with damaged or incompletely replicated DNA do not undergo cell division (Ciccia and Elledge, 2010). ATR is master regulator of the RSR. Upon fork stalling, ATR is activated and phosphorylates numerous proteins, including its main downstream effector kinase CHK1, to slow origin firing, stabilize stalled replication forks, and slow cell cycle progression (Saldivar et al., 2017).

HU is routinely used to induce replication stress and study the RSR. HU inhibits RNR, and thereby depletes cellular dNTP pools (Singh and Xu, 2016). Low dNTP levels stall replication forks and cause robust ATR signaling. However, HU-induced fork stalling stalls both leading and lagging strand synthesis. Recent evidence indicates that strand-specific DNA lesions affect replication forks differently. While lagging strand lesions are efficiently bypassed, leading strand lesions substantially reduce fork progression and result in DNA unwinding ahead of the lesion (Taylor and Yeeles, 2018). Given this difference, and the differences between leading and lagging strand DNA replication, it is tempting to speculate that strand-specific lesions may result in distinct RSRs. However, it is currently unknown if leading or lagging strand lesions activate RSRs distinct from each other or distinct from RSRs activated by stalling both strands.

Here, I used the small molecule CD437 to study the RSR upon lagging strand stalling. CD437 is a selective Pol α inhibitor that binds to and inhibits the Pol α catalytic subunit POLA1 (Han et al., 2016). Thus, at active replication forks CD437-dependent Pol α inhibition stalls lagging strand synthesis by preventing Okazaki fragment generation. CD437 causes an ~40% reduction in replication fork speed, the accumulation of ssDNA on the lagging strand, and eventually DSBs due to RPA exhaustion. Stalling lagging strand synthesis also activates TOPBP1-dependent ATR signaling, which prevents fork collapse upon strand uncoupling.

Results

Pol α inhibition causes rapid accumulation of ssDNA and eventually DSBs

To begin to explore how Pol α inhibition affects replication forks, I analyzed replication fork speed in cells treated with CD437. Cells were pulsed with CldU for 15 minutes to label ongoing replication forks, and then pulsed with IdU for 30 minutes in the absence or presence of CD437. Compared to untreated cells, replication forks in cells treated with CD437 slowed by approximately 35% (Fig 5.1A). I also measured ssDNA formation in cells treated with CD437. Compared to 30 minutes of HU, which induces no detectable ssDNA above the amount in untreated cells, 30 minutes of CD437 causes a substantial accumulation of ssDNA (Fig 5.1B). Prolonged treatment with CD437 causes an even greater accumulation of ssDNA (Fig 5.1C). The increase in ssDNA caused by Pol α inhibition is due to continued DNA synthesis by the leading strand because cells treated with HU and CD437 simultaneously, which stalls DNA synthesis on both strands, suppresses the ssDNA accumulation caused by CD437 alone (Fig 5.1B).

To more directly examine DNA damage caused by Pol α inhibition, I performed Comet assays to measure DSBs in cells treated with CD437. CD437 causes a modest increase in DSBs after 2 hours, and a larger and statistically significant increase after 3 hours (Fig 5.1D). Given the large amount of ssDNA generated by Pol α inhibition, I suspected the DSBs formed upon prolonged CD437 treatment were likely due to RPA exhaustion. To test this, I compared DSBs in cells treated with CD437 to DSBs in cells treated with CD437 that overexpressed RPA. RPA overexpression suppresses the DSBs that form after 3 hours of CD437 treatment (Fig 5.1E). Together, these results indicate that Pol α inhibition stalls lagging strand synthesis, but only partially reduces leading strand synthesis (strand uncoupling). Continued leading strand

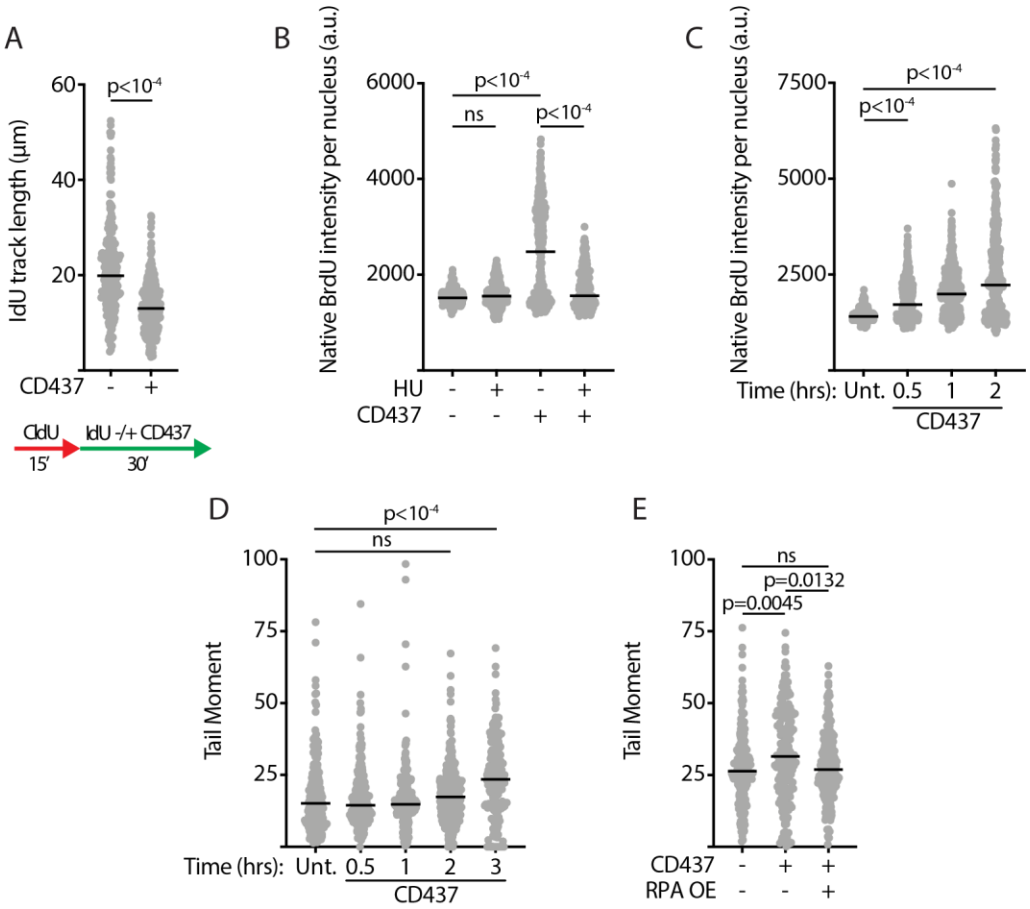

Figure 5.1 Pol α inhibition causes rapid accumulation of ssDNA and eventually DSBs. A) HeLa cells were pulsed with CldU and IdU +/- CD437 as indicated and processed for DNA combing. IdU tracks were measured manually. **B)** HeLa cells were labeled with 10 μM BrdU for 24 hours, synchronized overnight with 2 mM thymidine, and then were left untreated or treated with 3 mM HU, 5 μM CD437, or both for 30 minutes. Cells were fixed and stained for BrdU. **C)** HeLa cells were labeled with 10 μM BrdU for 24 hours, synchronized overnight with 2 mM thymidine, and then were left untreated or treated with 5 μM CD437 for 0.5-2 hours. Cells were fixed and stained for BrdU. **D)** Synchronized HeLa cells were treated with 5 μM CD437 for 0.5-3 hours and then processed for neutral comet assay. Tail moments were quantified using OpenComet software. **E)** Synchronized HeLa cells and cells overexpressing RPA were treated with 5 μM CD437 for 3 hours and then processed for neutral comet assay. Tail moments were quantified using OpenComet software. In all panels, statistical significance was calculated with a Kruskal-Wallis test and Dunn's multiple comparisons test. Black bars indicate medians.

synthesis upon lagging strand stalling causes ssDNA accumulation that eventually results in DSBs due to RPA exhaustion.

Pol α inhibition activates ATR

RPA-coated ssDNA recruits ATR-ATRIP to stalled replication forks through a direct interaction between ATRIP and RPA (Zou and Elledge, 2003). Because Pol α inhibition induces substantial ssDNA formation, we examined the recruitment of ATR-ATRIP to replication forks in response to CD437 using isolation of proteins on nascent DNA (iPOND). Indeed, ATR and ATRIP are two of the most highly enriched proteins at replication forks upon CD437 treatment (Mehta et al., in preparation). To directly examine ATR activation in response to CD437, I measured CHK1 and RPA32 phosphorylation. In HCT116 cells, compared to HU, CD437 results in very little CHK1 phosphorylation. By contrast, CD437 results in robust RPA32 phosphorylation, while HU induces no RPA32 phosphorylation above background levels (Fig 5.2A). Interestingly, when I assessed CD437-dependent ATR signaling in HEK293T cells, I observed that although CD437 results in less CHK1 phosphorylation than HU, CHK1 phosphorylation induced by these drugs is more similar in this cell line (Fig 5.2B). I compared HU- and CD437-dependent ATR signaling in three additional cell types and similar to HCT116 and HEK293T cells, found that CD437 results in more RPA32 phosphorylation, but less CHK1 phosphorylation compared to HU (Fig 5.2C-E). Differences between HU- and CD437-dependent CHK1 phosphorylation are likely cell-type specific. Another ATR substrate, MCM2, is phosphorylated similarly in response to CD437 or HU (Mehta, unpublished). Thus, strand uncoupling caused by Pol α inhibition results in recruitment and activation of ATR, but results in less CHK1 phosphorylation than occurs upon stalling of both strands.

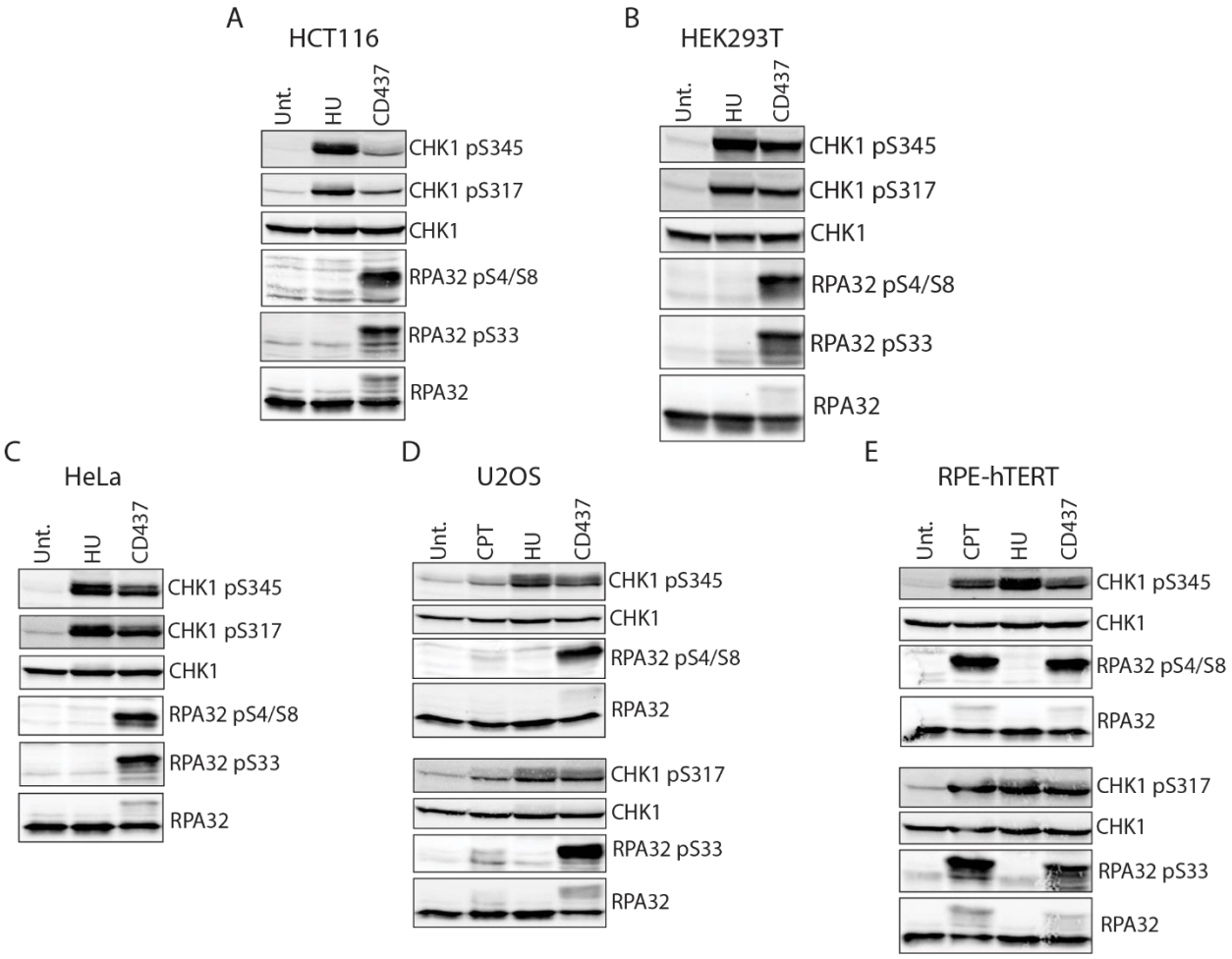

Figure 5.2 Pol α inhibition activates ATR. A-E) The indicated cells types were treated with 100 nM CPT for 4 hours (**D-E**), 3 mM HU for 30 minutes, or 5 μM CD437 for 30 minutes. Cells were lysed and proteins were separated by SDS-PAGE prior to detection by immunoblotting. RPE-hTERT cells were treated with 1 μM CD437 (**E**).

CLASPIN overexpression increases CHK1 phosphorylation upon strand uncoupling

Less CHK1 phosphorylation in response to lagging strand stalling compared to stalling both strands was surprising given that Pol α inhibition causes substantial ssDNA accumulation and results in more ATR-ATRIP recruitment to forks than is observed upon HU treatment (Mehta et al., in preparation). A closer examination of the iPOND dataset revealed that CLASPIN, which mediates ATR-dependent CHK1 phosphorylation in response to replication stress (Kumagai and Dunphy, 2000), is recruited to forks upon stalling both strands, but not upon lagging strand stalling (Mehta et al., in preparation). To determine if less CHK1 phosphorylation in response to Pol α inhibition is due to lack of CLASPIN recruitment, I overexpressed CLASPIN in HCT116 cells exposed to CD437. CLASPIN overexpression increases CD437-dependent CHK1 phosphorylation but does not increase CHK1 phosphorylation to the level observed upon HU treatment (Fig 5.3A).

CD437-dependent CHK1 phosphorylation is most similar to HU-dependent CHK1 phosphorylation in HEK293T cells. A comparison of CLASPIN expression levels between HCT116 and HEK293T cells revealed CLASPIN is more highly expressed in HEK293T cells than HCT116 cells (Fig 5.3B). Altogether, these results suggest that lagging strand stalling induces less CHK1 phosphorylation than stalling both strands because lagging strand stalling does not result in CLASPIN recruitment and that cell-type specific differences in CD437-dependent CHK1 phosphorylation are at least partially due to CLASPIN expression level differences.

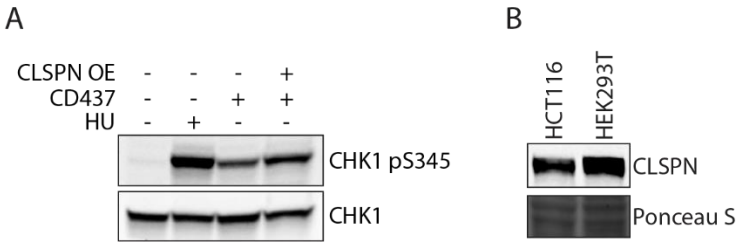

Figure 5.3 CLASPIN overexpression increases CHK1 phosphorylation upon strand uncoupling. A) HCT116 cells were treated with 3 mM HU or 5 μM CD437, and HCT116 cells overexpressing CLASPIN were treated with 5 μM CD437 for 30 minutes. Cells were lysed and proteins were separated by SDS-PAGE. CHK1 pS345 and CHK1 were detected by immunoblotting. **B)** Synchronized HCT116 and HEK293T cells were lysed and proteins were separated by SDS-PAGE. CLASPIN was detected by immunoblotting.

ATR prevents fork collapse upon strand uncoupling

ATR recruitment to and activation at stalled or damaged replication forks results in fork stabilization, promotes efficient fork restart, activates the intra-S phase checkpoint, and suppresses origin firing (Saldivar et al., 2017). Because Pol α inhibition causes ATR activation, I assessed the specific function(s) of ATR at replication forks where lagging strand synthesis is inhibited. While treatment of cells with CD437 for 1 hour causes no detectable increase in DSBs, co-treatment of cells with CD437 and ATRi for the same time does cause increased DSBs (Fig 5.4A). This result is not due to ATR inhibition alone as treatment of cells with ATRi for 2 hours causes no detectable increase in DSBs (Fig 5.4B). Thus, ATR activation in response to strand uncoupling prevents DSB formation.

DSBs caused by ATR inhibition could be the result of replication fork collapse, increased dormant origin firing, or both. I used DNA Combing to directly measure fork collapse in cells treated with CD437, ATRi, or both CD437 and ATRi. Cells were pulsed with CldU (red tracks) for 20 minutes in the absence or presence of drugs, then pulsed with IdU (green tracks) for 20 minutes. Tracks with both red and green indicate continued DNA synthesis after drug removal, while red only tracks indicate fork collapse. CD437 alone causes an increase in fork collapse (Fig 5.4C), which is surprising given that CD437 does not induce DSBs until at least 2 hours of treatment. One possible explanation for this discrepancy is that although short-term Pol α inhibition may cause a slight increase in fork collapse, DSBs are not observed by Comet assays until a majority of forks have collapsed. Compared to untreated cells, ATRi alone does not cause an increase in fork collapse. The combined treatment of CD437 and ATRi causes an even greater

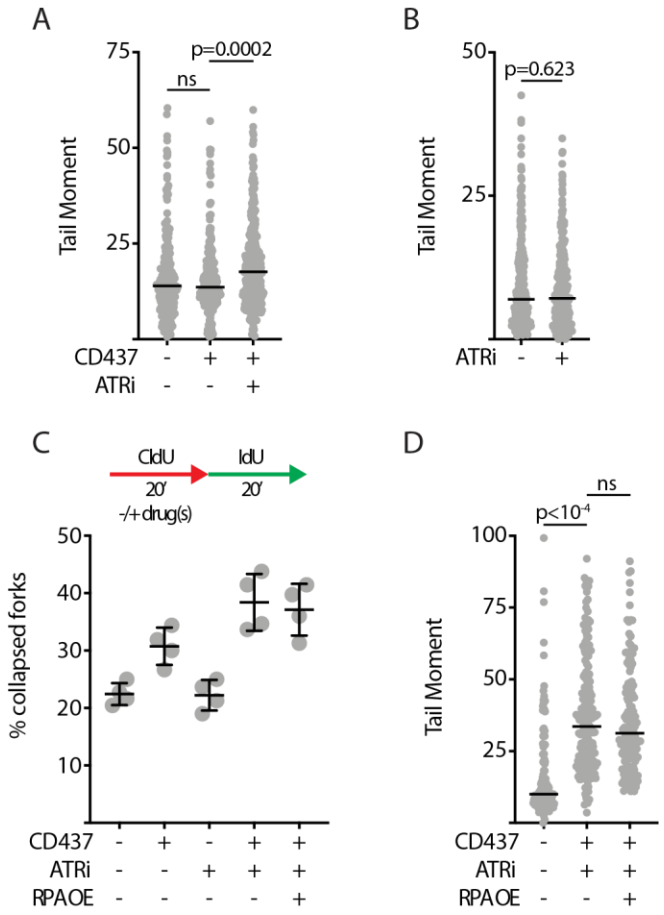

Figure 5.4 ATR prevents fork collapse upon strand uncoupling. A) Synchronized HeLa cells were untreated, treated with 5 μM CD437, or 5 μM CD437 and 1 μM ATRi (VX-970) for 1 hour and then processed for neutral comet assay. Tail moments were quantified using OpenComet software. **B)** Synchronized HeLa cells were untreated or treated with 1 μM ATRi (VX-970) for 2 hours and then processed for neutral comet assay. Tail moments were quantified using OpenComet software. **C)** HeLa cells and cells overexpressing RPA were pulsed with CldU +/- drugs and IdU as indicated and processed for DNA combing. Fork collapse percentage was quantitated manually. **D)** Synchronized HeLa cells or cells overexpressing RPA were treated with 5 μM CD437 and 1 μM ATRi (VX-970) for 1 hour and then processed for neutral comet assay. Tail moments were quantified using OpenComet software. In all panels where indicated, statistical significance was calculated with a Kruskal-Wallis test and Dunn's multiple comparisons test.

incidence of fork collapse compared to CD437 alone, indicating that ATR prevents fork collapse when lagging strand synthesis is inhibited (Fig 5.4C). Fork collapse in response to CD437+ATRi is not due to RPA exhaustion as RPA overexpression does not rescue fork collapse in this condition (Fig 5.4C). In addition, RPA overexpression does not prevent DSB formation in response to CD437+ATRi treatment (Fig 5.4D). Finally, DSBs caused by CD437+ATRi cannot be prevented by inhibiting origin firing (Mehta, unpublished). Together, these results indicate that in response to strand uncoupling, ATR prevents fork collapse not through inhibition of origin firing and RPA exhaustion, but more likely by preventing aberrant fork remodeling and/or nuclease-mediated cleavage of replication forks.

ATR activation in response to strand uncoupling is TOPBP1-dependent

ATR activation requires the assembly of a multi-protein complex that contains at least one ATR activating protein. Metazoan cells contain at least two ATR activating proteins, TOPBP1 and ETAA1 (Saldivar et al., 2017). TOPBP1 is the predominant ATR activator when cells are exposed to exogenous sources of replication stress, while ETAA1 is the primary activator in undamaged cells (Bass and Cortez, 2019; Saldivar et al., 2018). I assessed whether ATR activation in response to Pol α inhibition is TOPBP1- or ETAA1-dependent. Compared to control cells, cells depleted of RAD9, which disrupts TOPBP1-dependent ATR activation, exhibit less CHK1 and RPA32 phosphorylation in response to CD437. By contrast, cells depleted of ETAA1 show no detectable defect in CHK1 or RPA32 phosphorylation when treated with CD437 (Fig 5.5A). ETAA1Δ cells also exhibit no defect in CHK1 phosphorylation upon CD437 treatment, and only a slight reduction in RPA32 phosphorylation (Fig 5.5B). These results indicate that ATR activation caused by strand uncoupling is TOPBP1-dependent.

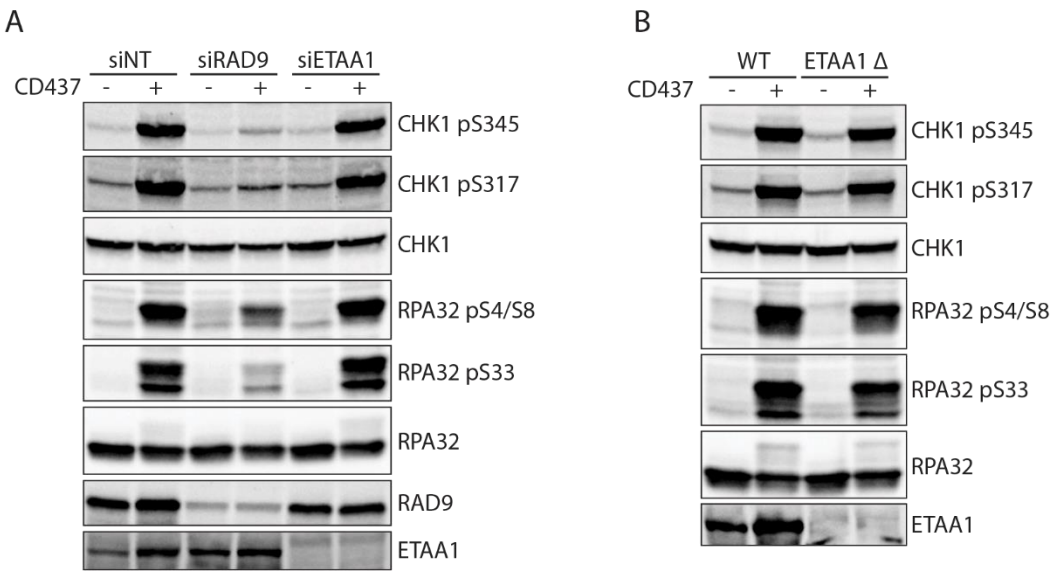

Figure 5.5 ATR activation in response to strand uncoupling is TOPBP1-dependent. A) HeLa cells, cells depleted of RAD9, or cells depleted of ETAA1 were untreated or treated with 5 μM CD437 for 30 minutes. Cells were lysed and proteins were separated by SDS-PAGE prior to detection by immunoblotting. **B)** HEK293T WT or ETAA1Δ cells were untreated or treated with 5 μM CD437 for 30 minutes. Cells were lysed and proteins were separated by SDS-PAGE prior to detection by immunoblotting.

Discussion

Pol α inhibition stalls lagging strand synthesis and partially inhibits leading strand synthesis, suggesting human cells possess a mechanism to at least partially couple leading and lagging strand synthesis during DNA replication. Previous studies examining leading and lagging strand replication coordination in *in vitro* systems found that lagging strand synthesis, and specifically primer synthesis on the lagging strand, slows leading strand polymerization (Lee et al., 2006; Yao et al., 2009). However, a more recent report found that leading and lagging strand polymerases function independently of each other within single replisomes (Graham et al., 2017). Another recent study reported that leading and lagging strand polymerases function independently of each other in mammalian cells upon Pol α inhibition (Ercilla et al., 2020). Several possibilities could explain these differences including the model system and/or type and dose of drugs used. My data indicates that while leading strand replication can occur in the absence of lagging strand replication, leading and lagging strand DNA synthesis are not completely autonomous processes.

Stalling lagging strand synthesis slows leading strand synthesis in multiple human cell types (Mehta et al., in preparation), but the mechanism for this slowing is not understood. One possibility is that ATR signaling upon strand uncoupling reduces CMG activity to slow DNA unwinding and limit ssDNA formation. Consistent with this hypothesis, Mec1 phosphorylates Mcm4 in response to replication stress (Randell et al., 2010), and deletion of Mec1-depedent phosphorylation sites within Mcm4 abrogates DNA damage checkpoint signaling (Sheu et al., 2014). In addition, Rad53 limits DNA unwinding and ssDNA formation in response to replication stress, and this result has been observed in cells and with a reconstituted *in vitro* system (Devbhandari and Remus, 2020; Gan et al., 2017). In human cells, both ATR and CHK1

have been shown to phosphorylate MCM complex components but whether ATR-CHK1-dependent MCM phosphorylation regulates CMG activity is not clear (Cortez et al., 2004; Han et al., 2015). Pol α inhibition induces ATR-dependent MCM2 phosphorylation, but interestingly, co-treatment of cells with CD437 and ATRi reduces leading strand synthesis even more than CD437 alone (Mehta, unpublished). However, this result could be due to increased fork collapse caused by accelerated leading strand synthesis, which would result in visualization of shorter replication forks.

ATR activation upon strand uncoupling prevents replication fork collapse, but how ATR preserves fork stability in this scenario is not clear. ATR prevents fork collapse upon stalling of both strands by reducing origin firing and regulating numerous RSR proteins, including the fork remodeler SMARCAL1 (Dungrawala et al., 2015; Toledo et al., 2013). ATR-dependent SMARCAL1 phosphorylation prevents aberrant fork remodeling and fork cleavage by SLX4-dependent nucleases (Couch et al., 2013). Given that fork collapse upon strand uncoupling is not due to RPA exhaustion caused by increased origin firing, it is possible that ATR inhibition upon lagging strand stalling results in fork collapse due to de-regulation of fork remodeling proteins and/or nuclease activity. Additional studies are needed to specifically elucidate how ATR stabilizes replication forks upon strand uncoupling.

ATR activation upon strand uncoupling is TOPBP1-dependent. TOPBP1-dependent ATR activation requires the 9-1-1 complex, which is loaded onto a ssDNA-dsDNA junction with a free 5’ end by RAD17-RFC2-5 (Bermudez et al., 2003; Ellison and Stillman, 2003; Zou et al., 2003). How this structure is generated upon lagging strand stalling remains an important, unanswered question. One possibility is that continued RNA primer synthesis on the lagging strand by Pol α-Primase to generate 5’ ssDNA-RNA-DNA junctions is sufficient for 9-1-1

loading. A second possibility is that fork reversal upon lagging strand stalling generates the TOPBP1-activating structure. However, current data does not support this model as depletion of SMARCAL1, HLTF, ZRANB3, or RAD51 upon Pol α inhibition does not affect ATR signaling (Mehta et al., in preparation). A third possibility is that RPA-coated ssDNA generated upon strand uncoupling recruits TOPBP1. In support of this hypothesis, a previous study found that TOPBP1 binds RPA-coated ssDNA in *Xenopus* egg extracts (Acevedo et al., 2016). A fourth possibility is that re-priming occurs on the lagging strand upon Pol α inhibition by another polymerase. Preliminary data indicates that depletion of PRIMPOL, a DNA dependent DNA primase-polymerase, partially reduces ATR signaling upon lagging strand stalling (data not shown and Mehta et al., in preparation). Thus, repriming on the lagging strand by PRIMPOL may be a mechanism by which the 5' ssDNA-dsDNA junction is generated upon strand uncoupling.

Despite more ssDNA generated and more ATR-ATRIP recruited to replication forks upon strand uncoupling than stalling both strands, strand uncoupling induces less CHK1 phosphorylation than stalling of both strands. This is due to lack of CLASPIN recruitment upon strand uncoupling. CLASPIN is an intrinsic component of the replisome and interacts with multiple replication factors including PCNA, CDC45, Pol ε, and RPA (Lee et al., 2005; Smits et al., 2019), but what causes increased CLASPIN recruitment to forks where both strands are stalled as opposed to just the lagging strand is not known.

In conclusion, using a selective Pol α inhibitor, I found that leading and lagging strand synthesis is partially coupled in human cells, and that strand uncoupling leads to recruitment and activation of ATR. TOPBP1-dependent ATR signaling upon lagging strand stalling regulates fork stability but does not induce robust replication checkpoint signaling.

Conclusions

Previous studies examining coordination of leading and lagging strand synthesis during DNA replication reported conflicting results. My data indicates leading and lagging strand synthesis is partially coupled in mammalian cells. Selectively stalling lagging strand synthesis causes strand uncoupling and ssDNA accumulation on the lagging strand, resulting in TOPBP1-dependent ATR activation. ATR activation induced by strand uncoupling prevents fork collapse; however, ATR-dependent checkpoint signaling in response to lagging strand stalling is substantially attenuated compared to checkpoint signaling induced by stalling both strands.

CHAPTER VI

DISCUSSION AND FUTURE DIRECTIONS

Mechanism of ATR^{Mec1} activation

Function of the predicted coiled coils and critical aromatic residues

Current data suggests that the Mec1 activators employ a similar mechanism to activate Mec1 and that the ATR activators employ a similar mechanism to activate ATR. A mutation in the ATR PRD that attenuates ATR activation by TOPBP1 also attenuates activation by ETAA1 (Bass et al., 2016). TOPBP1 binds the ATR-ATRIP complex through an interaction with the ATR PRD and ATRIP. A mutation in ATRIP, termed ATRIP-top, abrogates the TOPBP1-ATRIP interaction and impairs ATR-dependent checkpoint signaling (Mordes et al., 2008a). Interestingly, when an analogous mutation is introduced into Ddc2, termed ddc2-top, the Dpb11-Mec1-Ddc2 interaction is lost and Mec1 signaling is perturbed (Mordes et al., 2008a; Mordes et al., 2008b). It is currently unknown if the ATRIP-top mutation impairs ETAA1-dependent signaling, but together, this data suggests that the ATR^{Mec1} activation mechanism is conserved from yeast to humans.

Given that TOPBP1, and likely ETAA1, contact both ATR and ATRIP to stimulate ATR activity, the question arises as to which regions of the AADs contact ATR and which contact ATRIP? I have shown that the ETAA1 and TOPBP1 predicted coiled coils alone bind ATR-ATRIP, indicating that the predicted coiled coils are an ATR-ATRIP interacting surface on the AADs. Whether the predicted coiled coils contact ATR or ATRIP remains an open question. If the predicted coiled coils bind one subunit of the ATR-ATRIP complex, another AAD region

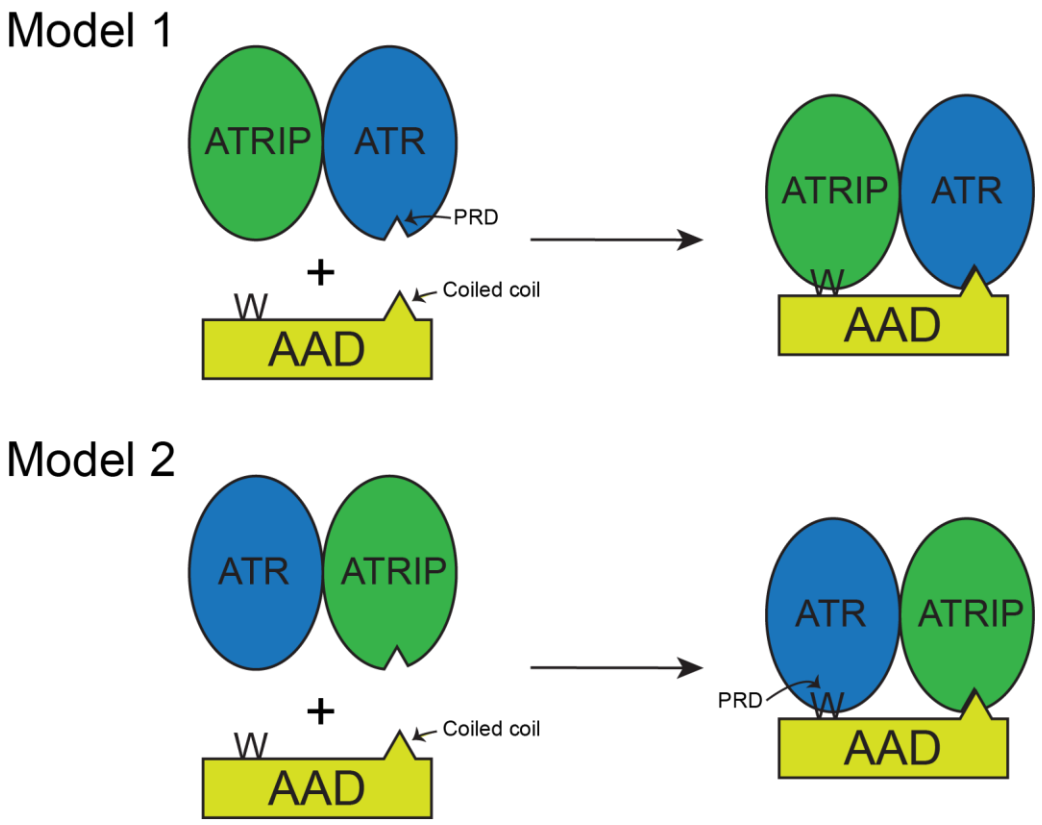

Figure 6.1: Models of ATR-ATRIP binding by an AAD. In one scenario, the predicted coiled coil binds the ATR PRD, while the critical tryptophan and surrounding residues bind ATRIP. In the other scenario, the reverse occurs.

must bind the other subunit (Fig 6.1). The likely candidate for this second binding interaction is the critical tryptophan in the AADs. Although there is no data demonstrating a direct interaction between the critical tryptophans and ATR-ATRIP, mutation of these residues reduces the ETAA1- and TOPBP1-ATR interactions and impairs ATR signaling. In addition, the critical tryptophans and adjacent residues are conserved from *Xenopus* to humans (Bass et al., 2016; Haahr et al., 2016; Kumagai et al., 2006; Lee et al., 2016). A high-resolution atomic structure of ATR-ATRIP bound to an AAD will delineate exactly how the AADs bind ATR-ATRIP to stimulate kinase activity.

If the ATR^{Mec1} activation mechanism is conserved from yeast to humans, the MADs would be expected to possess predicted coiled coils that bind Mec1-Ddc2. However, unlike ETAA1 residues 183-215 (p-score =0.01) and TOPBP1 residues 1054-1083 (p-score=0.074), the MADs contain no obvious predicted coiled coils (McDonnell et al., 2006). The residues in each MAD with the highest likelihood of forming coiled coils include Dpb11 residues 622-651 (p-score=0.095), Ddc1 residues 456-485 (p-score=0.15), and Dna2 residues 281-310 (p-score=0.099) (Fig 6.2A-C). The aforementioned residues in Ddc1 and Dna2 are not required for Mec1 activation because small peptides containing only the critical aromatic residues and immediately flanking amino acids are sufficient to activate Mec1 in an *in vitro* kinase assay (Wanrooij et al., 2016). It is worth noting however, that Mec1 activation by these small peptides is several orders of magnitude lower than by full-length MADs. Interestingly, the authors of this study were not able to generate a small peptide with the two aromatic residues from Dpb11 that was capable of activating Mec1. This result suggests that perhaps an additional component in the Dpb11 MAD is required for Mec1 activation and that Dpb11-dependent Mec1 activation may be

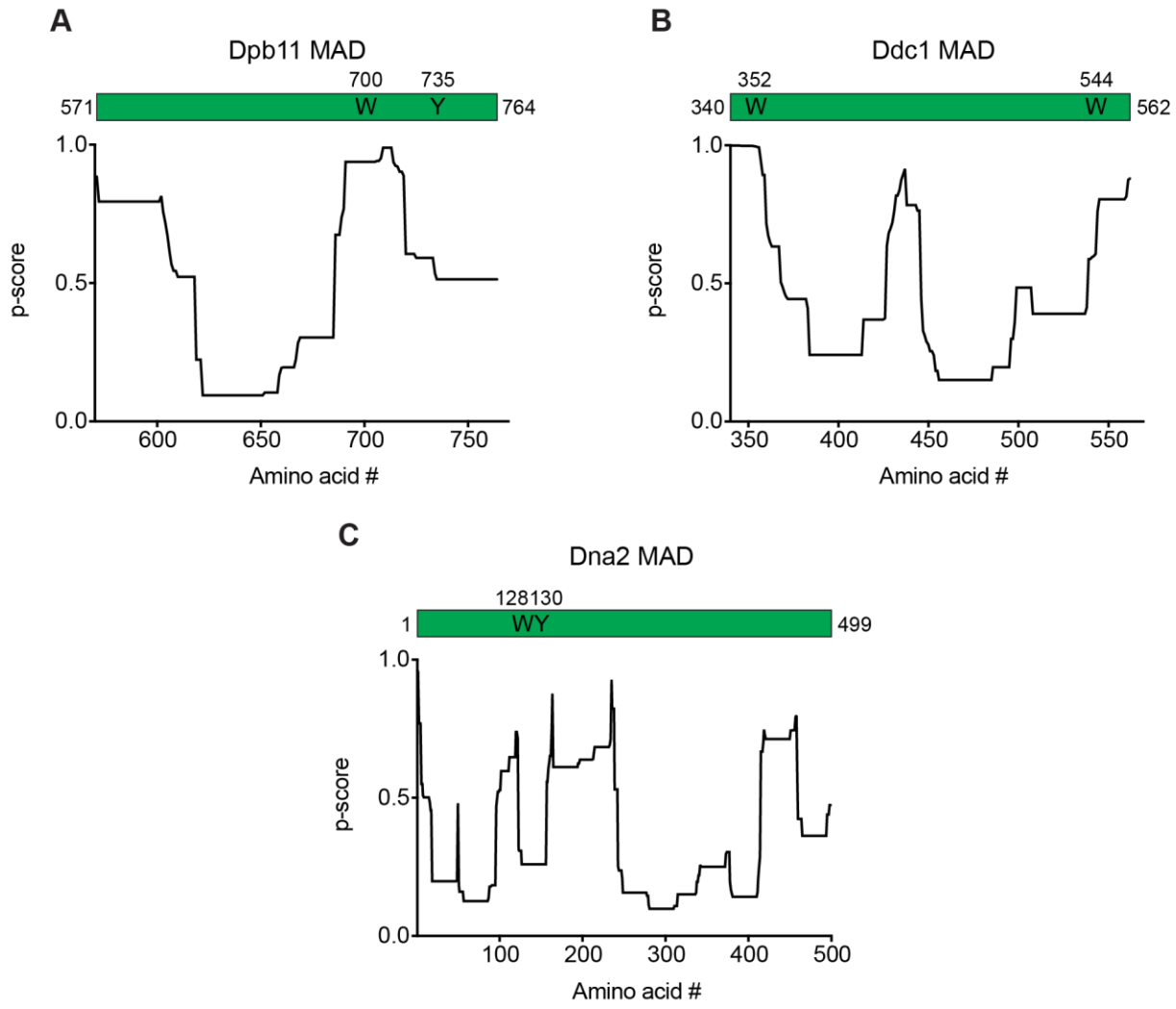

Figure 6.2: MAD coiled coil predictions. A-C)) Predicted coiled coil per residue p-scores of the Dpb11 MAD (**A**), Ddc1 MAD (**B**), and Dna2 MAD (**C**). Lower p-scores indicate a greater likelihood of forming a coiled coil. Predicted coiled coil p-scores were calculated using Paircoil2 (McDonnell et al., 2006). The critical aromatic amino acids within each MAD are also shown.

distinct from Ddc1- and Dna2-dependent Mec1 activation. Cellular data also indicates that Dpb11- and Ddc1-dependent Mec1 activation may occur via different mechanisms. Overexpression of Dpb11 rescues the HU sensitivity of ddc2-top yeast, but Ddc1 overexpression does not (Mordes et al., 2008b).

NBS1 was previously reported to be an ATR activator (Kobayashi et al., 2013), but the region of NBS1 that interacts with ATR, BRCT domain 2, bears no resemblance to the ETAA1 and TOPBP1 AADs. If NBS1 is indeed an ATR activator, then two distinct ATR activation mechanisms likely exist in metazoan cells. Therefore, it would not be unreasonable to hypothesize that more than one Mec1 activation mechanism exists in yeast. Perhaps $TOPBP1^{Dpb11}$-dependent ATR^{Mec1} activation is conserved from yeast to humans, but additional ATR^{Mec1} activating mechanisms (Ddc1 and Dna2 in yeast and NBS1 in metazoans) also exist. If biochemical activation of ATR^{Mec1} occurs through multiple, distinct mechanisms, it will be imperative to identify how these mechanisms differentially affect ATR^{Mec1} signaling in cells.

Mapping the predicted coiled coil interaction surface on ATR or ATRIP

As described above, an outstanding question is whether the AAD predicted coiled coils contact ATR or ATRIP. While a high-resolution atomic structure of ATR-ATRIP bound to an AAD would answer this question, alternative approaches could also be used. One possibility would be to perform a yeast-two-hybrid screen where AADs containing or lacking the predicted coiled coil are used as bait proteins to screen an ATR fragment library and ATRIP fragment library. AADs with an intact predicted coiled coil should bind the ATR PRD and ATRIP (Mordes et al., 2008a). However, if the predicted coiled coil directly contacts one subunit of the ATR-ATRIP complex, an AAD lacking this motif should only interact with either ATR or ATRIP. Another possibility would be to perform binding assays as described in Chapter III. A

purified GST-tagged predicted coiled coil could be incubated with nuclear extracts expressing only Flag-ATR or HA-ATRIP. To rule out the possibility of endogenous ATR or ATRIP bridging an interaction between the predicted coiled coil and Flag-ATR or HA-ATRIP, mutant forms of ATR and ATRIP that do not interact with each other could be used. It is important to note, however, that one caveat of this approach assumes the predicted coiled coil-ATR or ATRIP interaction occurs independently of ATR-ATRIP complex formation.

Regulation of ATR activation by TOPBP1 and ETAA1 dimerization

Consistent with the hypothesis that TOPBP1 and ETAA1 activate ATR via the same mechanism, I have found that TOPBP1 and ETAA1 AAD dimerization augments ATR activation. My data also implies that dimerization (or oligomerization) of full-length TOPBP1 and ETAA1 in cells positively regulates ATR signaling. Whether a similar mechanism is employed by the Mec1 activators to stimulate Mec1 signaling remains unknown. How or if MAD dimerization affects Mec1 activation or if Dpb11, Ddc1, and/or Dna2 form oligomeric complexes warrants investigation.

Further delineating how TOPBP1 and ETAA1 oligomerization are regulated also warrants investigation. AKT-dependent TOPBP1 AAD phosphorylation mediates TOPBP1 oligomerization via interactions between the AAD and BRCT7/8 domains, and this oligomerization reduces ATR signaling (Liu et al., 2013). However, ATM-dependent TOPBP1 AAD phosphorylation and CDK- and ATR-dependent ETAA1 AAD phosphorylation enhances TOPBP1- and ETAA1-dependent ATR activation respectively (discussed further below) (Achuthankutty et al., 2019; Yoo et al., 2007). Thus, differential AAD phosphorylation events have opposing effects on ATR activation, but whether the stimulatory phosphorylation events regulate TOPBP1 and/or ETAA1 oligomerization is unclear. Future studies are needed to address

these possibilities, but my data indicates ETAA1 oligomerization occurs independently of the AAD and is therefore unlikely to be affected by AAD phosphorylation.

ETAA1 oligomerization is mediated by at least two distinct regions within the protein, but the mechanism by which ETAA1 self-associates is not clear. Given that several regions within ETAA1 are predicted to be intrinsically disordered and that ETAA1 contains a repetitive sequence element, one possibility is that ETAA1 oligomerization occurs through formation of biomolecular condensates. Intrinsically disordered proteins often undergo phase separation to form biomolecular condensates via several weak intermolecular interactions mediated by repetitive sequence elements (Banani et al., 2017). Such phase separation would explain the difficulty in mapping ETAA1 oligomerization domains/motifs.

Consistent with the hypothesis that ETAA1 phase separation mediates oligomerization and hence function, several studies have shown that other proteins undergo functionally relevant phase separation at sites of DNA damage. Laser-induced microirradiation results in PARP-1-dependent recruitment and phase separation of intrinsically disordered proteins FUS/TLS (fused in sarcoma/translated in sarcoma), EWS (ewing sarcoma), and TAF15 (TATA box-binding protein-associated factor 68 KDa) at DNA strand breaks (Altmeyer et al., 2015; Patel et al., 2015), and 53BP1 phase separation in irradiated cells promotes DSB repair and regulates expression of p53 and p53-dependent genes (Kilic et al., 2019; Pessina et al., 2019). In addition, *Escherichia coli* single stranded (ss) DNA-binding protein (SSB) undergoes phase separation under cell-like conditions, and this phase separation occurs through a multitude of interactions involving both the intrinsically disordered linker (IDL) and structural regions of the protein. SSB phase separation has been proposed as a mechanism by which *E. coli* can more rapidly respond to genotoxic stress and repair DNA damage (Harami et al., 2020). Thus, similar ETAA1 phase

separation to increase local ETAA1 concentration at DNA damage sites may increase ATR activation and facilitate protein-protein interactions between ETAA1 and additional DDR proteins (discussed below).

Mechanisms of PIKK activation

The similar domain architectures and three-dimensional structures of the PIKKs predicts these kinases may be activated via similar mechanisms. One such similarity is the oligomeric state of PIKK activating proteins. TOPBP1 and ETAA1 form oligomeric complexes, and dimerization of these proteins is required for efficient ATR activation. Similarly, MRN and KU70/80, which activate ATM and DNA-PKcs respectively, are also dimers (Francoeur et al., 1986; Mimori et al., 1986; Reeves, 1985; Syed and Tainer, 2018). Biochemical experiments indicate RAD50 dimerization is essential for ATM activation (Lee et al., 2013), and KU70/80, which is an obligate heterodimer, together with DNA-PKcs forms the active DNA-PK holoenzyme (Blackford and Jackson, 2017). RHEB, which activates mTORC1, does not self-associate, but activation of the dimeric mTORC1 complex requires simultaneous binding of two RHEB molecules (Yang et al., 2017). Thus, PIKK activation likely requires binding of two activator molecules.

The predicted coiled coils in TOPBP1 and ETAA1 contact either ATRIP or the ATR PRD. However, potential interactions between PIKK activator predicted coiled coils and the corresponding PIKK PRDs does not appear to be a common activation mechanism. Our lab previously found that like ATR, mutations in the DNA-PKcs PRD disrupts DNA-PK activation (Mordes et al., 2008a), and another study proposed KU70/80 binds immediately C-terminal to the DNA-PKcs kinase domain (Spagnolo et al., 2006). Together, these results suggested a potential interaction between KU70/80 and the DNA-PKcs PRD; however, more recent

structural data indicates the KU80 C-terminus contacts DNA-PKcs through the circular cradle HEAT repeats rather than the PRD to initiate kinase activation (Sibanda et al., 2017). Likewise, the NBS1 C-terminus contacts ATM not at the PRD, but through the α-solenoid HEAT repeats to trigger ATM activation (Jansma and Hopfner, in press). The binding sites on DNA-PKcs and ATM of KU80 and NBS1 respectively are analogous to the ATRIP binding site on ATR rather than the TOPBP1 and ETAA1 binding site on ATR (Falck et al., 2005). As for ATR, the structure of the active ATM complex has yet to be solved, but current data indicates ATM and DNA-PKcs activation by MRN and KU70/80 exhibit at least some mechanistic differences than ATR activation by TOPBP1 and ETAA1. In addition, the KU80 and NBS1 C-termini are not predicted to be intrinsically disordered and do not contain predicted coiled coil motifs (McDonnell et al., 2006; Meszaros et al., 2018).

ETAA1 regulation

ETAA1 protein-protein interactions

In addition to ATR-ATRIP and RPA, ETAA1 interacts with BRCA1, BRCA2, BLM, and HLTF (Bass et al., 2016). Whether any of these interactions are direct or functionally relevant are important questions that require further investigation. BRCA1, BRCA2, BLM, and HLTF all function in recombination-based repair pathways (Bai et al., 2020; Bussen et al., 2007; Bussen et al., 2006; Tarsounas and Sung, 2020; Wu et al., 2006). ETAA1 also functions in recombination-based repair, as evidenced by the increase in sister-chromatid exchanges (SCEs) in ETAA1-deficient cells (Bass et al., 2016). BLM-deficiency causes an increase in SCEs also (Chaganti et al., 1974; Kuhn and Therman, 1986), but interestingly, SCEs are not further exacerbated upon combined ETAA1 and BLM loss (Bass et al., 2016), suggesting an epistatic relationship. However, like my attempts to identify a distinct oligomerization domain within ETAA1,

previous attempts to map a BLM interaction surface on ETAA1 were unsuccessful (Bass, unpublished). Thus, the ETAA1-BLM interaction may be the result of numerous multivalent interactions, possibly within biomolecular condensates. Indeed, previous studies have found BLM functions in such structures. Artificially created telomere clusters in promyelocytic leukemia (PML) bodies that mimic alternative lengthening of telomers (ALT) associated PML bodies (APBs), which are membrane-less condensates, only exhibit ALT-phenotypes upon BLM overexpression (Min et al., 2019). A separate study found that BLM localizes to telomeric foci in ALT cells, and that BLM overexpression increases telomeric DNA in these cells (Stavropoulos et al., 2002).

Biomolecular condensates are organization hubs within the cell and function to bring specific proteins together, while simultaneously also keeping others apart. For example, PARP-1 dependent FUS recruitment to liquid droplets at DNA strand breaks results in the co-recruitment of TAF15 and hnRNPUL1, a genome maintenance protein predicted to contain intrinsically disordered domains. In contrast, other DDR proteins including KU70, NBS1, MDC1, and 53BP1 are excluded from these condensates (Altmeyer et al., 2015). For 53BP1 specifically, biomolecular condensate formation at some DNA breaks while exclusion from condensates at other sites may regulate its function and protein-protein interactions. Likewise, some ETAA1 protein-protein interactions may occur within biomolecular condensates, and the composition of specific condensates may spatiotemporally regulate these interactions to modulate ETAA1 function.

ETAA1 regulation by phosphorylation

ETAA1 is phosphorylated during an unperturbed S-phase and in response to replication stress (Achuthankutty et al., 2019). In the absence of any exogenous DNA damage, ETAA1 is

phosphorylated in a CDK-dependent manner at S95 and S111. These residues are located within the AAD and phosphorylation of these sites potentiate ETAA1-dependent ATR activation. As such, mutation of both S95 and S111 cause mitotic chromosomal abnormalities that arise from unresolved replication intermediates (Achuthankutty et al., 2019). ETAA1 also undergoes ATR-dependent phosphorylation at S95 in response to exogenous DNA damage (Achuthankutty et al., 2019). Whether ATR directly phosphorylates S95 and/or if S95 phosphorylation in response to replications stress is functionally important is not known. However, previous studies indicate AAD^{MAD} phosphorylation potentiates ATR^{Mec1} activation by ATR^{Mec1} activating proteins. The TOPBP1 AAD is phosphorylated by ATM, and this phosphorylation is required for TOPBP1-dependent ATR activation in response to DSBs in *Xenopus* egg extracts (Yoo et al., 2007). Additionally, Dpb11 is phosphorylated within its MAD by Mec1, and this phosphorylation is required for Dpb11-dependent Mec1 activation both *in vitro* and in cells (Mordes et al., 2008b).

DNA replication stress regulates ETAA1 expression

ETAA1 expression levels are altered in response to DNA replication stress. Prolonged CPT exposure causes a decrease in ETAA1 expression as visualized by immunoblotting (Bass and Cortez, 2019). This decrease is due to ETAA1 phosphorylation as phosphatase treatment restores ETAA1 expression levels to those observed in untreated cells (Bass, unpublished). Interestingly, ETAA1 expression increases in response to HU or CD437 treatment (Fig 6.3). ETAA1 undergoes ATR-dependent phosphorylation in response to HU (Achuthankutty et al., 2019), but it is not known if CD437 induces ETAA1 phosphorylation. It is also not clear if the observed increase in ETAA1 expression upon HU or CD437 treatment is due to phosphorylation. The changes in ETAA1 expression level induced by exogenous replication stress could be due to accumulation of a substrate that preferentially activates ETAA1-dependent ATR signaling, such

as R-loops. Both HU and CPT cause an increase in R-loop formation (Hamperl et al., 2017; Marinello et al., 2013). While it is not known if CD437 causes R-loop accumulation, depletion of RTEL1 (regulator of telomere elongation helicase 1), which is known to resolve replication-transcript conflicts (Wu et al., 2020), exacerbates fork slowing upon CD437 treatment (Mehta, unpublished). Further fork slowing in response to CD437 and RTEL1 depletion is rescued by transcription inhibition (Mehta, unpublished). These results suggest R-loop formation may contribute to CD437-dependent fork slowing and that increased ETAA1 expression upon CD437 treatment could be due to R-loop accumulation. Further studies are needed to test these hypotheses. In addition, how differences in ETAA1 expression are regulated in response to different replication inhibitors warrants further investigation.

Division of labor between TOPBP1 and ETAA1

Current data indicates TOPBP1 is the primary ATR activator in response to DNA replication stress, while ETAA1 is the primary ATR activator during normal DNA replication (Bass and Cortez, 2019; Saldivar et al., 2018). A similar division of labor amongst the Mec1 activating proteins has also been proposed (de Oliveira et al., 2015). However, these models are likely oversimplified. ETAA1 is a replication stress response protein and was first identified as such (Bass et al., 2016; Haahr et al., 2016; Lee et al., 2016). ETAA1 is enriched at stalled replication forks (Dungrawala et al., 2015), and ETAA1 loss causes increased sensitivity to HU and CPT. ETAA1 loss also results in defective RPA32 phosphorylation in response to prolonged CPT treatment (Bass et al., 2016; Haahr et al., 2016; Lee et al., 2016). As for TOPBP1, TOPBP1-dependent ATR activation is essential in the absence of any exogenous DNA damage.

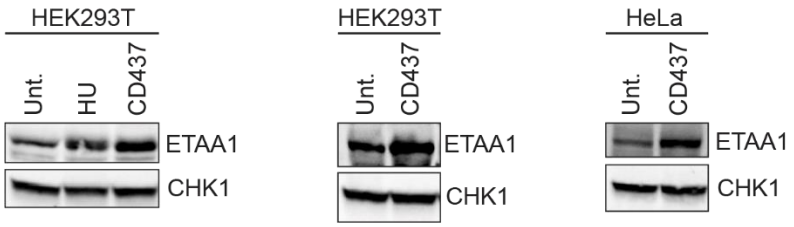

Figure 6.3: ETAA1 expression changes in response to replication stress. The indicated cell types were untreated or treated with 3 mM HU or 5 μM CD437 for 30 minutes. Cells were lysed and proteins were separated by SDS-PAGE and detected by immunoblotting.

Mutation of a single amino acid in the TOPBP1 AAD that prevents ATR activation causes cell and organismal lethality (Zhou et al., 2013). TOPBP1 is required for the initiation of DNA replication, and it is currently unknown if mutation of the TOPBP1 AAD causes DNA replication defects. However, the Dpb11 MAD is dispensable for DNA replication (Pfander and Diffley, 2011), which suggests that the lethality associated with TOPBP1 AAD mutations is not due to defective DNA replication.

The specific function(s) of ETAA1-dependent ATR activation in response to exogenous replication stress warrants further investigation. One hypothesis is that ETAA1 activates ATR specifically at R-loops. Because R-loops lack 5' ssDNA-dsDNA junctions, TOPBP1 recruitment to these structures is likely precluded. By contrast, ETAA1 recruitment to R-loops could occur through direct ETAA1-RPA interactions. R-loop accumulation in response to replication stress activates ATR (Hamperl et al., 2017; Matos et al., 2020), and R-loop formation at centromeres in mitosis results in ATR recruitment and activation (Kabeche et al., 2018). Thus, while centromeric R-loop formation likely mediates ETAA1-dependent ATR activation in mitosis, R-loop accumulation in S-phase due to replication stress could also activate ETAA1-dependent ATR signaling. As such, the HU and CPT sensitivity of ETAA1-deficient cells may be due to defective ATR signaling at, and resolution of, R-loops.

Likewise, the specific functions of TOPBP1- and ETAA1-dependent ATR activation during an unperturbed S-phase require further investigation. TOPBP1-dependent ATR activation is essential for cell and organismal viability (Zhou et al., 2013), while ETAA1-dependent ATR activation is not. ETAA1$^{-/-}$ mice exhibit defective T-cell clonal expansion in response to viral infection but are otherwise phenotypically normal. However, ETAA1 loss does result in partial

embryonic lethality (Miosge et al., 2017). These results indicate TOPBP1 is the more important ATR activator during unperturbed DNA replication.

ETAA1 loss reduces γH2AX formation during DNA replication, while TOPBP1 loss does not. Also, ATR controls an intrinsic S/G2 checkpoint that coordinates mitotic gene expression and S-phase progression (Saldivar et al., 2018), but whether this checkpoint is ETAA1- or TOPBP1-dependent is not clear. Loss of S/G2 checkpoint signaling increases genomic instability but does not result in cell lethality, suggesting ETAA1 may control this checkpoint. If ETAA1-dependent ATR activation regulates γH2AX induction and the S/G2 checkpoint under normal conditions, what is the essential function of TOPBP1-dependent ATR activation in unperturbed cells? ATR inhibition in otherwise unperturbed cells causes robust ssDNA accumulation, specifically in early S-phase cells, and eventually replication catastrophe. ssDNA accumulation and replication catastrophe result from increased origin firing and defective RRM2 accumulation (Buisson et al., 2015). Replication catastrophe causes excessive DNA damage that prevents further cell proliferation and is thus incompatible with viability (Toledo et al., 2013). TOPBP1-dependent regulation of origin firing and dNTP levels to prevent replication catastrophe could explain why TOPBP1-dependent ATR activation is essential for cell and organismal viability. While these hypotheses require further testing, I propose that TOPBP1 is the primary ATR activator during normal and stressed DNA replication. In both scenarios, TOPBP1-dependent ATR activation stabilizes stalled replication forks, regulates origin firing, and ensures adequate dNTP levels to prevent replication catastrophe. In response to DNA damage, TOPBP1 also solely regulates cell cycle checkpoints (Fig 6.4A and B). By contrast, I hypothesize ETAA1 has more specialized functions during both normal and stressed

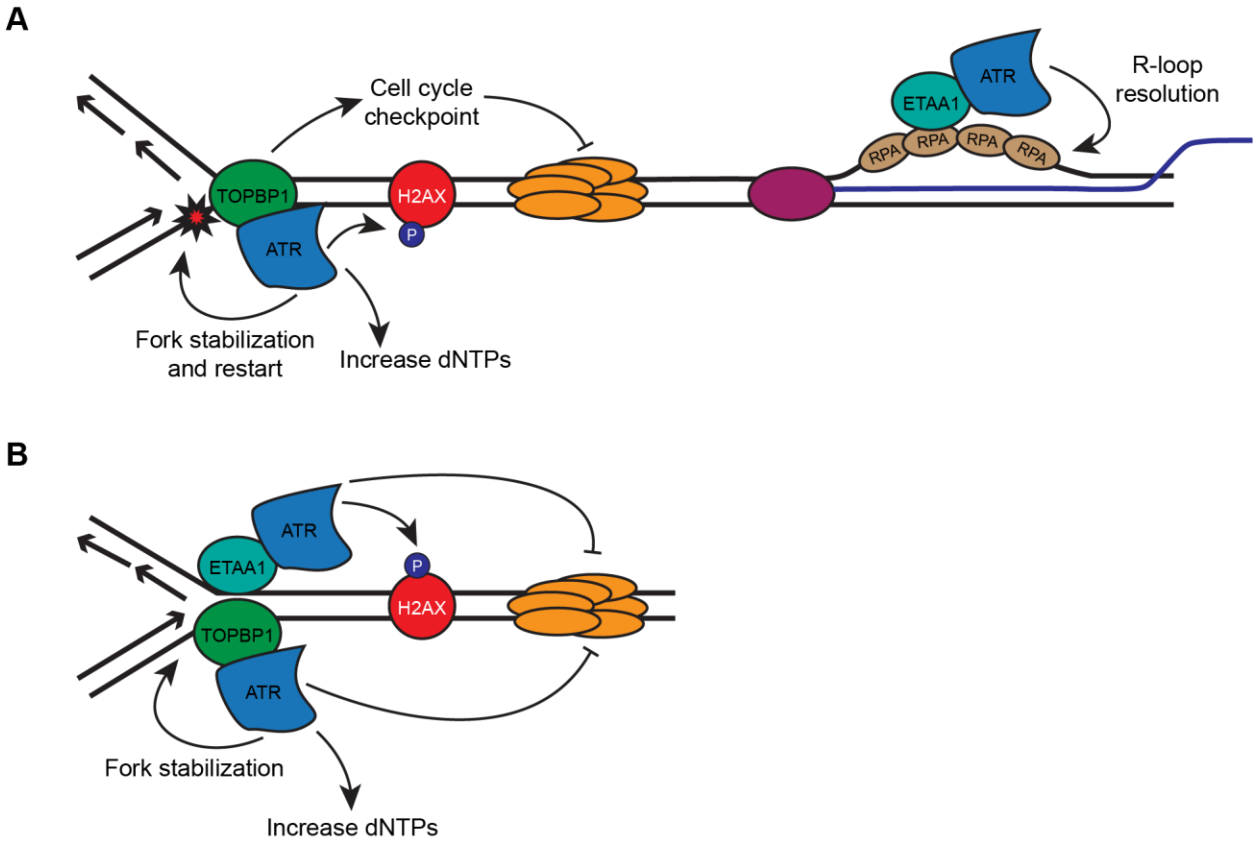

Figure 6.4 Proposed model of TOPBP1- and ETAA1-dependent ATR signaling events. A) In response to replication stress caused by exogenous DNA damaging agents, ATR signaling is predominantly TOPBP1-dependent. TOPBP1-dependent ATR signaling increases dNTP levels, promotes replication fork stabilization and restart, activates cell cycle checkpoints, and phosphorylates the majority of ATR-dependent substrates including H2AX. ETAA1-dependent ATR signaling occurs at R-loops to promote R-loop resolution. **B)** During unperturbed DNA replication, TOPBP1-dependent ATR signaling activates cell cycle checkpoints to restrain origin firing, stabilizes replication forks, and ensures adequate dNTP levels. ETAA1-dependent ATR signaling also contributes to checkpoint activation to restrain origin firing and mediates H2AX phosphorylation.

DNA replication. In the absence of exogenous stress, ETAA1 together with TOPBP1 controls cell cycle checkpoints, whereas in the presence of exogenous DNA damage, ETAA1-dependent ATR activation promotes R-loop resolution (Fig 6.4A and B). These ETAA1-dependent processes, while not essential for viability, are important for maintenance of genome stability. ETAA1-dependent regulation of recombination pathways, such as Holliday junction dissolution during HR or recombination-based replication fork restart, may also contribute to maintenance of genome stability.

Defining the ATR checkpoint activating structure

Leading vs. lagging strand lesions

Using a selective Pol α inhibitor, I found that stalling only the lagging strand results in a much less robust DNA replication checkpoint in comparison to stalling both strands. Despite the increase in ssDNA accumulation and ATR recruitment to replication forks upon lagging strand stalling, CHK1 phosphorylation in this scenario is less than CHK1 phosphorylation in response to stalling both strands (Fig 6.5A). In fact, when CHK1 phosphorylation is normalized to RPA32 phosphorylation, CHK1 phosphorylation is 10x higher in response to HU treatment than CD437 treatment (Fig 6.5B). These results indicate one, that ssDNA generation at replication forks is not sufficient to activate replication checkpoint signaling and two, that robust replication checkpoint signaling occurs only in response to leading strand stalling. Lagging strand synthesis occurs discontinuously via Okazaki fragment generation (Burgers and Kunkel, 2017); therefore, in response to lagging strand specific DNA lesions, DNA re-priming past the lesion would facilitate continued lagging strand synthesis without impeding fork progression and not activate the replication checkpoint. In contrast, leading strand specific lesions that interfere with DNA polymerization would cause helicase-polymerase uncoupling, fork slowing, and activate the

replication checkpoint. As such, helicase-polymerase uncoupling in *Xenopus* egg extracts results in robust ATR activation (Byun et al., 2005). Therefore, I propose that ATR checkpoint signaling in response to replication stress is primarily triggered by leading strand replication impediments. This hypothesis is consistent with *in vitro* results demonstrating that only leading strand specific lesions interfere with fork progression (Taylor and Yeeles, 2018). Additionally, this model predicts that selective Pol ε inhibition should cause robust checkpoint signaling similar to what is observed upon HU treatment.

During unperturbed DNA replication, ATR^{Mec1} activation is primarily mediated by Okazaki fragment generation on the lagging strand, and many Mec1 substrates during unperturbed replication are distinct from those that are induced by replication stress (de Oliveira et al., 2015). Distinct mechanisms of ATR^{Mec1} activation that occur on the lagging and leading strand may therefore control the replication stress response. While lagging strand replication functions to activate ATR during a normal S-phase, leading strand impeding lesions caused by replication stress likely increase ATR signaling beyond basal levels to activate the replication checkpoint. This transition, along with simultaneous changes in the fork proteome such as CLASPIN recruitment, which only occurs upon leading strand stalling, likely directs ATR to phosphorylate the requisite substrates needed to maintain replication fork stability in the presence of exogenously induced DNA damage.

Generation of the ATR activating structure

The canonical structure that supports TOPBP1-dependent ATR signaling at stalled replication forks is the 5’ ssDNA-dsDNA junction (MacDougall et al., 2007), which is generated by Pol α re-priming downstream of the lesion (Byun et al., 2005; Van et al., 2010). All data

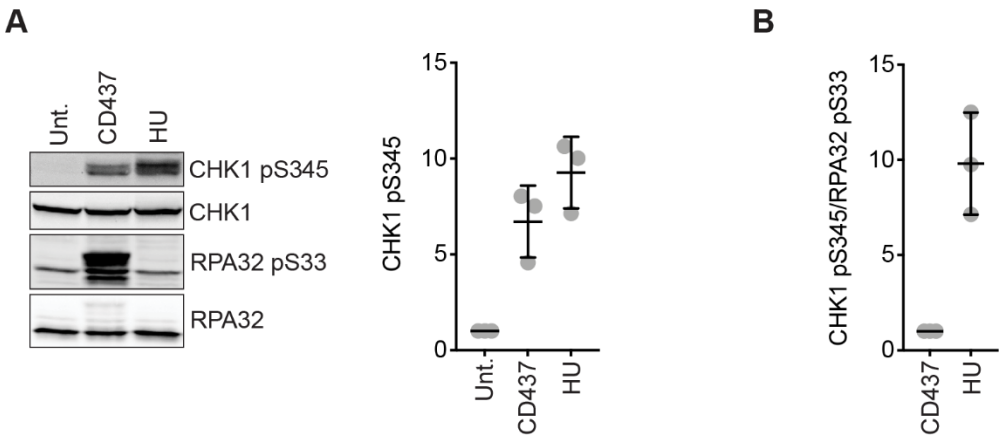

Figure 6.5: HU induces more robust replication checkpoint signaling than CD437. A) HeLa cells were untreated or treated with 5 μM CD437 or 3 mM HU for 30 minutes. Cells were lysed and proteins were separated by SDS-PAGE and detected by immunoblotting. CHK1 phosphorylation was quantified in three independent experiments (Mean +/- SD). **B)** Quantification of CHK1 phosphorylation normalized to RPA32 phosphorylation in HeLa cells upon treatment with 5 μM CD437 or 3 mM HU for 30 minutes (Mean +/- SD).

currently supporting this model are derived from experiments performed in *Xenopus* egg extracts, and it is not known if Pol α re-priming is required for ATR activation at stalled forks in cells. To test this, I treated cells with either HU, CD437, or both HU and CD437 and examined CHK1 phosphorylation. Surprisingly, compared to cells treated with HU, cells treated with HU and CD437 exhibit increased CHK1 phosphorylation, and this difference is observed in at least two cell types (Fig 6.6). The same result was reported in another study (Ercilla et al., 2020). This result indicates that in human cells, Pol α activity is not required for ATR signaling at stalled replication forks.

Several possibilities can explain the apparent discrepancy about Pol α re-priming being necessary for ATR activation in *Xenopus* egg extracts but not human cells. First, it is possible that 5' ssDNA-dsDNA junctions generated by primer synthesis are not required for ATR activation at stalled forks in human cells. However, given that RAD9, RAD1, and HUS1 are three of the most highly enriched proteins at HU-stalled replication forks and are required for TOPBP1-dependent CHK1 phosphorylation (Dungrawala et al., 2015), it is likely that primer synthesis facilitates their recruitment. A second possibility is that re-priming at stalled forks can occur in a Pol α-independent manner. Because CD437 does not inhibit primase activity of Pol α-Primase, it is possible that generation of RNA-primers downstream of a stalled fork is sufficient to facilitate 9-1-1 loading. Experiments examining this possibility in *Xenopus* egg extracts have been inconclusive however, because RNA primers annealed to ssDNA are rapidly degraded in this system (MacDougall et al., 2007). Pol α-independent re-priming could also be mediated by PRIMPOL. PRIMPOL re-priming downstream of UV-induced lesions is required for efficient fork restart (Mouron et al., 2013); therefore, PRIMPOL re-priming at stalled forks may function

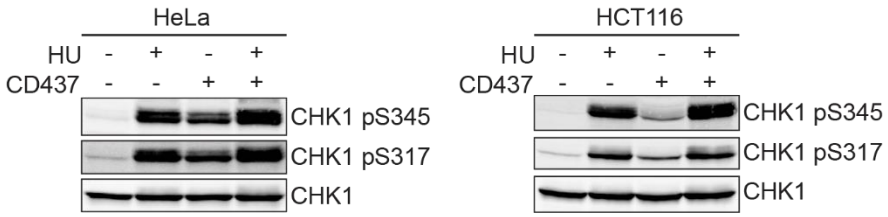

Figure 6.6: Pol α activity is not required for replication checkpoint signaling upon fork stalling. The indicated cell types were untreated, treated with 3 mM HU, 5 μM CD437, or 3 mM HU and 5 μM CD437 for 30 minutes. Cells were lysed and proteins were separated by SDS-PAGE and detected by immunoblotting.

to generate the ATR activating structure. Further studies are needed to test this hypothesis. A third possibility is that the ATR activating structure at stalled forks in human cells is generated by fork remodeling. As discussed in Chapter I, fork reversal could generate the ATR activating structure if the nascent leading strand is longer than the nascent lagging strand. If the nascent lagging strand is longer than the nascent leading strand, fork reversal followed by 5'-3' resection would generate the ATR activating structure. While depletion of DNA2, which catalyzes 5'-3' resection, reduces ATR signaling upon fork stalling (Thangavel et al., 2015), there is currently scant evidence that inhibiting fork reversal impairs ATR activation (Saldivar et al., 2017). However, given that numerous enzymes regulate at least two distinct fork reversal pathways (Liu et al., 2020), more genetic analyses are needed to better determine how or if fork reversal promotes checkpoint signaling by generating the ATR activating structure.

ATR future directions

Since its discovery 25 years ago, ATR has been extensively studied. Recently, many reports have focused on how ATR regulates DNA replication and genomic stability in the absence of exogenous DNA damage. As mentioned above, phosphoproteomic analyses revealed many Mec1 substrates during unperturbed DNA replication are distinct from those induced by exogenous replication stress (de Oliveira et al., 2015). While several phosphoproteomic screens to identify damage-specific ATR substrates have been performed, a comprehensive list of ATR substrates phosphorylated during unperturbed conditions is lacking. Many ATR substrates phosphorylated in unperturbed and perturbed settings are likely to be the same, but several substrates may also be differentially phosphorylated in these two settings. Identification of differentially phosphorylated proteins in unstressed and stressed conditions may aid in determining which candidate ATR downstream effectors that when inhibited, could increase

efficacy of radio- and/or chemotherapy while reducing adverse side effects. Furthermore, identifying TOPBP1- and ETAA1-dependent ATR substrates during an unperturbed cell cycle will increase our understanding of the specific functions of each activator during normal DNA replication.

Replication fork reversal occurs in response to numerous genotoxic drugs and preserves fork stability by preventing nascent strand degradation and by promoting lesion repair in the context of duplex DNA (Cortez, 2019). Damaged replication forks can also be stabilized and restarted by PRIMPOL-dependent re-priming, and recent studies indicate fork reversal and re-priming pathways function antagonistically at replication forks. Upon loss of HLTF, which prevents fork reversal, unrestrained DNA synthesis occurs in a PRIMPOL-dependent manner (Bai et al., 2020). Additionally, in response to repeated cisplatin doses, BRCA1-deficient cells down-regulate fork reversal and up-regulate PRIMPOL-dependent restart. Fork reversal can also be suppressed by PRIMPOL overexpression (Quinet et al., 2020). The balance between fork reversal and PRIMPOL-dependent re-priming is regulated by ATR, but the underlying mechanism(s) are incompletely understood. ATR signaling promotes reversal of damaged replication forks, but it also activates fork reversal globally to stabilize undamaged forks (Mutreja et al., 2018). However, ATR signaling also mediates PRIMPOL-dependent fork restart in BRCA1-deficient cells, but only after multiple cisplatin treatments (Quinet et al., 2020). Together, this data suggests that ATR primarily mediates fork stabilization and repair through fork reversal, but in response to repeated genotoxic stress and/or loss of certain DNA repair proteins, ATR signaling is rewired to promote PRIMPOL-dependent re-priming. Understanding how differences in ATR signaling regulate these opposing pathways may be useful for developing therapeutic strategies to treat cancers with specific DNA repair defects.

ATR functions in pathways other than the DDR including in response to nuclear envelope mechanical stress (Kumar et al., 2014). A recent report also found that Mec1 is required to maintain proteostasis and that defective Mec1 signaling results in widespread, toxic protein aggregation (Corcoles-Saez et al., 2018). Similarly, it was found that defective ATM activation upon oxidative stress causes severe protein aggregation (Lee et al., 2018). It is not clear if defective ATR signaling causes aberrant protein aggregation; however, in my studies I have noticed that whole cell lysates from HEK293T ΔETAA1 cells consistently have higher protein concentrations than whole cell lysates from an equivalent cell number of HEK293T wild type cells. Whether this difference is attributable to protein aggregation and/or aberrant autophagy remains unknown, but this observation indicates that ATR signaling may regulate proteostasis in an ETAA1-dependent manner. More experiments are needed to test this hypothesis directly, but this finding could open a new avenue of research by directly linking genome maintenance with protein homeostasis.

Conclusions

In summary, I have more thoroughly defined the mechanism of ATR activation by TOPBP1 and ETAA1. In Chapter III, I identified the minimal TOPBP1 and ETAA1 AADs required for ATR activation and found that each AAD contains a predicted coiled coil motif that is required for ATR binding and activation. The predicted coiled coils are essential for ATR activation because they directly contact the ATR-ATRIP complex. In Chapter IV, I determined that TOPBP1 and ETAA1 AAD dimerization enhances ATR activation, and that ETAA1 forms oligomeric complexes in cells. Although I did not identify a distinct oligomerization domain within ETAA1, I found that an oligomerization-defective ETAA1 mutant is unable to restore ATR signaling and genome stability to ETAA1-deficient cells unless it is induced to dimerize

through a heterologous dimerization domain. In Chapter V, I analyzed the replication stress response activated by selectively stalling the lagging strand and found that leading and lagging strand replication are partially coupled in human cells. Additionally, I found that while lagging strand stalling activates ATR in a TOPBP1-dependent manner to prevent replication fork collapse, it does not induce robust replication checkpoint signaling.

Future studies that describe atomic-resolution structures of the active ATR^{Mec1}-$ATRIP^{Ddc2}$ complex will enhance our understanding of the mechanism of ATR activation and likely show how the predicted coiled coils contact ATR-ATRIP and how AAD dimerization transitions ATR from an inactive to active state. In addition, more ETAA1 structure-function analyses will further define ETAA1 oligomerization surfaces and also elucidate the functional relevance of ETAA1 protein-protein interactions and post-translational modifications. Finally, identifying how strand-specific lesions affect ATR signaling may reveal how specific ATR substrates modulate replication fork fidelity and cell cycle checkpoints in both unstressed and stressed conditions.

REFERENCES

Acevedo, J., Yan, S., and Michael, W.M. (2016). Direct Binding to Replication Protein A (RPA)-coated Single-stranded DNA Allows Recruitment of the ATR Activator TopBP1 to Sites of DNA Damage. Journal of Biological Chemistry *291*, 13124-13131.

Achuthankutty, D., Thakur, R.S., Haahr, P., Hoffmann, S., Drainas, A.P., Bizard, A.H., Weischenfeldt, J., Hickson, I.D., and Mailand, N. (2019). Regulation of ETAA1-mediated ATR activation couples DNA replication fidelity and genome stability. Journal of Cell Biology *218*, 3943-3953.

Adams, K.E., Medhurst, A.L., Dart, D.A., and Lakin, N.D. (2006). Recruitment of ATR to sites of ionising radiation-induced DNA damage requires ATM and components of the MRN protein complex. Oncogene *25*, 3894-3904.

Ahlskog, J.K., Larsen, B.D., Achanta, K., and Sorensen, C.S. (2016). ATM/ATR-mediated phosphorylation of PALB2 promotes RAD51 function. Embo Reports *17*, 671-681.

Ahnesorg, P., Smith, P., and Jackson, S.P. (2006). XLF interacts with the XRCC4-DNA ligase IV complex to promote DNA nonhomologous end-joining. Cell *124*, 301-313.

Altmeyer, M., Neelsen, K.J., Teloni, F., Pozdnyakova, I., Pellegrino, S., Grofte, M., Rask, M.B.D., Streicher, W., Jungmichel, S., Nielsen, M.L., *et al.* (2015). Liquid demixing of intrinsically disordered proteins is seeded by poly(ADP-ribose). Nature Communications *6*.

Ammazzalorso, F., Pirzio, L.M., Bignami, M., Franchitto, A., and Pichierri, P. (2010). ATR and ATM differently regulate WRN to prevent DSBs at stalled replication forks and promote replication fork recovery. Embo Journal *29*, 3156-3169.

Bai, G.S., Kermi, C., Stoy, H., Schiltz, C.J., Bacal, J., Zaino, A.M., Hadden, M.K., Eichman, B.F., Lopes, M., and Cimprich, K.A. (2020). HLTF Promotes Fork Reversal, Limiting Replication Stress Resistance and Preventing Multiple Mechanisms of Unrestrained DNA Synthesis. Molecular Cell *78*, 1237-+.

Bakkenist, C.J., and Kastan, M.B. (2003). DNA damage activates ATM through intermolecular autophosphorylation and dimer dissociation. Nature *421*, 499-506.

Ball, H.L., and Cortez, D. (2005). ATRIP oligomerization is required for ATR-dependent checkpoint signaling. J Biol Chem *280*, 31390-31396.

Ball, H.L., Ehrhardt, M.R., Mordes, D.A., Glick, G.G., Chazin, W.J., and Cortez, D. (2007). Function of a conserved checkpoint recruitment domain in ATRIP proteins. Molecular and Cellular Biology *27*, 3367-3377.

Balmus, G., Pilger, D., Coates, J., Demir, M., Sczaniecka-Clift, M., Barros, A.C., Woods, M., Fu, B., Yang, F., Chen, E., *et al.* (2019). ATM orchestrates the DNA-damage response to counter toxic non-homologous end-joining at broken replication forks. Nature Communications *10*.

Banani, S.F., Lee, H.O., Hyman, A.A., and Rosen, M.K. (2017). Biomolecular condensates: organizers of cellular biochemistry. Nature Reviews Molecular Cell Biology *18*, 285-298.

Baretic, D., Pollard, H.K., Fisher, D.I., Johnson, C.M., Santhanam, B., Truman, C.M., Kouba, T., Fersht, A.R., Phillips, C., and Williams, R.L. (2017). Structures of closed and open conformations of dimeric human ATM. Science Advances *3*.

Bass, T.E., and Cortez, D. (2019). Quantitative phosphoproteomics reveals mitotic function of the ATR activator ETAA1. Journal of Cell Biology *218*, 1235-1249.

Bass, T.E., Luzwick, J.W., Kavanaugh, G., Carroll, C., Dungrawala, H., Glick, G.G., Feldkamp, M.D., Putney, R., Chazin, W.J., and Cortez, D. (2016). ETAA1 acts at stalled replication forks to maintain genome integrity. Nature Cell Biology *18*, 1185-+.

Bermudez, V.P., Lindsey-Boltz, L.A., Cesare, A.J., Maniwa, Y., Griffith, J.D., Hurwitz, J., and Sancar, A. (2003). Loading of the human 9-1-1 checkpoint complex onto DNA by the checkpoint clamp loader hRad17-replication factor C complex in vitro. Proceedings of the National Academy of Sciences of the United States of America *100*, 1633-1638.

Berti, M., Cortez, D., and Lopes, M. (2020). The plasticity of DNA replication forks in response to clinically relevant genotoxic stress. Nature Reviews Molecular Cell Biology *21*, 633-651.

Blackford, A.N., and Jackson, S.P. (2017). ATM, ATR, and DNA-PK: The Trinity at the Heart of the DNA Damage Response. Molecular Cell *66*.

Brown, J.S., Sundar, R., and Lopez, J. (2018). Combining DNA damaging therapeutics with immunotherapy: more haste, less speed. British Journal of Cancer *118*, 312-324.

Buisson, R., Boisvert, J.L., Benes, C.H., and Zou, L. (2015). Distinct but Concerted Roles of ATR, DNA-PK, and Chk1 in Countering Replication Stress during S Phase. Molecular Cell *59*, 1011-1024.

Burgers, P.M.J., and Kunkel, T.A. (2017). Eukaryotic DNA Replication Fork. Annual Review of Biochemistry *86*, 417-438.

Burkhard, P., Stetefeld, J., and Strelkov, S.V. (2001). Coiled coils: a highly versatile protein folding motif. Trends in Cell Biology *11*, 82-88.

Bussen, W., Raynard, S., Busygina, V., Singh, A.K., and Sung, P. (2007). Holliday junction processing activity of the BLM-topo III alpha-BLAP75 complex. Journal of Biological Chemistry *282*, 31484-31492.

Bussen, W.L., Raynard, S.J., and Sung, P. (2006). A double-holliday junction dissolvasome comprising BLM, topoisomerase IIIalpha, and BLAP75. Environmental and Molecular Mutagenesis *47*, 423-423.

Byun, T.S., Pacek, M., Yee, M.C., Walter, J.C., and Cimprich, K.A. (2005). Functional uncoupling of MCM helicase and DNA polymerase activities activates the ATR-dependent checkpoint. Genes & Development *19*, 1040-1052.

Chaganti, R.S., Schonberg, S., and German, J. (1974). MANIFOLD INCREASE IN SISTER CHROMATID EXCHANGES IN BLOOMS SYNDROME LYMPHOCYTES. Proceedings of the National Academy of Sciences of the United States of America *71*, 4508-4512.

Chanut, P., Britton, S., Coates, J., Jackson, S.P., and Calsou, P. (2016). Coordinated nuclease activities counteract Ku at single-ended DNA double-strand breaks. Nature Communications *7*.

Chen, J., Harding, S.M., Natesan, R., Tian, L., Benci, J.L., Li, W.H., Minn, A.J., Asangani, I.A., and Greenberg, R.A. (2020). Cell Cycle Checkpoints Cooperate to Suppress DNA- and RNA-Associated Molecular Pattern Recognition and Anti-Tumor Immune Responses. Cell Reports *32*.

Chen, L., Chen, J.Y., Huang, Y.J., Gu, Y., Qiu, J.S., Qian, H., Shao, C.W., Zhang, X., Hu, J., Li, H.R., *et al.* (2018). The Augmented R-Loop Is a Unifying Mechanism for Myelodysplastic Syndromes Induced by High-Risk Splicing Factor Mutations. Molecular Cell *69*, 412-+.

Ciccia, A., and Elledge, S.J. (2010). The DNA Damage Response: Making It Safe to Play with Knives. Molecular Cell *40*, 179-204.

Cimprich, K.A., and Cortez, D. (2008). ATR: an essential regulator of genome integrity. Nature Reviews Molecular Cell Biology *9*, 616-627.

Clackson, T., Yang, W., Rozamus, L.W., Hatada, M., Amara, J.F., Rollins, C.T., Stevenson, L.F., Magari, S.R., Wood, S.A., Courage, N.L., *et al.* (1998). Redesigning an FKBP-ligand interface to generate chemical dimerizers with novel specificity. Proceedings of the National Academy of Sciences of the United States of America *95*, 10437-10442.

Corcoles-Saez, I., Dong, K.Z., Johnson, A.L., Waskiewicz, E., Costanzo, M., Boone, C., and Cha, R.S. (2018). Essential Function of Mec1, the Budding Yeast ATM/ATR Checkpoint-Response Kinase, in Protein Homeostasis. Developmental Cell *46*, 495-+.

Cortez, D. (2019). Replication-Coupled DNA Repair. Molecular Cell *74*, 866-876.

Cortez, D., Glick, G., and Elledge, S.J. (2004). Minichromosome maintenance proteins are direct targets of the ATM and ATR checkpoint kinases. Proceedings of the National Academy of Sciences of the United States of America *101*, 10078-10083.

Cortez, D., Guntuku, S., Qin, J., and Elledge, S.J. (2001). ATR and ATRIP: Partners in checkpoint signaling. Science *294*, 1713-1716.

Cortez, D., Wang, Y., Qin, J., and Elledge, S.J. (1999). Requirement of ATM-dependent phosphorylation of BRCA1 in the DNA damage response to double-strand breaks. Science *286*, 1162-1166.

Cotta-Ramusino, C., McDonald, E.R., Hurov, K., Sowa, M.E., Harper, J.W., and Elledge, S.J. (2011). A DNA Damage Response Screen Identifies RHINO, a 9-1-1 and TopBP1 Interacting Protein Required for ATR Signaling. Science *332*, 1313-1317.

Couch, F.B., Bansbach, C.E., Driscoll, R., Luzwick, J.W., Glick, G.G., Betous, R., Carroll, C.M., Jung, S.Y., Qin, J., Cimprich, K.A., *et al.* (2013). ATR phosphorylates SMARCAL1 to prevent replication fork collapse. Genes & Development *27*, 1610-1623.

Critchlow, S.E., Bowater, R.P., and Jackson, S.P. (1997). Mammalian DNA double-strand break repair protein XRCC4 interacts with DNA ligase IV. Current Biology *7*, 588-598.

Crossley, M.P., Bocek, M., and Cimprich, K.A. (2019). R-Loops as Cellular Regulators and Genomic Threats. Molecular Cell *73*, 398-411.

Cuadrado, M., Martinez-Pastor, B., Murga, M., Toledo, L.I., Gutierrez-Martinez, P., Lopez, E., and Fernandez-Capetillo, O. (2006). ATM regulates ATR chromatin loading in response to DNA double-strand breaks. Journal of Experimental Medicine *203*, 297-303.

D'Angiolella, V., Donato, V., Forrester, F.M., Jeong, Y.T., Pellacani, C., Kudo, Y., Saraf, A., Florens, L., Washburn, M.P., and Pagano, M. (2012). Cyclin F-Mediated Degradation of Ribonucleotide Reductase M2 Controls Genome Integrity and DNA Repair. Cell *149*, 1023-1034.

Daniel, J.A., Pellegrini, M., Lee, J.H., Paull, T.T., Feigenbaum, L., and Nussenzweig, A. (2008). Multiple autophosphorylation sites are dispensable for murine ATM activation in vivo. Journal of Cell Biology *183*, 777-783.

Davies, S.L., North, P.S., Dart, A., Lakin, N.D., and Hickson, I.D. (2004). Phosphorylation of the Bloom's syndrome helicase and its role in recovery from S-phase arrest. Molecular and Cellular Biology *24*, 1279-1291.

de Oliveira, F.M.B., Kim, D., Cussiol, J.R., Das, J., Jeong, M.C., Doerfler, L., Schmidt, K.H., Yu, H.Y., and Smolka, M.B. (2015). Phosphoproteomics Reveals Distinct Modes of Mec1/ATR Signaling during DNA Replication. Molecular Cell *57*, 1124-1132.

Delacroix, S., Wagner, J.M., Kobayashi, M., Yamamoto, K., and Karnitz, L.M. (2007). The Rad9-Hus1-Rad1 (9-1-1) clamp activates checkpoint signaling via TopBP1. Genes & Development *21*, 1472-1477.

Devbhandari, S., and Remus, D. (2020). Rad53 limits CMG helicase uncoupling from DNA synthesis at replication forks. Nature Structural & Molecular Biology *27*, 461-+.

Dungrawala, H., Rose, K.L., Bhat, K.P., Mohni, K.N., Glick, G.G., Couch, F.B., and Cortez, D. (2015). The Replication Checkpoint Prevents Two Types of Fork Collapse without Regulating Replisome Stability. Molecular Cell *59*, 998-1010.

Duursma, A.M., Driscoll, R., Elias, J.E., and Cimprich, K.A. (2013). A Role for the MRN Complex in ATR Activation via TOPBP1 Recruitment. Molecular Cell *50*, 116-122.

Ellison, V., and Stillman, B. (2003). Biochemical characterization of DNA damage checkpoint complexes: Clamp loader and clamp complexes with specificity for 5 ' recessed DNA. Plos Biology *1*, 231-243.

Ercilla, A., Benada, J., Amitash, S., Zonderland, G., Baldi, G., Somyajit, K., Ochs, F., Costanzo, V., Lukas, J., and Toledo, L. (2020). Physiological Tolerance to ssDNA Enables Strand Uncoupling during DNA Replication. Cell Reports *30*, 2416-2429.e2417.

Falck, J., Coates, J., and Jackson, S.P. (2005). Conserved modes of recruitment of ATM, ATR and DNA-PKcs to sites of DNA damage. Nature *434*, 605-611.

Falck, J., Mailand, N., Syljuasen, R.G., Bartek, J., and Lukas, J. (2001). The ATM-Chk2-Cdc25A checkpoint pathway guards against radioresistant DNA synthesis. Nature *410*, 842-847.

Ferrao, P.T., Bukczynska, E.P., Johnstone, R.W., and Mcarthur, G.A. (2012). Efficacy of CHK inhibitors as single agents in MYC-driven lymphoma cells. Oncogene *31*, 1661.

Forey, R., Poveda, A., Sharma, S., Barthe, A., Padioleau, I., Renard, C., Lambert, R., Skrzypczak, M., Ginalski, K., Lengronne, A., *et al.* (2020). Mec1 Is Activated at the Onset of Normal S Phase by Low-dNTP Pools Impeding DNA Replication. Molecular Cell *78*, 396-+.

Forment, J.V., and O'Connor, M.J. (2018). Targeting the replication stress response in cancer. Pharmacology & Therapeutics *188*, 155-167.

Fradet-Turcotte, A., Canny, M.D., Escribano-Diaz, C., Orthwein, A., Leung, C.C.Y., Huang, H., Landry, M.C., Kitevski-LeBlanc, J., Noordermeer, S.M., Sicheri, F., *et al.* (2013). 53BP1 is a reader of the DNA-damage-induced H2A Lys 15 ubiquitin mark. Nature *499*, 50-+.

Francoeur, A.M., Peebles, C.L., Gompper, P.T., and Tan, E.M. (1986). IDENTIFICATION OF KI KU, P70/P80 AUTOANTIGENS AND ANALYSIS OF ANTI-KI AUTOANTIBODY REACTIVITY. Journal of Immunology *136*, 1648-1653.

Frattini, C., Promonet, A., Alghoul, E., Vidal-Eychenie, S., Lamarque, M., Blanchard, M.-P., Urbach, S., Basbous, J., and Constantinou, A. (2021). TopBP1 assembles nuclear condensates to switch on ATR signaling. Molecular cell.

Gan, H.Y., Yu, C.H., Devbhandari, S., Sharma, S., Han, J.H., Chabes, A., Remus, D., and Zhang, Z.G. (2017). Checkpoint Kinase Rad53 Couples Leading- and Lagging-Strand DNA Synthesis under Replication Stress. Molecular Cell *68*, 446-+.

Gandhi, L., Rodriguez-Abreu, D., Gadgeel, S., Esteban, E., Felip, E., De Angelis, F., Domine, M., Clingan, P., Hochmair, M.J., Powell, S.F., *et al.* (2018). Pembrolizumab plus Chemotherapy in Metastatic Non-Small-Cell Lung Cancer. New England Journal of Medicine *378*, 2078-2092.

Gatei, M., Young, D., Cerosaletti, K.M., Desai-Mehta, A., Spring, K., Kozlov, S., Lavin, M.F., Gatti, R.A., Concannon, P., and Khanna, K. (2000). ATM-dependent phosphorylation of nibrin in response to radiation exposure. Nature Genetics *25*, 115-119.

Gell, D., and Jackson, S.P. (1999). Mapping of protein-protein interactions within the DNA-dependent protein kinase complex. Nucleic Acids Research *27*, 3494-3502.

Graham, J.E., Marians, K.J., and Kowalczykowski, S.C. (2017). Independent and Stochastic Action of DNA Polymerases in the Replisome. Cell *169*, 1201-+.

Graham, T.G.W., Walter, J.C., and Loparo, J.J. (2016). Two-Stage Synapsis of DNA Ends during Non-homologous End Joining. Molecular Cell *61*, 850-858.

Grawunder, U., Wilm, M., Wu, X.T., Kulesza, P., Wilson, T.E., Mann, M., and Lieber, M.R. (1997). Activity of DNA ligase IV stimulated by complex formation with XRCC4 protein in mammalian cells. Nature *388*, 492-495.

Greenberg, R.A. (2018). Assembling a protective shield. Nature Cell Biology *20*, 862-863.

Guo, C., Kumagai, A., Schlacher, K., Shevchenko, A., and Dunphy, W.G. (2015). Interaction of Chk1 with Treslin Negatively Regulates the Initiation of Chromosomal DNA Replication. Molecular Cell *57*, 492-505.

Haahr, P., Hoffmann, S., Tollenaere, M.A.X., Ho, T., Toledo, L.I., Mann, M., Bekker-Jensen, S., Raschle, M., and Mailand, N. (2016). Activation of the ATR kinase by the RPA-binding protein ETAA1. Nature Cell Biology *18*, 1196-+.

Hamperl, S., Bocek, M.J., Saldivar, J.C., Swigut, T., and Cimprich, K.A. (2017). Transcription-Replication Conflict Orientation Modulates R-Loop Levels and Activates Distinct DNA Damage Responses. Cell *170*, 774-+.

Han, T., Goralski, M., Capota, E., Padrick, S.B., Kim, J., Xie, Y., and Nijhawan, D. (2016). The antitumor toxin CD437 is a direct inhibitor of DNA polymerase alpha. Nature Chemical Biology *12*, 511-+.

Han, X.Z., Pozo, F.M., Wisotsky, J.N., Wang, B.L., Jacobberger, J.W., and Zhang, Y.W. (2015). Phosphorylation of Minichromosome Maintenance 3 (MCM3) by Checkpoint Kinase 1 (Chk1) Negatively Regulates DNA Replication and Checkpoint Activation. Journal of Biological Chemistry *290*, 12370-12378.

Hanahan, D., and Weinberg, R.A. (2011). Hallmarks of Cancer: The Next Generation. Cell *144*, 646-674.

Harami, G.M., Kovacs, Z.J., Pancsa, R., Palinkas, J., Barath, V., Tarnok, K., Malnasi-Csizmadia, A., and Kovacs, M. (2020). Phase separation by ssDNA binding protein controlled via protein-protein and protein-DNA interactions. Proceedings of the National Academy of Sciences of the United States of America *117*, 26206-26217.

Hodroj, D., Recolin, B., Serhal, K., Martinez, S., Tsanov, N., Abou Merhi, R., and Maiorano, D. (2017). An ATR-dependent function for the Ddx19 RNA helicase in nuclear R-loop metabolism. Embo Journal *36*, 1182-1198.

Huang, J., Zhang, J., Bellani, M.A., Pokharel, D., Gichimu, J., James, R.C., Gali, H., Ling, C., Yan, Z.J., Xu, D.Y., *et al.* (2019). Remodeling of Interstrand Crosslink Proximal Replisomes Is Dependent on ATR, FANCM, and FANCD2. Cell Reports *27*, 1794-+.

Huen, M.S.Y., Grant, R., Manke, I., Minn, K., Yu, X.C., Yaffe, M.B., and Chen, J.J. (2007). RNF8 transduces the DNA-damage signal via histone ubiquitylation and checkpoint protein assembly. Cell *131*, 901-914.

Hung, P.J., Johnson, B., Chen, B.R., Byrum, A.K., Bredemeyer, A.L., Yewdell, W.T., Johnson, T.E., Lee, B.J., Deivasigamani, S., Hindi, I., *et al.* (2018). MRI Is a DNA Damage Response Adaptor during Classical Non-homologous End Joining. Molecular Cell *71*, 332-+.

Hustedt, N., Alvarez-Quilon, A., McEwan, A., Yuan, J.Y., Cho, T., Koob, L., Hart, T., and Durocher, D. (2019). A consensus set of genetic vulnerabilities to ATR inhibition. Open Biology *9*.

Imseng, S., Aylett, C.H.S., and Maier, T. (2018). Architecture and activation of phosphatidylinositol 3-kinase related kinases. Current Opinion in Structural Biology *49*, 177-189.

Jazayeri, A., Falck, J., Lukas, C., Bartek, J., Smith, G.C.M., Lukas, J., and Jackson, S.P. (2006). ATM- and cell cycle-dependent regulation of ATR in response to DNA double-strand breaks. Nature Cell Biology *8*, 37-U13.

Jette, N., and Lees-Miller, S.P. (2015). The DNA-dependent protein kinase: A multifunctional protein kinase with roles in DNA double strand break repair and mitosis. Progress in Biophysics & Molecular Biology *117*, 194-205.

Jiang, W.X., Crowe, J.L., Liu, X.Y., Nakajima, S., Wang, Y.Y., Li, C., Lee, B.J., Dubois, R.L., Liu, C., Yu, X.C., *et al.* (2015). Differential Phosphorylation of DNA-PKcs Regulates the Interplay between End-Processing and End-Ligation during Nonhomologous End-Joining. Molecular Cell *58*, 172-185.

Jiang, X.F., Sun, Y.L., Chen, S.J., Roy, K., and Price, B.D. (2006). The FATC domains of PIKK proteins are functionally equivalent and participate in the Tip60-dependent activation of DNA-PKcs and ATM. Journal of Biological Chemistry *281*, 15741-15746.

Jungmichel, S., Clapperton, J.A., Lloyd, J., Hari, F.J., Spycher, C., Pavic, L., Li, J.J., Haire, L.F., Bonalli, M., Larsen, D.H., *et al.* (2012). The molecular basis of ATM-dependent dimerization of the Mdc1 DNA damage checkpoint mediator. Nucleic Acids Research *40*, 3913-3928.

Kabeche, L., Nguyen, H.D., Buisson, R., and Zou, L. (2018). A mitosis-specific and R loop-driven ATR pathway promotes faithful chromosome segregation. Science *359*, 108-113.

Kilic, S., Lezaja, A., Gatti, M., Bianco, E., Michelena, J., Imhof, R., and Altmeyer, M. (2019). Phase separation of 53BP1 determines liquid-like behavior of DNA repair compartments. Embo Journal *38*.

Kim, A., Montales, K., Ruis, K., Senebandith, H., Gasparyan, H., Cowan, Q., and Michael, W.M. (2020). Biochemical analysis of TOPBP1 oligomerization. DNA repair *96*, 102973-102973.

Kim, W., Zhao, F., Wu, R.T., Qin, S.S., Nowsheen, S., Huang, J.Z., Zhou, Q., Chen, Y.P., Deng, M., Guo, G.J., *et al.* (2019). ZFP161 regulates replication fork stability and maintenance of genomic stability by recruiting the ATR/ATRIP complex. Nature Communications *10*.

Kobayashi, M., Hayashi, N., Takata, M., and Yamamoto, K. (2013). NBS1 directly activates ATR independently of MRE11 and TOPBP1. Genes to Cells *18*, 238-246.

Kolas, N.K., Chapman, J.R., Nakada, S., Ylanko, J., Chahwan, R., Sweeney, F.D., Panier, S., Mendez, M., Wildenhain, J., Thomson, T.M., *et al.* (2007). Orchestration of the DNA-damage response by the RNF8 ubiquitin ligase. Science *318*, 1637-1640.

Kuhn, E.M., and Therman, E. (1986). CYTOGENETICS OF BLOOMS SYNDROME. Cancer Genetics and Cytogenetics *22*, 1-18.

Kumagai, A., and Dunphy, W.G. (2000). Claspin, a novel protein required for the activation of Chk1 during a DNA replication checkpoint response in Xenopus egg extracts. Molecular Cell *6*, 839-849.

Kumagai, A., Lee, J., Yoo, H.Y., and Dunphy, W.G. (2006). TopBP1 activates the ATR-ATRIP complex. Cell *124*, 943-955.

Kumar, A., Mazzanti, M., Mistrik, M., Kosar, M., Beznoussenko, G.V., Mironov, A.A., Garre, M., Parazzoli, D., Shivashankar, G.V., Scita, G., *et al.* (2014). ATR Mediates a Checkpoint at the Nuclear Envelope in Response to Mechanical Stress. Cell *158*, 633-646.

Kumar, S., and Burgers, P.M. (2013). Lagging strand maturation factor Dna2 is a component of the replication checkpoint initiation machinery. Genes & Development *27*, 313-321.

Kwok, M., Davies, N., Agathanggelou, A., Smith, E., Oldreive, C., Petermann, E., Stewart, G., Brown, J., Lau, A., Pratt, G., *et al.* (2016). ATR inhibition induces synthetic lethality and overcomes chemoresistance in TP53- or ATM-defective chronic lymphocytic leukemia cells. Blood *127*, 582.

Kwok, M., Davies, N., Agathanggelou, A., Smith, E., Petermann, E., Yates, E., Brown, J., Lau, A., and Stankovic, T. (2015). Synthetic lethality in chronic lymphocytic leukaemia with DNA damage response defects by targeting the ATR pathway. Lancet *385*, 58-58.

Lamm, N., Read, M.N., Nobis, M., Van Ly, D., Page, S.G., Masamsetti, V.P., Timpson, P., Biro, M., and Cesare, A.J. (2020). Nuclear F-actin counteracts nuclear deformation and promotes fork repair during replication stress. Nature Cell Biology *22*, 1460-+.

Lanz, M.C., Dibitetto, D., and Smolka, M.B. (2019). DNA damage kinase signaling: checkpoint and repair at 30 years. Embo Journal *38*.

Lee, J., Gold, D.A., Shevchenko, A., and Dunphy, W.G. (2005). Roles of replication fork-interacting and Chk1-activating domains from claspin in a DNA replication checkpoint response. Molecular Biology of the Cell *16*, 5269-5282.

Lee, J., Kumagai, A., and Dunphy, W.G. (2001). Positive regulation of Wee1 by Chk1 and 14-3-3 proteins. Molecular Biology of the Cell *12*, 551-563.

Lee, J.-H., Mand, M.R., Deshpande, R.A., Kinoshita, E., Yang, S.-H., Wyman, C., and Paull, T.T. (2013). Ataxia telangiectasia-mutated (ATM) kinase activity is regulated by ATP-driven conformational changes in the Mre11/Rad50/Nbs1 (MRN) complex. The Journal of biological chemistry *288*, 12840.

Lee, J.B., Hite, R.K., Hamdan, S.M., Xie, X.S., Richardson, C.C., and van Oijen, A.M. (2006). DNA primase acts as a molecular brake in DNA replication. Nature *439*, 621-624.

Lee, J.H., Mand, M.R., Kao, C.H., Zhou, Y., Ryu, S.W., Richards, A.L., Coon, J.J., and Paull, T.T. (2018). ATM directs DNA damage responses and proteostasis via genetically separable pathways. Science Signaling *11*.

Lee, J.H., and Paull, T.T. (2004). Direct activation of the ATM protein kinase by the Mre11/Rad50/Nbs1 complex. Science *304*, 93-96.

Lee, J.H., and Paull, T.T. (2005). ATM activation by DNA double-strand breaks through the Mre11-Rad50-Nbs1 complex. Science *308*, 551-554.

Lee, J.H., Xu, B., Lee, C.H., Ahn, J.Y., Song, M.S., Lee, H., Canman, C.E., Lee, J.S., Kastan, M.B., and Lim, D.S. (2003). Distinct functions of Nijmegen breakage syndrome in ataxia telangiectasia mutated-dependent responses to DNA damage. Molecular Cancer Research *1*, 674-681.

Lee, Y.C., Zhou, Q., Chen, J.J., and Yuan, J.S. (2016). RPA-Binding Protein ETAA1 Is an ATR Activator Involved in DNA Replication Stress Response. Current Biology *26*, 3257-3268.

Lemmens, B., Hegarat, N., Akopyan, K., Sala-Gaston, J., Bartek, J., Hochegger, H., and Lindqvist, A. (2018). DNA Replication Determines Timing of Mitosis by Restricting CDK1 and PLK1 Activation. Molecular Cell *71*, 117-+.

Li, F., Kozono, D., Deraska, P., Branigan, T., Dunn, C., Zheng, X.F., Parmar, K., Nguyen, H., DeCaprio, J., Shapiro, G.I., *et al.* (2020). CHK1 Inhibitor Blocks Phosphorylation of FAM122A and Promotes Replication Stress. Molecular Cell *80*, 410-+.

Lim, D.S., Kim, S.T., Xu, B., Maser, R.S., Lin, J.Y., Petrini, J.H.J., and Kastan, M.B. (2000). ATM phosphorylates p95/nbs1 in an S-phase checkpoint pathway. Nature *404*, 613-+.

Lin, J.J., and Dutta, A. (2007). ATR pathway is the primary pathway for activating G(2)/m checkpoint induction after re-replication. Journal of Biological Chemistry *282*, 30357-30362.

Lindsey-Boltz, L.A., Kemp, M.G., Capp, C., and Sancar, A. (2015). RHINO forms a stoichiometric complex with the 9-1-1 checkpoint clamp and mediates ATR-Chk1 signaling. Cell Cycle *14*, 99-108.

Liu, H., Takeda, S., Kumar, R., Westergard, T.D., Brown, E.J., Pandita, T.K., Cheng, E.H.Y., and Hsieh, J.J.D. (2010). Phosphorylation of MLL by ATR is required for execution of mammalian S-phase checkpoint. Nature *467*, 343-U126.

Liu, J.P., Luo, S.K., Zhao, H.C., Liao, J., Li, J., Yang, C.Y., Xu, B., Stern, D.F., Xu, X.Z., and Ye, K.Q. (2012). Structural mechanism of the phosphorylation-dependent dimerization of the MDC1 forkhead-associated domain. Nucleic Acids Research *40*, 3898-3912.

Liu, K., Graves, J.D., Scott, J.D., Li, R.B., and Lin, W.C. (2013). Akt Switches TopBP1 Function from Checkpoint Activation to Transcriptional Regulation through Phosphoserine Binding-Mediated Oligomerization. Molecular and Cellular Biology *33*, 4685-4700.

Liu, K., Paik, J.C., Wang, B., Lin, F.T., and Lin, W.C. (2006). Regulation of TopBP1 oligomerization by Akt/PKB for cell survival. Embo Journal *25*, 4795-4807.

Liu, S.Z., Shiotani, B., Lahiri, M., Marechal, A., Tse, A., Leung, C.C.Y., Glover, J.N.M., Yang, X.H.H., and Zou, L. (2011). ATR Autophosphorylation as a Molecular Switch for Checkpoint Activation. Molecular Cell *43*, 192-202.

Liu, W., Krishnamoorthy, A., Zhao, R., and Cortez, D. (2020). Two replication fork remodeling pathways generate nuclease substrates for distinct fork protection factors. Science Advances *6*.

Lopez-Contreras, A.J., Specks, J., Barlow, J.H., Ambrogio, C., Desler, C., Vikingsson, S., Rodrigo-Perez, S., Green, H., Rasmussen, L.J., Murga, M., *et al.* (2015). Increased Rrm2 gene dosage reduces fragile site breakage and prolongs survival of ATR mutant mice. Genes & Development *29*, 690-695.

Lossaint, G., Larroque, M., Ribeyre, C., Bec, N., Larroque, C., Decaillet, C., Gari, K., and Constantinou, A. (2013). FANCD2 Binds MCM Proteins and Controls Replisome Function upon Activation of S Phase Checkpoint Signaling. Molecular Cell *51*, 678-690.

Luis, I.T., Matilde, M., Rafal, Z., Rebeca, S., Antonio, R., Sonia, M., Julen, O., Joaquin, P., James, R.B., and Oscar, F.-C. (2011). A cell-based screen identifies ATR inhibitors with synthetic lethal properties for cancer-associated mutations. Nature Structural & Molecular Biology *18*, 721.

Lukas, J., Lukas, C., and Bartek, J. (2004). Mammalian cell cycle checkpoints: signalling pathways and their organization in space and time. DNA Repair *3*, 997-1007.

Lyu, K., Kumagai, A., and Dunphy, W.G. (2019). RPA-coated single-stranded DNA promotes the ETAA1-dependent activation of ATR. Cell Cycle *18*, 898-913.

Ma, Y.M., Pannicke, U., Schwarz, K., and Lieber, M.R. (2002). Hairpin opening and overhang processing by an Artemis/DNA-dependent protein kinase complex in nonhomologous end joining and V(D)J recombination. Cell *108*, 781-794.

MacDougall, C.A., Byun, T.S., Van, C., Yee, M.C., and Cimprich, K.A. (2007). The structural determinants of checkpoint activation. Genes & Development *21*, 898-903.

Macheret, M., and Halazonetis, T.D. (2015). DNA Replication Stress as a Hallmark of Cancer. Annual Review of Pathology: Mechanisms of Disease *10*, 425-448.

Mailand, N., Bekker-Jensen, S., Faustrup, H., Melander, F., Bartek, J., Lukas, C., and Lukas, J. (2007). RNF8 ubiquitylates histones at DNA double-strand breaks and promotes assembly of repair proteins. Cell *131*, 887-900.

Mailand, N., Falck, J., Lukas, C., Syljuasen, R.G., Welcker, M., Bartek, J., and Lukas, L. (2000). Rapid destruction of human Cdc25A in response to DNA damage. Science *288*, 1425-1429.

Marinello, J., Chillemi, G., Bueno, S., Manzo, S.G., and Capranico, G. (2013). Antisense transcripts enhanced by camptothecin at divergent CpG-island promoters associated with bursts of topoisomerase I-DNA cleavage complex and R-loop formation. Nucleic Acids Research *41*, 10110-10123.

Matilde, M., Stefano, C., Andres, J.L.-C., Luis, I.T., Rebeca, S., Maria, F.M., Luana, D.A., Thomas, S., Carmen, G., Elena, G., *et al.* (2011). Exploiting oncogene-induced replicative stress for the selective killing of Myc-driven tumors. Nature Structural & Molecular Biology *18*, 1331.

Matos, D.A., Zhang, J.M., Ouyang, J., Nguyen, H.D., Genois, M.M., and Zou, L. (2020). ATR Protects the Genome against R Loops through a MUS81-Triggered Feedback Loop. Molecular Cell *77*, 514-+.

Matsuoka, S., Ballif, B.A., Smogorzewska, A., McDonald, E.R., Hurov, K.E., Luo, J., Bakalarski, C.E., Zhao, Z.M., Solimini, N., Lerenthal, Y., *et al.* (2007). ATM and ATR substrate analysis reveals extensive protein networks responsive to DNA damage. Science *316*, 1160-1166.

McDonnell, A.V., Jiang, T., Keating, A.E., and Berger, B. (2006). Paircoil2: improved prediction of coiled coils from sequence. Bioinformatics *22*, 356-358.

McElhinny, S.A.N., Gordenin, D.A., Stith, C.M., Burgers, P.M.J., and Kunkel, T.A. (2008). Division of labor at the eukaryotic replication fork. Molecular Cell *30*, 137-144.

McTigue, M.A., Williams, D.R., and Tainer, J.A. (1995). CRYSTAL-STRUCTURES OF A SCHISTOSOMAL DRUG AND VACCINE TARGET - GLUTATHIONE-S-TRANSFERASE FROM SCHISTOSOMA-JAPONICA AND ITS COMPLEX WITH THE LEADING ANTISCHISTOSOMAL DRUG PRAZIQUANTEL. Journal of Molecular Biology *246*, 21-27.

Melander, F., Bekker-Jensen, S., Falck, J., Bartek, J., Mailand, N., and Lukas, J. (2008). Phosphorylation of SDT repeats in the MDC1 N terminus triggers retention of NBS1 at the DNA damage-modified chromatin. Journal of Cell Biology *181*, 213-226.

Memisoglu, G., Lanz, M.C., Eapen, V.V., Jordan, J.M., Lee, K., Smolka, M.B., and Haber, J.E. (2019). Mec1(ATR) Autophosphorylation and Ddc2(ATRIP) Phosphorylation Regulates DNA Damage Checkpoint Signaling. Cell Reports *28*, 1090-+.

Menezes, D.L., Holt, J., Tang, Y., Feng, J., Barsanti, P., Pan, Y., Ghoddusi, M., Zhang, W., Thomas, G., Holash, J., *et al.* (2015). A Synthetic Lethal Screen Reveals Enhanced Sensitivity to ATR Inhibitor Treatment in Mantle Cell Lymphoma with ATM Loss-of-Function. Molecular Cancer Research *13*, 120-129.

Menolfi, D., and Zha, S. (2020). ATM, ATR and DNA-PKcs kinases-the lessons from the mouse models: inhibition ≠ deletion. Cell & bioscience *10*, 8.

Meszaros, B., Erdos, G., and Dosztanyi, Z. (2018). IUPred2A: context-dependent prediction of protein disorder as a function of redox state and protein binding. Nucleic Acids Research *46*, W329-W337.

Michelena, J., Gatti, M., Teloni, F., Imhof, R., and Altmeyer, M. (2019). Basal CHK1 activity safeguards its stability to maintain intrinsic S-phase checkpoint functions. Journal of Cell Biology *218*, 2865-2875.

Mimori, T., Hardin, J.A., and Steitz, J.A. (1986). CHARACTERIZATION OF THE DNA-BINDING PROTEIN ANTIGEN-KU RECOGNIZED BY AUTOANTIBODIES FROM PATIENTS WITH RHEUMATIC DISORDERS. Journal of Biological Chemistry *261*, 2274-2278.

Min, A., Im, S.-A., Jang, H., Kim, S., Lee, M., Kim, D.K., Yang, Y., Kim, H.-J., Lee, K.-H., Kim, J.W., *et al.* (2017). AZD6738, A Novel Oral Inhibitor of ATR, Induces Synthetic Lethality with ATM Deficiency in Gastric Cancer Cells. Molecular cancer therapeutics *16*, 566.

Min, J., Wright, W.E., and Shay, J.W. (2019). Clustered telomeres in phase-separated nuclear condensates engage mitotic DNA synthesis through BLM and RAD52. Genes & Development *33*, 814-827.

Miosge, L.A., Sontani, Y., Chuah, A., Horikawa, K., Russell, T.A., Mei, Y., Wagle, M.V., Howard, D.R., Enders, A., Tscharke, D.C., *et al.* (2017). Systems-guided forward genetic screen reveals a critical role of the replication stress response protein ETAA1 in T cell clonal expansion. Proceedings of the National Academy of Sciences of the United States of America *114*, E5216-E5225.

Moiseeva, T.N., Yin, Y.D., Calderon, M.J., Qian, C.A., Schamus-Haynes, S., Sugitani, N., Osmanbeyoglu, H.U., Rothenberg, E., Watkins, S.C., and Bakkenist, C.J. (2019). An ATR and CHK1 kinase signaling mechanism that limits origin firing during unperturbed DNA replication. Proceedings of the National Academy of Sciences of the United States of America *116*, 13374-13383.

Morafraile, E.C., Hanni, C., Allen, G., Zeisner, T., Clarke, C., Johnson, M.C., Santos, M.M., Carroll, L., Minchell, N.E., Baxter, J., *et al.* (2019). Checkpoint inhibition of origin firing prevents DNA topological stress. Genes & Development *33*, 1539-1554.

Mordes, D.A., Glick, G.G., Zhao, R.X., and Cortez, D. (2008a). TopBP1 activates ATR through ATRIP and a PIKK regulatory domain. Genes & Development *22*, 1478-1489.

Mordes, D.A., Nam, E.A., and Cortez, D. (2008b). Dpb11 activates the Mec1-Ddc2 complex. Proceedings of the National Academy of Sciences of the United States of America *105*, 18730-18734.

Mouron, S., Rodriguez-Acebes, S., Martinez-Jimenez, M.I., Garcia-Gomez, S., Chocron, S., Blanco, L., and Mendez, J. (2013). Repriming of DNA synthesis at stalled replication forks by human Prim Pol. Nature Structural & Molecular Biology *20*, 1383-1389.

Munoz, I.M., Jowsey, P.A., Toth, R., and Rouse, J. (2007). Phospho-epitope binding by the BRCT domains of hPTIP controls multiple aspects of the cellular response to DNA damage. Nucleic Acids Research *35*, 5312-5322.

Murphy, A.K., Fitzgerald, M., Ro, T., Kim, J.H., Rabinowitsch, A.I., Chowdhury, D., Schildkraut, C.L., and Borowiec, J.A. (2014). Phosphorylated RPA recruits PALB2 to stalled DNA replication forks to facilitate fork recovery. Journal of Cell Biology *206*, 493-507.

Mutreja, K., Krietsch, J., Hess, J., Ursich, S., Berti, M., Roessler, F.K., Zellweger, R., Patra, M., Gasser, G., and Lopes, M. (2018). ATR-Mediated Global Fork Slowing and Reversal Assist Fork Traverse and Prevent Chromosomal Breakage at DNA Interstrand Cross-Links. Cell Reports *24*, 2629-+.

Myers, J.S., and Cortez, D. (2006). Rapid activation of ATR by ionizing radiation requires ATM and Mre11. Journal of Biological Chemistry *281*, 9346-9350.

Nam, E.A., Zhao, R.X., Glick, G.G., Bansbach, C.E., Friedman, D.B., and Cortez, D. (2011). Thr-1989 Phosphorylation Is a Marker of Active Ataxia Telangiectasia-mutated and Rad3-related (ATR) Kinase. Journal of Biological Chemistry *286*, 28707-28714.

Navadgi-Patil, V.M., and Burgers, P.M. (2008). Yeast DNA Replication Protein Dpb11 Activates the Mec1/ATR Checkpoint Kinase. Journal of Biological Chemistry *283*, 35853-35859.

Navadgi-Patil, V.M., and Burgers, P.M. (2009). The Unstructured C-Terminal Tail of the 9-1-1 Clamp Subunit Ddc1 Activates Mec1/ATR via Two Distinct Mechanisms. Molecular Cell *36*, 743-753.

Navadgi-Patil, V.M., Kumar, S., and Burgers, P.M. (2011). The Unstructured C-terminal Tail of Yeast Dpb11 (Human TopBP1) Protein Is Dispensable for DNA Replication and the S Phase Checkpoint but Required for the G(2)/M Checkpoint. Journal of Biological Chemistry *286*, 40999-41007.

Neelsen, K.J., and Lopes, M. (2015). Replication fork reversal in eukaryotes: from dead end to dynamic response. Nature Reviews Molecular Cell Biology *16*, 207-220.

O'Driscoll, M., Ruiz-Perez, V.L., Woods, C.G., Jeggo, P.A., and Goodship, J.A. (2003). A splicing mutation affecting expression of ataxia-telangiectasia and Rad3-related protein (ATR) results in Seckel syndrome. Nature Genetics *33*, 497-501.

Ochi, T., Blackford, A.N., Coates, J., Jhujh, S., Mehmood, S., Tamura, N., Travers, J., Wu, Q., Draviam, V.M., Robinson, C.V., *et al.* (2015). PAXX, a paralog of XRCC4 and XLF, interacts with Ku to promote DNA double-strand break repair. Science *347*, 185-188.

Oconnell, M.J., Raleigh, J.M., Verkade, H.M., and Nurse, P. (1997). Chk1 is a wee1 kinase in the G(2) DNA damage checkpoint inhibiting cdc2 by Y15 phosphorylation. Embo Journal *16*, 545-554.

Okazaki, R., Okazaki, T., Sakabe, K., Sugimoto, K., Kainuma, R., Sugino, A., and Iwatsuki, N. (1968). IN VIVO MECHANISM OF DNA CHAIN GROWTH. Cold Spring Harbor Symposia on Quantitative Biology *33*, 129-&.

Patel, A., Lee, H.O., Jawerth, L., Maharana, S., Jahnel, M., Hein, M.Y., Stoynov, S., Mahamid, J., Saha, S., Franzmann, T.M., *et al.* (2015). A Liquid-to-Solid Phase Transition of the ALS Protein FUS Accelerated by Disease Mutation. Cell *162*, 1066-1077.

Paull, T.T. (2015). Mechanisms of ATM Activation. Annual Review of Biochemistry, Vol 84 *84*, 711-738.

Pellegrini, M., Celeste, A., Difilippantonio, S., Guo, R., Wang, W.D., Feigenbaum, L., and Nussenzweig, A. (2006). Autophosphorylation at serine 1987 is dispensable for murine Atm activation in vivo. Nature *443*, 222-225.

Peng, C.Y., Graves, P.R., Thoma, R.S., Wu, Z.Q., Shaw, A.S., and PiwnicaWorms, H. (1997). Mitotic and G(2) checkpoint control: Regulation of 14-3-3 protein binding by phosphorylation of Cdc25C on serine-216. Science *277*, 1501-1505.

Perkhofer, L., Schmitt, A., Romero Carrasco, M.C., Ihle, M., Hampp, S., Ruess, D.A., Hessmann, E., Russell, R., Lechel, A., Azoitei, N., *et al.* (2017). ATM Deficiency Generating Genomic Instability Sensitizes Pancreatic Ductal Adenocarcinoma Cells to Therapy-Induced DNA Damage. Cancer research *77*, 5576.

Pessina, F., Giavazzi, F., Yin, Y.D., Gioia, U., Vitelli, V., Galbiati, A., Barozzi, S., Garre, M., Oldani, A., Flaus, A., *et al.* (2019). Functional transcription promoters at DNA double-strand breaks mediate RNA-driven phase separation of damage-response factors. Nature Cell Biology *21*, 1286-+.

Pfander, B., and Diffley, J.F.X. (2011). Dpb11 coordinates Mec1 kinase activation with cell cycle-regulated Rad9 recruitment. Embo Journal *30*, 4897-4907.

Pursell, Z.F., Isoz, I., Lundstrom, E.B., Johansson, E., and Kunkel, T.A. (2007). Yeast DNA polymerase epsilon participates in leading-strand DNA replication. Science *317*, 127-130.

Qiu, Z.J., Oleinick, N.L., and Zhang, J.R. (2018). ATR/CHK1 inhibitors and cancer therapy. Radiotherapy and Oncology *126*, 450-464.

Quinet, A., Tirman, S., Jackson, J., Svikovic, S., Lemacon, D., Carvajal-Maldonado, D., Gonzalez-Acosta, D., Vessoni, A.T., Cybulla, E., Wood, M., *et al.* (2020). PRIMPOL-Mediated Adaptive Response Suppresses Replication Fork Reversal in BRCA-Deficient Cells. Molecular Cell *77*, 461-+.

Randell, J.C.W., Fan, A., Chan, C., Francis, L.I., Heller, R.C., Galani, K., and Bell, S.P. (2010). Mec1 Is One of Multiple Kinases that Prime the Mcm2-7 Helicase for Phosphorylation by Cdc7. Molecular Cell *40*, 353-363.

Rao, Q.H., Liu, M.J., Tian, Y., Wu, Z.H., Hao, Y.H., Song, L., Qin, Z.Y., Ding, C., Wang, H.W., Wang, J.W., *et al.* (2018). Cryo-EM structure of human ATR-ATRIP complex. Cell Research *28*, 143-156.

Rappas, M., Oliver, A.W., and Pearl, L.H. (2011). Structure and function of the Rad9-binding region of the DNA-damage checkpoint adaptor TopBP1. Nucleic Acids Research *39*, 313-324.

Reeves, W.H. (1985). USE OF MONOCLONAL-ANTIBODIES FOR THE CHARACTERIZATION OF NOVEL DNA-BINDING PROTEINS RECOGNIZED BY HUMAN AUTOIMMUNE SERA. Journal of Experimental Medicine *161*, 18-39.

Riballo, E., Kuhne, M., Rief, N., Doherty, A., Smith, G.C.M., Recio, M.J., Reis, C., Dahm, K., Fricke, A., Krempler, A., *et al.* (2004). A pathway of double-strand break rejoining dependent upon ATM, artemis, and proteins locating to gamma-H2AX foci. Molecular Cell *16*, 715-724.

Saldivar, J.C., Cortez, D., and Cimprich, K.A. (2017). The essential kinase ATR: ensuring faithful duplication of a challenging genome. Nature Reviews Molecular Cell Biology *18*, 622-636.

Saldivar, J.C., Hamperl, S., Bocek, M.J., Chung, M.Y., Bass, T.E., Cisneros-Soberanis, F., Samejima, K., Xie, L.F., Paulson, J.R., Earnshaw, W.C., *et al.* (2018). An intrinsic S/G(2) checkpoint enforced by ATR. Science *361*, 806-809.

Sanchez, Y., Wong, C., Thoma, R.S., Richman, R., Wu, R.Q., PiwnicaWorms, H., and Elledge, S.J. (1997). Conservation of the Chk1 checkpoint pathway in mammals: Linkage of DNA damage to Cdk regulation through Cdc25. Science *277*, 1497-1501.

Sato, H., Niimi, A., Yasuhara, T., Permata, T.B.M., Hagiwara, Y., Isono, M., Nuryadi, E., Sekine, R., Oike, T., Kakoti, S., *et al.* (2017). DNA double-strand break repair pathway regulates PD-L1 expression in cancer cells. Nature Communications *8*.

Sawicka, M., Wanrooij, P.H., Darbari, V.C., Tannous, E., Hailemariam, S., Bose, D., Makarova, A.V., Burgers, P.M., and Zhang, X. (2016). The Dimeric Architecture of Checkpoint Kinases

Mec1ATR and Tel1ATM Reveal a Common Structural Organization. The Journal of biological chemistry *291*, 13436-13447.

Saxena, S., Dixit, S., Somyajit, K., and Nagaraju, G. (2019). ATR Signaling Uncouples the Role of RAD51 Paralogs in Homologous Recombination and Replication Stress Response. Cell Reports *29*, 551-+.

Schmitt, A., Knittel, G., Welcker, D., Yang, T.-P., George, J., Nowak, M., Leeser, U., Büttner, R., Perner, S., Peifer, M., *et al.* (2017). Deficiency Is Associated with Sensitivity to PARP1- and ATR Inhibitors in Lung Adenocarcinoma. Cancer research *77*, 3040.

Scully, R., Panday, A., Elango, R., and Willis, N.A. (2019). DNA double-strand break repair-pathway choice in somatic mammalian cells. Nature Reviews Molecular Cell Biology *20*, 698-714.

Scully, R., and Xie, A.Y. (2013). Double strand break repair functions of histone H2AX. Mutation Research-Fundamental and Molecular Mechanisms of Mutagenesis *750*, 5-14.

Sen, T., Tong, P., Stewart, C.A., Cristea, S., Valliani, A., Shames, D.S., Redwood, A.B., Fan, Y.H., Li, L., Glisson, B.S., *et al.* (2017). CHK1 Inhibition in Small-Cell Lung Cancer Produces Single-Agent Activity in Biomarker-Defined Disease Subsets and Combination Activity with Cisplatin or Olaparib. Cancer research *77*, 3870.

Shastri, N., Tsai, Y.C., Hile, S., Jordan, D., Powell, B., Chen, J., Maloney, D., Dose, M., Lo, Y., Anastassiadis, T., *et al.* (2018). Genome-wide Identification of Structure-Forming Repeats as Principal Sites of Fork Collapse upon ATR Inhibition. Molecular Cell *72*, 222-+.

Sheu, Y.J., Kinney, J.B., Lengronne, A., Pasero, P., and Stillman, B. (2014). Domain within the helicase subunit Mcm4 integrates multiple kinase signals to control DNA replication initiation and fork progression. Proceedings of the National Academy of Sciences of the United States of America *111*, E1899-E1908.

Shibata, A., Conrad, S., Birraux, J., Geuting, V., Barton, O., Ismail, A., Kakarougkas, A., Meek, K., Taucher-Scholz, G., Lobrich, M., *et al.* (2011). Factors determining DNA double-strand break repair pathway choice in G2 phase. Embo Journal *30*, 1079-1092.

Shiloh, Y., and Ziv, Y. (2013). The ATM protein kinase: regulating the cellular response to genotoxic stress, and more. Nature Reviews Molecular Cell Biology *14*, 197-210.

Sibanda, B.L., Chirgadze, D.Y., Ascher, D.B., and Blundell, T.L. (2017). DNA-PKcs structure suggests an allosteric mechanism modulating DNA double-strand break repair. Science *355*, 520-+.

Singh, A., and Xu, Y.J. (2016). The Cell Killing Mechanisms of Hydroxyurea. Genes *7*.

Singleton, B.K., Torres-Arzayus, M.I., Rottinghaus, S.T., Taccioli, G.E., and Jeggo, P.A. (1999). The C terminus of Ku80 activates the DNA-dependent protein kinase catalytic subunit. Molecular and Cellular Biology *19*, 3267-3277.

Smits, V.A.J., Cabrera, E., Freire, R., and Gillespie, D.A. (2019). Claspin - checkpoint adaptor and DNA replication factor. Febs Journal *286*, 441-455.

Sorensen, C.S., Syluasen, R.G., Falck, J., Schroeder, T., Ronnstrand, L., Khanna, K.K., Zhou, B.B., Bartek, J., and Lukas, J. (2003). Chk1 regulates the S phase checkpoint by coupling the physiological turnover and ionizing radiation-induced accelerated proteolysis of Cdc25A. Cancer Cell *3*, 247-258.

Spagnolo, L., Rivera-Calzada, A., Pearl, L.H., and Llorca, O. (2006). Three-dimensional structure of the human DNA-PKcs/Ku70/Ku80 complex assembled on DNA and its implications for DNA DSB repair. Molecular Cell *22*, 511-519.

Spycher, C., Miller, E.S., Townsend, K., Pavic, L., Morrice, N.A., Janscak, P., Stewart, G.S., and Stucki, M. (2008). Constitutive phosphorylation of MDC1 physically links the MRE11-RAD50-NBS1 complex to damaged chromatin. Journal of Cell Biology *181*, 227-240.

Stavropoulos, D.J., Bradshaw, P.S., Li, X.B., Pasic, I., Truong, K., Ikura, M., Ungrin, M., and Meyn, M.S. (2002). The Bloom syndrome helicase BLM interacts with TRF2 in ALT cells and promotes telomeric DNA synthesis. Human Molecular Genetics *11*, 3135-3144.

Stucki, M., Clapperton, J.A., Mohammad, D., Yaffe, M.B., Smerdon, S.J., and Jackson, S.P. (2005). MDC1 directly binds phosphorylated histone H2AX to regulate cellular responses to DNA double-strand breaks. Cell *123*, 1213-1226.

Sun, Y.L., Xu, Y., Roy, K., and Price, B.D. (2007). DNA damage-induced acetylation of lysine 3016 of ATM activates ATM kinase activity. Molecular and Cellular Biology *27*, 8502-8509.

Syed, A., and Tainer, J.A. (2018). The MRE11-RAD50-NBS1 Complex Conducts the Orchestration of Damage Signaling and Outcomes to Stress in DNA Replication and Repair. Annual Review of Biochemistry, Vol 87 *87*, 263-294.

Tannous, E., Yates, L., Zhang, X., and Burgers, P. (2020). Mechanism of auto-inhibition and activation of Mec1ATR checkpoint kinase. Nature Structural & Molecular Biology, undefined-undefined.

Tannous, E.A., Yates, L.A., Zhang, X.D., and Burgers, P.M. (2021). Mechanism of auto-inhibition and activation of Mec1(ATR) checkpoint kinase. Nature Structural & Molecular Biology *28*.

Tarsounas, M., and Sung, P.R. (2020). The antitumorigenic roles of BRCA1-BARD1 in DNA repair and replication. Nature Reviews Molecular Cell Biology *21*, 284-299.

Taylor, M.R.G., and Yeeles, J.T.P. (2018). The Initial Response of a Eukaryotic Replisome to DNA Damage. Molecular Cell *70*, 1067-+.

Thada, V., and Cortez, D. (2019). Common motifs in ETAA1 and TOPBP1 required for ATR kinase activation. The Journal of biological chemistry *294*, 8395.

Thangavel, S., Berti, M., Levikova, M., Pinto, C., Gomathinayagam, S., Vujanovic, M., Zellweger, R., Moore, H., Lee, E.H., Henclrickson, E.A., *et al.* (2015). DNA2 drives processing and restart of reversed replication forks in human cells. Journal of Cell Biology *208*, 545-562.

Thorslund, T., Ripplinger, A., Hoffmann, S., Wild, T., Uckelmann, M., Villumsen, B., Narita, T., Sixma, T.K., Choudhary, C., Bekker-Jensen, S., *et al.* (2015). Histone H1 couples initiation and amplification of ubiquitin signalling after DNA damage. Nature *527*, 389-+.

Toledo, L.I., Altmeyer, M., Rask, M.B., Lukas, C., Larsen, D.H., Povlsen, L.K., Bekker-Jensen, S., Mailand, N., Bartek, J., and Lukas, J. (2013). ATR Prohibits Replication Catastrophe by Preventing Global Exhaustion of RPA. Cell *155*, 1088-1103.

Van, C., Yan, S., Michael, W.M., Waga, S., and Cimprich, K.A. (2010). Continued primer synthesis at stalled replication forks contributes to checkpoint activation. Journal of Cell Biology *189*, 233-246.

Vassin, V.M., Anantha, R.W., Sokolova, E., Kanner, S., and Borowiec, J.A. (2009). Human RPA phosphorylation by ATR stimulates DNA synthesis and prevents ssDNA accumulation during DNA-replication stress. Journal of Cell Science *122*, 4070-4080.

Wang, C., Wang, G., Feng, X., Shepherd, P., Zhang, J., Tang, M.F., Chen, Z., Srivastava, M., McLaughlin, M.E., Navone, N.M., *et al.* (2019). Genome-wide CRISPR screens reveal synthetic lethality of RNASEH2 deficiency and ATR inhibition. Oncogene *38*, 2451-2463.

Wang, H.L., Shi, L.Z., Wong, C.C.L., Han, X.M., Hwang, P.Y.H., Truong, L.N., Zhu, Q.Y., Shao, Z.P., Chen, D.J., Berns, M.W., *et al.* (2013). The Interaction of CtIP and Nbs1 Connects CDK and ATM to Regulate HR-Mediated Double-Strand Break Repair. Plos Genetics *9*.

Wang, X.J., Chu, H.Y., Lv, M.J., Zhang, Z.H., Qiu, S.W., Liu, H.Y., Shen, X.T., Wang, W.W., and Cai, G. (2016). Structure of the intact ATM/Tel1 kinase. Nature Communications *7*.

Wang, X.J., Ran, T.T., Zhang, X., Xin, J.Y., Zhang, Z.H., Wu, T.W., Wang, W.W., and Cai, G. (2017). 3.9 angstrom structure of the yeast Mec1-Ddc2 complex, a homolog of human ATR-ATRIP. Science *358*, 1206-1209.

Wanrooij, P.H., Tannous, E., Kumar, S., Navadgi-Patil, V.M., and Burgers, P.M. (2016). Probing the Mec1(ATR) Checkpoint Activation Mechanism with Small Peptides. Journal of Biological Chemistry *291*, 393-401.

Woodbine, L., Neal, J.A., Sasi, N.K., Shimada, M., Deem, K., Coleman, H., Dobyns, W.B., Ogi, T., Meek, K., Davies, E.G., *et al.* (2013). PRKDC mutations in a SCID patient with profound neurological abnormalities. Journal of Clinical Investigation *123*, 2969-2980.

Wu, L., Bachrati, C.Z., Ou, J.W., Xu, C., Yin, J.H., Chang, M., Wang, W.D., Li, L., Brown, G.W., and Hickson, I.D. (2006). BLAP75/RMI1 promotes the BLM-dependent dissolution of homologous recombination intermediates. Proceedings of the National Academy of Sciences of the United States of America *103*, 4068-4073.

Wu, W., Bhowmick, R., Vogel, I., zer, Ghisays, F., Thakur, R.S., de Leon, E.S., Richter, P.H., Ren, L.Q., Petrini, J.H., *et al.* (2020). RTEL1 suppresses G-quadruplex-associated R-loops at difficult-to-replicate loci in the human genome. Nature Structural & Molecular Biology *27*, 424-+.

Wyatt, H.D.M., Sarbajna, S., Matos, J., and West, S.C. (2013). Coordinated Actions of SLX1-SLX4 and MUS81-EME1 for Holliday Junction Resolution in Human Cells. Molecular Cell *52*, 234-247.

Yan, S., and Michael, W.M. (2009). TopBP1 and DNA polymerase-alpha directly recruit the 9-1-1 complex to stalled DNA replication forks. Journal of Cell Biology *184*, 793-804.

Yang, H.J., Jiang, X.L., Li, B.R., Miller, M., Yang, A., Dhar, A., and Pavletich, N.P. (2017). Mechanisms of mTORC1 activation by RHEB and inhibition by PRAS40. Nature *552*, 368-+.

Yao, N.Y., Georgescu, R.E., Finkelstein, J., and O'Donnell, M.E. (2009). Single-molecule analysis reveals that the lagging strand increases replisome processivity but slows replication fork progression. Proceedings of the National Academy of Sciences of the United States of America *106*, 13236-13241.

Yazdi, P.T., Wang, Y., Zhao, S., Patel, N., Lee, E., and Qin, J. (2002). SMC1 is a downstream effector in the ATM/NBS1 branch of the human S-phase checkpoint. Genes & Development *16*, 571-582.

Yekezare, M., Gomez-Gonzalez, B., and Diffley, J.F.X. (2013). Controlling DNA replication origins in response to DNA damage - inhibit globally, activate locally. Journal of Cell Science *126*, 1297-1306.

Yin, X.T., Liu, M.J., Tian, Y., Wang, J.W., and Xu, Y.H. (2017). Cryo-EM structure of human DNA-PK holoenzyme. Cell Research *27*, 1341-1350.

Yoo, H.Y., Kumagai, A., Shevchenko, A., and Dunphy, W.G. (2007). Ataxia-telangiectasia mutated (ATM)-dependent activation of ATR occurs through phosphorylation of TopBP1 by ATM. Journal of Biological Chemistry *282*, 17501-17506.

Zachos, G., Black, E.J., Walker, M., Scott, M.T., Vagnarelli, P., Earnshaw, W.C., and Gillespie, D.A.F. (2007). Chk1 is required for spindle checkpoint function. Developmental Cell *12*, 247-260.

Zeman, M.K., and Cimprich, K.A. (2014). Causes and consequences of replication stress. Nature Cell Biology *16*, 2-9.

Zhao, S., Weng, Y.C., Yuan, S.S.F., Lin, Y.T., Hsu, H.C., Lin, S.C.J., Gerbino, E., Song, M.H., Zdzienicka, M.Z., Gatti, R.A., *et al.* (2000). Functional link between ataxia-telangiectasia and Nijmegen breakage syndrome gene products. Nature *405*, 473-477.

Zhou, Z.W., Liu, C., Li, T.L., Bruhn, C., Krueger, A., Min, W., Wang, Z.Q., and Carr, A.M. (2013). An Essential Function for the ATR-Activation-Domain (AAD) of TopBP1 in Mouse Development and Cellular Senescence. Plos Genetics *9*.

Zou, L., and Elledge, S.J. (2003). Sensing DNA damage through ATRIP recognition of RPA-ssDNA complexes. Science *300*, 1542-1548.

Zou, L., Liu, D., and Elledge, S.J. (2003). Replication protein A-mediated recruitment and activation of Rad17 complexes. Proceedings of the National Academy of Sciences of the United States of America *100*, 13827-13832.